Probing the Role of the Active-Site Cysteine of Azurin by Site-Directed Mutagenesis

Thesis by

Tadashi Jack Mizoguchi

In Partial Fulfillment of the Requirements

for the Degree of

Doctor of Philosophy

California Institute of Technology

Pasadena, California

1996

(Submitted December 1, 1995)

Acknowledgments

First of all, I want to thank my advisors, Harry Gray and Jack Richards, for giving me the freedom to pave my own path towards a Ph.D. degree while always being willing and able to dispense "words of wisdom" when I felt lost or when experiments were not going well. On a more personal note, I want to thank Jack for convincing me that Stanford was *not* the place for me and Harry for turning me into a well-traveled gourmand. I also want to offer a special thank you to Mr. Cairo, my 9th grade chemistry teacher, who first got me hooked on chemistry through his enthusiasm for the subject and his often explosive demos.

I thank all the people who contributed to the work described in this thesis: Dave Goodin, Mike Hill, Tim Karpishin, Claudio Luchinat, Paul Saltman, Natalie Declerck, Angelo Di Bilio, Mario Piccioli, Tom Chang, Salem Faham, Ralf Langen, Ben Ramirez, Claire Slutter, and Toshi Takeuchi.

I would never have survived my stay at Caltech without the support of my friends. I met my "original" Caltech friends through a study group for Bi/Ch 110a. If we (Gary, Jerome, Max, Yonchu, and I) weren't arguing over the finer points of biochemistry, we were probably amusing ourselves over the latest antics of "the paranoiac"! Then, we all got sucked into lab. Now, five years later, I find myself in the company of Don, Kevin, and Yonchu who provided me with numerous fun-filled distractions during my thesis-writing days. Thank you. Thanks to all my friends!

Finally, I must thank my family for its continuing support during my seemingly endless journey through academics. Mama, Papa, Chichan, Chachan, Dave, Ken, Machan: You have always been and always will be an important part of my life.

Abstract

The coordination chemistry and electron-transfer properties of a single-site mutant of the mononuclear copper electron-transfer protein azurin from *Pseudomonas aeruginosa* have been studied. The active-site cysteine at position 112 was replaced by an aspartate (Cys112Asp) to assess directly the importance of this ligand to the structure-function properties of azurin. Although the mutant protein retains a high-affinity copper-binding active site, the absorption and EPR spectra of Cu^{II} Cys112Asp azurin are quite distinct from those of the wild-type protein and indicate the presence of a normal (type 2) copper center. A $Cu^{II/I}$ reduction potential of 180 mV *vs.* NHE (pH 7.0) was obtained through a redox titration experiment with cytochrome c_{551}. The Co^{II} derivative of Cys112Asp azurin was prepared and found to be amenable to paramagnetic NMR spectroscopy. In conjunction with electronic absorption data, the NMR data were used to generate a computer model of the Co^{II} active-site structure in which the metal is coordinated by two histidines (His46 and His117), a polypeptide backbone carbonyl oxygen (of Gly 45), and an out-of-plane, asymmetrically-bound bidentate aspartate (Asp112) in an overall distorted square pyramidal geometry. The 2.4-Å resolution X-ray crystal structure of Cu^{II} Cys112Asp azurin is reported and confirms this ligand set and geometry. Ni^{II}-substituted Cys112Asp azurin was also made, but unlike Cu^{II} and Co^{II}, the Ni^{II} ion is much less tightly bound by the protein. The electronic spectroscopy of Ni^{II} Cys112Asp azurin suggests the existence of some bonding interaction with the thioether sulfur atom of Met121. In contrast to Cys112-containing azurins, laser-induced *intra*molecular electron-transfer reactions from the reduced copper center of Asp112-containing azurins to surface histidine-bound bis(bipyridyl)(imidazole)ruthenium(III) labels could not be observed. However, the kinetics of *inter*molecular protein-protein electron transfer between Cys112Asp and wild-type azurins were recorded by stopped-flow spectrophotometry. Analysis of the bimolecular

kinetic data suggests that the Cys-to-Asp mutation has diminished significantly the electronic coupling between the copper and ruthenium centers in the intramolecular electron-transfer systems.

Table of Contents

List of Tables and Figures

Carpe Diem

because

Tempus Fugit

and

Don't Peak Too soon!

Chapter 1

Introduction: Blue Copper and *Pseudomonas aeruginosa* Azurin

Blue (or type 1) copper proteins[1] constitute a very large class of copper-containing proteins that are found in organisms ranging from bacteria to humans. As such, these proteins probably appeared very early in the evolutionary history of life on Earth.[2] The defining feature of a blue copper protein is the presence of a so-called blue copper site, which contains a single redox-active copper ion that is characterized (in the oxidized state) by: (1) an intense absorption band centered ~600 nm ($\varepsilon > 2000\ M^{-1}cm^{-1}$), (2) a small hyperfine coupling constant in the EPR spectrum ($A_{\|} < 100 \times 10^{-4}\ cm^{-1}$), and (3) a high reduction potential ($E° > 150$ mV *vs.* NHE). The function of blue copper sites in proteins is storage and transfer of one oxidizing (or reducing) equivalent to other physiological agents by outer-sphere electron transfer. The properties of blue copper are in stark contrast to those observed for most small molecule Cu^{II} complexes (Table 1.1) and other mononuclear copper proteins, such as Cu/Zn superoxide dismutase and galactose oxidase, that contain normal (or type 2) copper sites. (It should be noted that a given protein may contain more than one type of copper.[1d])

Early EPR work[4] on blue copper proteins suggested that their unique spectroscopic properties arose from a single Cu^{II} ion residing in a specific protein environment. The concept of rack-induced bonding in blue copper proteins,[5] which states that the polypeptide fold is responsible for creating an unusual coordination site and stabilizing a *strained* Cu^{II} complex, was introduced, thereby conferring an important role to the protein in the creation of blue copper sites. Subsequently, extensive spectroscopic studies of blue copper proteins led to the assignment of the intense 600-nm absorption band as a cysteine thiolate-to-Cu^{II} ligand-to-metal charge-transfer transition and the proposal of a pseudotetrahedral Cu^{II} coordination geometry defined in part by a two histidines and a cysteine.[1a] However, it was not until the first report of the crystal structure of a blue copper protein (Cu^{II} plastocyanin[6]) that these prior conclusions based on indirect spectroscopic techniques were shown, for the most part, to be correct.

Nearly 20 years have passed since the original plastocyanin structure was published, but interest among chemists in blue copper remains strong as new and more detailed questions continue to be addressed. Apart from studying naturally occurring blue copper proteins directly, other methods have been developed to study and understand blue copper in general. These methods can be divided into three general categories: theory, modeling, and mutagenesis.

Theory. With the availability of high-resolution structures of blue copper proteins, sophisticated theoretical investigations[7] have been undertaken to obtain detailed descriptions of the electronic structures of oxidized blue copper. For example, the Cu^{II}-cysteine thiolate bond has been shown to be highly covalent such that the ground-state unpaired electron of the formally d^9 Cu^{II} center is delocalized significantly onto the sulfur atom of the cysteine ligand; the half-occupied orbital has been calculated to possess < 50% Cu character.[8] Furthermore, the covalency of the Cu^{II}-cysteine thiolate bond has been used to explain the anomalously small hyperfine coupling constants observed in the EPR spectra of blue copper complexes and to show that the cysteine ligand provides an extremely well-coupled electron-transfer route into the Cu^{II} center.

Owing to the closed-shell d^{10} electronic configuration of Cu^{I}, few spectroscopic techniques are available to probe the reduced blue copper site (without interference from other chromophores). Nevertheless, the reduced site is functionally as important as the oxidized site. Theoretical calculations similar to those used to dissect the oxidized site, however, have provided a means to obtain an equally quantitative description of the electronic structure of reduced blue copper.[9] Results from these calculations suggest that the polypeptide fold forces a strained low symmetry (C_s) geometry on the reduced Cu^{I} center and that the geometry of the Cu^{II} center is actually *not* energetically unfavorable, thereby calling into question the validity of rack-induced bonding in blue copper proteins.

Modeling. The creation and study of artificial blue copper sites have also provided valuable insights into certain aspects of native blue copper sites. A successful blue copper model compound must mimic the ability of the polypeptide fold to overcome two major chemical obstacles associated with the Cu^{II} ion: (1) the preference of Cu^{II} to adopt a tetragonal coordination geometry (characteristic of normal copper) and (2) the tendency of Cu^{II} to react with thiolates to form Cu^{I} and disulfides. Therefore, a foreknowledge of the general structure of blue copper sites does not necessarily make the synthesis of a blue copper model compound a trivial synthetic exercise. In fact, it serves only to amplify the importance of the choice of ligands in avoiding these thermodynamic traps.[10]

A Cu^{II} complex with spectroscopic properties indicative of blue copper was, in fact, reported[11] *before* the report of the first blue copper protein crystal structure, but only recently has a structurally well characterized blue copper model compound been reported.[12] Nevertheless, the design of both systems is nearly identical. Bulky, substituted hydridotris(pyrazol-1-yl)borate (TPB) ligands[13] were used to occupy three coordination sites and a bulky thiolate to complete the pseudotetrahedral arrangement around the copper center. Interestingly, the crystal structure of Cu^{II}(hydridotris(3,5-diisopropylpyrazol-1-yl)borate)(pentafluorothiophenolate)[12] shows an unsymmetrically bound substituted TPB ligand, thereby distorting the overall structure of the complex towards trigonal pyramidal in which one of the pyrazoles occupies an axial position with a significantly longer bond to the Cu^{II} center than the other two pyrazoles. Similar geometries are known to exist in a number of crystallographically characterized blue copper proteins.[1d] The fact that a relatively unconstrained model compound can adopt a natural blue copper-like structure suggests that such a Cu^{II} geometry may be inherently stable so long as the possibility of tetragonal coordination is prevented. Such a conclusion provides experimental evidence against rack-induced bonding in blue copper proteins.

An advantage of synthetic model chemistry lies in the relative ease with which chemical modifications can be made to a given system to ascertain their effects on specific properties. The results from a resonance Raman study of a series of synthetic blue copper TPB model compounds with different thiolates were instrumental in explaining the observed multiple resonance Raman bands (centered ~400 cm^{-1}) associated with the Cu^{II}-S(Cys) stretching mode in blue copper proteins.[14] When secondary or tertiary thiolates were used in the model compounds, only the Cu^{II} compound with the lesser substituted thiolate exhibited similarly complex resonance Raman spectra; the others gave only a singe band. The origin of the splitting has, therefore, been ascribed to vibrational coupling between the Cu^{II}-S(Cys) stretching mode and several heavy atom bending modes associated with the primary thiolate ligand cysteine side chain.

Another approach to artificial blue copper sites involves the use of pre-existing protein metal-binding sites that are to some degree preorganized towards a blue copper-type geometry. For example, the Cu^{II}-substituted insulin hexamer has been shown to exhibit blue copper spectral characteristics with the addition of certain exogenous thiolates.[15] Three histidines from three of the six insulin molecules provide three of the copper ion ligands, while the thiolate ligand is provided from solution to complete a putative pseudotetrahedral coordination structure. A blue copper site has also been introduced within a single protein, Cu/Zn superoxide dismutase (SOD), by mutating one of the histidine ligands in the pseudotetrahedral Zn^{II} site (His80) to a cysteine.[16] In addition to a characteristic blue copper band (λ_{max} = 595 nm), the Cu^{II} derivative of His80Cys SOD exhibits another intense absorption band (λ_{max} = 459 nm) that also derives from a Cys(thiolate)-to-Cu^{II} charge-transfer transition.[8b,17] In fact, this second charge-transfer band is observed with varying intensities in all blue copper proteins, and a survey of blue copper sites in proteins has revealed an empirical correlation among: (1) the ratio of intensities of the absorption bands centered ~460 nm and ~600 nm (A_{460}/A_{600}), (2) the

rhombicity of the EPR spectra, and (3) the coordination geometry (trigonal ↔ trigonal pyramidal ↔ tetrahedral) of the Cu^{II} centers.[16b,17] $A_{460}/A_{600} < 0.2$ predicts an axial EPR spectrum and a structure approximating trigonal, while $A_{460}/A_{600} > 0.2$ a rhombic EPR spectrum and a structure approaching pseudotetrahedral.

Mutagenesis. We and others have studied blue copper sites in proteins by recording and interpreting the effects of amino acid substitution(s) on their structure, spectroscopy, and function as electron-transfer proteins.[18] Proteins like azurin and plastocyanin, which do not contain cofactors aside from the one copper ion, represent the simplest systems for studying blue copper sites in proteins. Since mutagenesis studies (including ours) have focused mainly on one blue copper protein, azurin from *Pseudomonas aeruginosa*, a description of this protein and its mutants is presented below.

P. aeruginosa azurin is a small (128 residues[19]), remarkably thermostable (T_m = ~80 °C (ref 20)) electron-transfer protein. The protein is found in the periplasm of *P. aeruginosa*,[21] and, as a consequence, its gene[22] is found to code for a preprotein with 20 extra N-terminal residues that are cleaved upon secretion. Originally purified as a "blue protein" in 1958,[23] it and similar proteins from other bacteria were not dubbed azurins until 1963.[24] The absorption spectrum of pure Cu^{II} azurin (Figure 1.1A) shows the characteristic 600-nm charge-transfer band centered at 628 nm ($\varepsilon_{628} = 5.7 \times 10^3\ M^{-1}cm^{-1}$ (ref 25)). The highly structured 280-nm protein absorption band with the distinguishing spike at 292 nm is attributable to the single tryptophan residue (at position 48) in a highly hydrophobic and rigid environment.[26] Consistent with this assignment is the fact that photoexcitation into the tryptophan chromophore leads to one of the highest energy room-temperature tryptophan fluorescence emission maxima (λ_{max} = 308 nm) known for proteins.[27] The absorption spectrum of the colorless Cu^{I} azurin (Figure 1.1B) retains the 292-nm absorption spike and shows increased absorptions in the near-UV that are attributable to Cu^{I}-centered transitions.[28] In particular, based on work on Au^{I}-substituted

azurins,[29] the absorption shoulder to the red of the protein band is assigned tentatively to a 3d-to-4p metal-centered transition of Cu^{I} in a trigonal coordination environment. Meanwhile, the EPR spectrum of Cu^{II} azurin (Figure 1.2) is axial (A_{460}/A_{600} = ~0.07) with $A_{\parallel}$ = ~60 x 10^{-4} cm^{-1}; E° = ~300 mV *vs.* NHE at pH 7.0.

Cu^{II} azurin from *P. aeruginosa* represents the second blue copper protein to have its three-dimensional structure determined. The original 3 Å resolution structure[30] was improved to 2.7 Å,[31] but even higher 1.93 Å resolution structures at two pH values (5.5 and 9.0) have recently become available.[32] (Apart from a main-chain peptide bond flip between Pro36 and Gly37, there is little difference between the pH 5.5 and pH 9.0 structures.) The overall structure of the protein consists of a single 8-stranded β-barrel with a small helical appendage (Figure 1.3). The copper center is located at one end of the β-barrel, and an intramolecular disulfide bond connects the side chains of Cys3 and Cys26 at the other end.

A view of the blue copper site of Cu^{II} azurin (Figure 1.4) reveals a Cu^{II} ion coordinated by two histidines (His46 and His117) and a cysteine (Cys112) in a nearly trigonal planar geometry. These three ligands are, in fact, strictly conserved in all native blue copper sites in proteins.[1d] There are also two other potential donor ligand atoms provided by Met121 and the backbone carbonyl group of Gly45 located at either of the two axial positions. The ~3 Å distances between the axial donor atoms and the copper center preclude the existence of strong bonds; electronic structure calculations suggest[33] that some degree of covalent interaction exists between the copper and the S(thioether) of Met121 but not the Gly45 carbonyl oxygen. All of the active-site residues and the metal center are effectively buried inside the protein except for the His117 side chain, which is partially exposed to solvent. Although the structure of Cu^{I} *P. aeruginosa* azurin is not available, the crystal structures of both oxidized and reduced forms of azurin from *Alcaligenes denitrificans* show that change in redox state is accompanied by only minimal changes in structure.[34] The structural invariance of the copper center and the limited communication

between the copper ion and the bulk solvent have significant implications with respect to promoting efficient electron transfer as the energies required for both inner-sphere nuclear and outer-sphere solvent reorganizations,[35] respectively, are minimized.

The crystal structure of apo *P. aeruginosa* azurin has been determined[36] and shows two different azurin forms co-crystallized within the crystal lattice. One form is structurally very similar to Cu^{II} azurin except for the absence of electron density associated with the copper center. The fact that the arrangement of the metal-binding ligands is preserved regardless of the presence of a coordinated metal has been used to bolster the validity of rack-induced bonding in azurin.[5c] However, the existence of a second apo azurin form, characterized by significant alterations in the active-site region, demonstrates that apo azurin is not held rigidly in a single rack conformer. The solvent-exposed active site of the second apo form also suggests that this form may be important for metal incorporation, particularly in view of the solvent inaccessibility of the active site in the rack structure. Crystal structures of Zn^{II}-[37] and Ni^{II}-substituted[38] *P. aeruginosa* azurins have also been reported. Although very close in structure to native Cu^{II} azurin, both metal-substituted derivatives show similar movements of the metal ion and the Gly45 carbonyl group toward each other, thereby creating a bond between the metal and the carbonyl oxygen atom while simultaneously removing any metal-(S)thioether bonding interaction that might otherwise have existed with Met121. Therefore, the active site of holo azurin is not absolutely rigid as some metal-derived preference in coordination geometry (towards tetrahedral for Zn^{II} and Ni^{II}) is apparently possible.

The successful heterologous overexpression of *P. aeruginosa* azurin[39] has provided researchers with access to the power of directed mutagenesis[40] as a means to assess the importance of specific residues to certain properties of the wild-type (WT) protein. The significance of mutagenesis to the study of azurin is apparent when one considers the number of mutants that have been reported in the literature. For convenience, these mutants

can be divided into those that do not involve active-site residues (His46, Cys112, His117, and Met121) and those that do. (Crystal structures of five *P. aeruginosa* azurin mutants are currently available: His35Gln (Cu^{II}),[41] His35Leu (Cu^{II}),[41] Asn47Asp (Zn^{II}),[42] Phe114Ala (Cu^{II}),[43] and Trp48Met (Ni^{II}).[44])

The role of the Cys3-Cys26 disulfide bond to the structural integrity of azurin was examined recently by making the Cys3Ser and Cys26Ser single and Cys3Ser/Cys26Ser double mutants.[45] The double mutation apparently causes significant structural changes to the overall protein fold, leading to the destruction of the blue copper active site. The single mutants are characterized by the isolation of various poorly defined forms of which only some retain blue copper-type properties. These results demonstrate the importance of the native disulfide bond to the overall structural stability and homogeneity of azurin. In a separate study, the Ile7Ser and Phe110Ser variants of azurin were prepared to determine the effect of the mutations on the photophysical properties of Trp48.[26] The replacement of Ile7 and Phe110 with a smaller and less hydrophobic serine resulted in red-shifted tryptophan fluorescence emission maxima along with a distribution of shorter fluorescence lifetimes. As both Ile7 and Phe110 make close contacts to Trp48, these observations are consistent with increased polarity around and flexibility of the Trp48 indole ring.

Mutagenesis has had a major impact in our understanding of the electron-transfer properties of azurin and proteins in general.[46] To gain insights into the physiological importance of specific residues, bimolecular protein-protein electron-transfer reactions between azurin and its native redox partners (*e.g.*, cytochrome c_{551} and nitrite reductase) must be considered. Although these reactions are generally low in thermodynamic driving force, they are observed to be very efficient. Reactions with cytochrome c_{551} have been shown[47] to exhibit electron-transfer rate constants on the order of 10^6 $M^{-1}s^{-1}$. Meanwhile, NMR line-broadening techniques[48] have been used to estimate the electron self-exchange rate constant of native azurin also to be ~10^6 $M^{-1}s^{-1}$. A series of surface mutations

(His35Lys,[49] His35Phe,[50] His35Leu,[50] His35Gln,[50] Met44Lys,[50,51] Met64Glu,[52] Glu91Gln[49]) have been introduced to locate the region(s) of the azurin surface responsible for electron-transfer-competent interactions with physiologically relevant redox partners. The observed changes in electron-transfer kinetics with itself, cytochrome c_{551}, nitrite reductase, and even the surface of an edge-plane graphite electrode were consistent with the hypothesis that the same hydrophobic region (defined by Met13, Leu39, Pro40, Val43, Met44, Phe114, Pro115, Gly116, Ala119, and Leu120 (ref 43)) around the solvent-exposed portion of the His117 ligand is the docking site when exchanging electrons with these reactants and that His117 imidazole group acts as the port of entry/exit of electrons to/from the copper center.[41,50-53]

Although bimolecular electron-transfer reactions can provide valuable information concerning the *in vivo* structure-function relationship of an electron-transfer protein, a quantitative understanding of the observed rate constants within theoretical frameworks is made difficult by the existence of multiple electron-transfer-competent encounter complexes and by the contribution of many difficult-to-define factors that control and stabilize their formation. However, by considering intramolecular reactions, the level of complexity of an electron-transfer system is diminished significantly, and the analysis of the data becomes more tractable.[54] The simplest intramolecular electron-transfer system reported for *P. aeruginosa* azurin involves only oxidized protein and near-UV light. Photoexcitation of Trp48 in Cu^{II} azurin leads to Cu^{II}-dependent quenching of the Trp48 triplet excited state that has been proposed to occur by an electron-transfer mechanism.[55] However, this conclusion remains open to interpretation as transient formation of Cu^{I} and a tryptophan cation radical was not observed.

An intramolecular system for which transient depletion of both donor and acceptor chromophores can be observed directly but independently in unmodified azurin has been developed using pulse radiolysis techniques[18c] in which $CO_2^{\cdot-}$ is used to reduce the native

disulfide bond of oxidized azurin. Intramolecular electron transfer over a distance of ~25 Å between the anion radical of the Cys3-Cys26 disulfide bond and the Cu^{II} center has then been shown to occur by transient absorption spectroscopy.[56] Similar experiments have been performed using azurin mutants that might provide general insights into the nature of long-range electron transfer in proteins. The surface mutations, His35Gln and Met44Lys, resulted in only minor changes in electron-transfer rate constants.[57] These difference were rationalized within the context of Marcus theory[35] as arising from changes in reduction potential and reorganization energy. Meanwhile, the Trp48Leu and Trp48Met internal mutants were studied[58] to test the importance of aromatic groups situated between the donor and acceptor sites. Again, only minor changes in electron-transfer rate constants were observed. It was concluded, therefore, that the π-system of Trp48 does not play a significant role in long-range electron transfer in this particular system. (Theoretical calculations have confirmed that the Trp48 side chain is not important in increasing the electronic coupling between the disulfide and copper center.[59])

Another method for studying intramolecular electron transfer in *P. aeruginosa* azurin has employed the generally applicable method of covalently attaching redox-active ruthenium complexes to surface histidine residues.[54] WT azurin provides only one accessible surface histidine (at position 83) ~15 Å away from the copper center. Both low-[60] and high-driving[61] force reactions utilizing His83 have been reported. With mutagenesis, however, one is not limited to one histidine labeling site. A series of azurin double mutants has been made to assess the electronic coupling through a single β-strand of azurin (containing Met121).[62] The His83Gln mutation, which removes the WT surface histidine, was common to all the mutants, while the labeling site was systematically moved away from the copper center from position 122 (Lys122His; ~12 Å metal-to-metal distance), 124 (Thr124His; ~17 Å), and finally to 126 (Thr126His; ~22 Å). The intramolecular electron-transfer rate constants from Cu^{I} to a highly oxidizing Ru^{III}(bis(2,2'-

bipyridyl))(imidazole)-(His) moiety (ΔG° = ~-0.75 eV) were measured using laser flash-photolysis techniques and were shown to be distance dependent with an exponential decay constant (β) of ~1.1 $Å^{-1}$. These experiments showed that the β-strand, owing to its extended polypeptide conformation, is more conductive than an α-helix with respect to long-range electron transfer.

Theoretical methods have also been employed to map the relative coupling energies between the copper center of azurin and arbitrary locations on the surface of the protein. Single pathway analyses of electronic coupling in proteins[63] have given way to more sophisticated tube analyses in which sets of similar pathways are considered together within a single tube.[61] Results of the calculations show that the hydrogen-bonding network that defines the β-sheet structure of azurin is a significant contributor to enhancing electron tunneling. In addition, with estimates for the relative couplings between the copper center and its ligands, the tube model was able to predict the relative rate constants of the intramolecular electron-transfer reactions between Cu^I and the Ru^{III}(bis(2,2'-bipyridyl))(imidazole)(His) labels that had been examined experimentally. Taken together, the study of intramolecular electron-transfer in azurin and its mutants has provided further theoretical and experimental support for the importance of the protein matrix in modulating electronic coupling between donor and acceptor sites.[64]

Most of the mutants described above were made with the intention of preserving the WT blue copper site so that issues pertaining to other parts of the azurin structure could be addressed in isolation. Owing to the complex set of interactions that ultimately determine the structure of proteins, however, even changes well removed from the active site can affect the copper center. For example, the reduction potential of azurin has manifested itself as a property that is extremely sensitive to changes far from the copper center.[65] Mutagenesis studies of active-site residues, on the other hand, are meant to probe directly their role in

defining the blue copper site of azurin by introducing potentially significant perturbations that may very well result in the destruction of the blue copper site.

Met121 represents the active-site residue of azurin that has been studied most extensively by mutagenesis. The WT methionine has been substituted by all other naturally occurring amino acids,[39c,66] a stop codon,[39c,66] and even a selenomethionine[67] (by *in vivo* mutagenesis). Significantly, all of the mutants, including the one in which the polypeptide chain ends at position 120, retain blue copper-like properties, although many exhibit reduced copper affinity. The original work on the Met121Leu mutant[68] showed that whatever bonding interaction that might exist between Met121 and the oxidized copper center is not critical for creating a blue copper site; the significantly higher reduction potential of the mutant (E° = 375 mV *vs.* NHE (pH 7.2)) was ascribed to increased hydrophobicity of the active site. The electron-transfer properties of Met121Leu azurin have also been examined by pulse radiolysis.[58] Analysis of the kinetic data suggests an increase in reorganization energy, implying greater flexibility within the active site. The Met121Glu and Met121Lys mutants[66] show very interesting pH-dependent properties attributable to ligation of the position 121 side chains under deprotonating conditions (pK_a(Glu121) ~5, pK_a(Lys121) ~6). Meanwhile, the Met121Gly mutant was recently re-examined[69] and was shown to bind small anions (azide, thiocyanate, and cyanide). Overall, the Met121 residue of azurin appears to be important for general active-site stability (*e.g.*, copper binding, rigidity, exclusion of exogenous ligands) and tuning of the reduction potential.

The ligand histidine at position 46 of azurin has also been converted to all other amino acids and a stop codon, but only the His46Asp mutant has been studied in any detail, as only the aspartate substitution results in a blue copper protein.[39c,70] Although His46 is not obligatory for blue copper binding, the fact that only Asp can take its place suggests that a residue with metal-binding capabilities is required. The extra negative charge introduced

by an Asp is reflected in a blue-shifted 600-nm blue copper band (λ_{max} = 612 nm) and a lower reduction potential (E° = 260 mV *vs.* NHE (pH 8.5)). In addition, the EPR spectrum of Cu^{II} His46Asp azurin was shown to exhibit signals characteristic of blue copper in HEPES buffer but normal copper in NH_4Cl buffer. This buffer-dependent phenomenon has been attributed to binding of an ammonia molecule (occupying a cavity created by the His-to-Asp mutation) to the active-site copper to make a tetragonal Cu^{II} site. Therefore, apart from its importance in metal binding, His46 appears to serve a role very similar to that of Met121.

His117Gly azurin represents the only reported mutant involving the partially solvent-exposed His117 residue.[71] This substitution creates a hole allowing certain exogenous ligands access to the copper center. Depending on the specific ligand, the spectroscopic properties of the resulting adducts indicate the generation of either a blue or normal copper site. Since the His117Gly mutation should partially relax the putative blue copper protein rack, the fact that a non-covalently attached ligand can restore blue copper binding has been used to argue against rack-induced bonding in azurin.[72] Although blue copper spectroscopy can be reconstituted using a variety of imidazole derivatives, chemical reduction of the blue copper centers was shown to be irreversible.[71b] A covalently attached imidazole group is apparently critical for the proper electron-transfer function of azurin.

The Gly45 carbonyl group can not be altered using standard mutagenesis techniques. However, a Gly45Ala mutant has been reported,[65] and although significant structural rearrangements around the metal site might be expected to accommodate the replacement of a hydrogen atom with a much larger methyl group, only very minor changes in optical, EPR, and electrochemical properties were observed. Therefore, this substitution apparently does little to perturb the structure of the blue copper site of azurin.

Previous to the work described in the subsequent chapters, the role of the ligand cysteine, which dominates the spectroscopy of blue copper sites, had not been investigated

by mutagenesis. We chose to make two azurin mutants: (1) Cys112Ser, which represents the nearly isosteric substitution of the cysteine sulfur with a serine oxygen, and (2) Cys112Asp, which represents the replacement of the anionic cysteine thiolate with a carboxylate group. Preliminary results from the Cys112Ser mutant suggested that, although the protein itself was stable, the substitution had destroyed the metal-binding ability of azurin. In contrast, the Cys112Asp mutant exhibited metal-binding properties that resulted in the generation of metalloproteins with spectroscopic, structural, and functional properties quite distinct from those of the WT protein. Chapter 2 describes the mutagenesis, expression, isolation, and purification of *P. aeruginosa* azurin. Chapters 3, 4, and 5 describe work on the Cu^{II}/Cu^{I}, Co^{II}, and Ni^{II} derivatives of Cys112Asp azurin, respectively. Finally, a brief summary of our work is presented in Chapter 6.

References

(1) For general reviews, see: (a) Gray, H. B.; Solomon, E. I. In *Copper Proteins*, Spiro, T. G., Ed.; Wiley: New York, 1981; Chapter 1, pp 1-39. (b) Sykes, A. G. *Struct. Bonding* **1990**, *75*, 175-224. (c) Sykes, A. G. *Adv. Inorg. Chem.* **1991**, *36*, 377-408. (d) Adman, E. T. *Adv. Protein Chem.* **1991**, *42*, 145-197.

(2) Scharf, B.; Engelhard, M. *Biochemistry* **1993**, *32*, 12894-12900.

(3) McMillin, D. R. *J. Chem. Ed.* **1985**, *62*, 997-1001.

(4) (a) Broman, L.; Malmström, B. G.; Aasa, R.; Vänngård, T. *Biochim. Biophys. Acta* **1963**, *75*, 365-376. (b) Mason, H. S. *Biochem. Biophys. Res. Commun.* **1963**, *10*, 11-13.

(5) (a) Malmström, B. G. In *Oxidases and Related Redox Systems*, King, T. E.; Mason, H. S.; Morrison, M., Eds.; Wiley: New York, 1965; Vol. 1, pp 207-216. (b) Gray, H. B.; Malmström, B. G. *Comments Inorg. Chem.* **1983**, *2*, 203-209. (c) Malmström, B. G. *Eur. J. Biochem.* **1994**, *223*, 711-718.

(6) Colman, P. M.; Freeman, H. C.; Guss, J. M.; Murata, M.; Norris, V. A.; Ramshaw, J. A. M.; Venkatappa, M. P. *Nature* **1978**, *272*, 319-324.

(7) For reviews on electronic structure calculation of metalloprotein active sites, see: (a) Solomon, E. I.; Baldwin, M. J.; Lowery, M. D. *Chem. Rev.* **1992**, *92*, 521-542. (b) Solomon, E. I.; Lowery, M. D. *Science* **1993**, *259*, 1575-1581.

(8) (a) Penfield, K. W.; Gewirth, A. A.; Solomon, E. I. *J. Am. Chem. Soc.* **1985**, *107*, 4519-4529. (b) Gewirth, A. A.; Solomon, E. I. *J. Am. Chem. Soc.* **1988**, *110*, 3811-3819. (c) Larsson, S.; Broo, A.; Sjölin, L. *J. Phys. Chem.* **1995**, *99*, 4860-4865.

(9) Guckert, J. A.; Lowery, M. D.; Solomon, E. I. *J. Am. Chem. Soc.* **1995**, *117*, 2817-2844.

(10) Lippard, S. J.; Berg, J. M. *Principles of Bioinorganic Chemistry*; University Science Books: Mill Valley, 1994; Chapter 12, pp 37-39.

(11) Thompson, J. S.; Marks, T. J.; Ibers, J. A. *Proc. Natl. Acad. Sci. USA* **1977**, *74*, 3114-3118.

(12) Kitajima, N.; Fujisawa, K.; Tanaka, M.; Moro-oka, Y. *J. Am. Chem. Soc.* **1992**, *114*, 9232-9233.

(13) For a sampling of the utility of substituted TPB ligands in modeling metalloprotein active sites, see: Moro-oka, Y.; Fujisawa, K.; Kitajima, N. *Pure & Appl. Chem.* **1995**, *67*, 241-248.

(14) Qui, D.; Kilpatrick, L.; Kitajima, N.; Spiro, T. G. *J. Am. Chem. Soc.* **1994**, *116*, 2585-2590.

(15) (a) Brader, M. L.; Dunn, M. F. *J. Am. Chem. Soc.* **1990**, *112*, 4585-4587. (b) Brader, M. L.; Borchardt, D.; Dunn, M. F. *J. Am. Chem. Soc.* **1992**, *114*, 4480-4486.
(16) (a) Lu, Y.; Gralla, E. B.; Roe, J. A.; Valentine, J. S. *J. Am. Chem. Soc.* **1992**, *114*, 3560-3562. (b) Lu, Y.; LaCroix, L. B.; Lowery, M. D.; Solomon, E. I.; Bender, C. J.; Peisach, J.; Roe, J. A.; Gralla, E. B.; Valentine, J. S. *J. Am. Chem. Soc.* **1993**, *115*, 5907-5918.
(17) Han, J.; Loehr, T. M.; Lu, Y.; Valentine, J. S.; Averill, B. A.; Sanders-Loehr, J. *J. Am. Chem. Soc.* **1993**, *115*, 4256-4263.
(18) For reviews of electron-transfer studies of blue copper proteins, see: (a) Farver, O.; Pecht, I. In *Copper Proteins*, Spiro, T. G., Ed.; Wiley: New York, 1981; Chapter 4, pp 1-39. (b) Gray, H. B. *Chem. Soc. Rev.* **1986**, *15*, 17-30. (c) Farver, O.; Pecht, I. *Biophys. Chem.* **1994**, *50*, 203-216.
(19) Ambler, R. P.; Brown, L. H. *Biochem. J.* **1967**, *104*, 784-825. (Although this article claims to describe the amino acid sequence of *P. fluorescens* azurin, the reported sequence is actually that currently accepted for *P. aeruginosa* azurin.)
(20) Engeseth, H. R.; McMillan, D. R. *Biochemistry* **1986**, *25*, 2448-2455.
(21) Wood, P. M. *FEBS Lett.* **1978**, *92*, 214-218.
(22) Canters, G. W. *FEBS Lett.* **1987**, *212*, 168-172.
(23) Horio, T. *J. Biochem.* **1958**, *45*, 195-205.
(24) Sutherland, I. W.; Wilkinson, J. F. *J. Gen. Microbiol.* **1963**, *30*, 105-112.
(25) Rosen. P.; Pecht, I. *Biochemistry* **1976**, *15*, 775-786.
(26) Gilardi, G.; Mei, G.; Rosato, N.; Canters, G. W.; Finazzi-Agrò, A. *Biochemistry* **1994**, *33*, 1425-1432.
(27) Finazzi-Agrò, A.; Rotilio, G.; Avigliano, L.; Guerrieri, P.; Boffi, V.; Mondovì, B. *Biochemistry* **1970**, *9*, 2009-2014. (Although this article claims to describe the fluorometric properties of *P. fluorescens* azurin, we suspect the protein used was actually *P. aeruginosa* azurin as the authors refer to ref 19 with regard to the primary structure of the protein.)
(28) Tamilarasan, R.; McMillan, D. R. *Inorg. Chem.* **1986**, *25*, 2037-2040.
(29) McCleskey, T. M.; Mizoguchi, T. J.; Richards, J. H.; Gray, H. B., submitted.
(30) Adman, E. T.; Stenkamp; R. E.; Sieker, L. C.; Jensen, L. H. *J. Mol. Biol.* **1978**, *123*, 35-47.
(31) Adman, E. T.; Jensen, L. H. *Isr. J. Chem.* **1981**, *21*, 8-12.
(32) Nar, H.; Messerschmidt, A.; Huber, R.; van de Kamp, M.; Canters, G. W. *J. Mol. Biol.* **1991**, *221*, 765-772.
(33) Lowery, M. D.; Solomon, E. I. *Inorg. Chim. Acta* **1992**, *198-200*, 233-243.

(34) Shepard, W. E. B.; Anderson, B. F.; Lewandoski, D. A.; Norris, G. E.; Baker, E. N. *J. Am. Chem. Soc.* **1990**, *112*, 7817-7819.

(35) Marcus, R. A.; Sutin, N. *Biochim. Biophys. Acta* **1985**, *811*, 265-322.

(36) Nar, H.; Messerschmidt, A.; Huber, R.; van de Kamp, M.; Canters, G. W. *FEBS Lett.* **1992**, *306*, 119-124.

(37) Nar, H.; Huber, R.; Messerschmidt, A.; Filippou, A. C.; Barth, M.; Jaquinod, M.; van de Kamp, M.; Canters, G. W. *Eur. J. Biochem.* **1992**, *205*, 1123-1129.

(38) Moratal, J. M.; Romero, A.; Salgado, J.; Perales-Alarcón, A.; Jiménez, H. R. *Eur. J. Biochem.* **1995**, *228*, 653-657.

(39) (a) Karlsson, B. G.; Pascher, T.; Nordling, M.; Arvidsson, R. H. A.; Lundberg, L. G. *FEBS Lett.* **1989**, *246*, 211-217. (b) van de Kamp, M.; Hali, F. C.; Rosato, N.; Finazzi Agro, A.; Canters, G. W. *Biochim. Biophys. Acta* **1990**, *1019*, 283-292. (c) Chang, T. K.; Iverson, S. A.; Rodrigues, C. G.; Kiser, C. N.; Lew, A. Y. C.; Germanas, J. P.; Richards, J. H. *Proc. Natl. Acad. Sci. USA* **1991**, *88*, 1325-1329.

(40) For a review, see: Canters, G. W.; Gilardi, G. *FEBS Lett.* **1993**, *325*, 39-48.

(41) Nar, H.; Messerschmidt, A.; Huber, R.; van de Kamp, M.; Canters, G. W. *J. Mol. Biol.* **1991**, *218*, 427-447.

(42) Sjölin, L.; Tsai, L.-C.; Langer, V.; Pascher, T.; Karlsson, G.; Nordling, M.; Nar, H. *Acta Crystallogr., Sect. D* **1993**, *49*, 449-457.

(43) Tsai, L.-C.; Sjölin, L.; Langer, V.; Pascher, T.; Nar, H. *Acta Crystallogr., Sect. D* **1995**, *51*, 168-176.

(44) Tsai, L.-C.; Sjölin, L.; Langer, V.; Bonander, N.; Karlsson, B. G.; Vänngård, T.; Hammann, C.; Nar, H. *Acta Crystallogr., Sect. D* **1995**, *51*, 711-717.

(45) Bonander, N.; Karlsson, B. G.; Vänngård, T. *Biochim. Biophys. Acta* **1995**, *1251*, 48-54.

(46) For a review, see: Wuttke, D. S.; Gray, H. B. *Curr. Opin. Struct. Biol.* **1993**, *3*, 555-563.

(47) Antonini, E.; Finazzi-Agrò, A.; Avigliano, L.; Guerrieri, P.; Rotilio, G.; Mondovì, B. *J. Biol. Chem.* **1970**, *245*, 4847-4849.

(48) Groeneveld, C. M.; Canters, G. W. *Eur. J. Biochem.* **1985**, *153*, 559-564.

(49) Pascher, T.; Bergström, J.; Malmström, B. G.; Vänngård, T.; Lundberg, L. G. *FEBS Lett.* **1989**, *258*, 266-268.

(50) van de Kamp, M.; Silvestrini, M. C.; Brunori, M.; Van Beeumen, J.; Hali, F. C.; Canters, G. W. *Eur. J. Chem.* **1990**, *194*, 109-118.

(51) van de Kamp, M.; Floris, R.; Hali, F. C.; Canters, G. W. *J. Am. Chem. Soc.* **1990**, *112*, 907-908.

(52) Van Pouderoyen, G.; Mazumdar, S.; Hunt, N. I.; Hill, H. A. O.; Canters, G. W. *Eur. J. Biochem.* **1994**, *222*, 583-588.

(53) Mikkelsen, K. V.; Skov, L. K.; Nar, H.; Farver, O. *Proc. Natl. Acad. Sci. USA* **1993**, *90*, 5443-5445.

(54) Winkler, J. R.; Gray, H. B. *Chem. Rev.* **1992**, *92*, 369-379.

(55) Klemens, F. K.; McMillan, D. R. *Photochem. Photobiol.* **1992**, *55*, 671-676.

(56) Farver, O.; Pecht, I. *Proc. Natl. Acad. Sci. USA* **1989**, *86*, 6968-6972.

(57) Farver, O.; Skov, L. K.; van de Kamp, M.; Canters, G. W.; Pecht, I. *Eur. J. Biochem.* **1992**, *210*, 399-403.

(58) Farver, O.; Skov, L. K.; Pascher, T.; Karlsson, B. G.; Nordling, M.; Lundberg, L. G.; Vänngård, T.; Pecht, I. *Biochemistry* **1993**, *32*, 7317-7322.

(59) Broo, A.; Larsson, S. *J. Phys. Chem.* **1991**, *95*, 4925-4928.

(60) Kostic, N. M.; Margalit, R.; Che, C.-M.; Gray, H. B. *J. Am. Chem. Soc.* **1983**, *105*, 7765-7767.

(61) Regan, J. J.; Di Bilio, A. J.; Langen, R.; Skov, L. K.; Winkler, J. R.; Gray, H. B.; Onuchic, J. N. *Chem. Biol.* **1995**, *2*, 489-496.

(62) Langen, R.; Chang, I-J.; Germanas, J. P.; Richards, J. H.; Winkler, J. R.; Gray, H. B. *Science* **1995**, *268*, 1733-1735.

(63) Beratan, D. N.; Onuchic, J. N.; Winkler, J. R.; Gray, H. B. *Science* **1992**, *258*, 1740-1741.

(64) For reviews, see: (a) Canters, G. W.; van de Kamp, M. *Curr. Opin. Struct. Biol.* **1992**, *2*, 859-869. (b) Friesner, R. A. *Structure*, **1994**, *2*, 339-343.

(65) Pascher, T.; Karlsson, B. G.; Nordling, M.; Malmström, B. G.; Vänngård, T. *Eur. J. Biochem.* **1993**, *212*, 289-296.

(66) Karlsson, B. G.; Nordling, M.; Pascher, T.; Tsai, L.-C.; Sjölin, L.; Lundberg, L. G. *Protein Eng.* **1991**, *4*, 343-349.

(67) Frank, P.; Licht, A.; Tullius, T. D.; Hodgson, K. O.; Pecht, I. *J. Biol. Chem.* **1985**, *260*, 5518-5525.

(68) Karlsson, B. G.; Aasa, R.; Malmström, B. G.; Lundberg, L. G. *FEBS Lett.* **1989**, *253*, 99-102.

(69) Vidakovic, M.; Germanas, J. P. *Angew. Chem. Int. Ed. Engl.* **1995**, *34*, 1622-1624.

(70) Germanas, J. P.; Di Bilio, A. J.; Gray, H. B.; Richards, J. H. *Biochemistry* **1993**, *32*, 7698-7702.

(71) (a) den Blaauwen, T.; van de Kamp, M.; Canters, G. W. *J. Am. Chem. Soc.* **1991**, *113*, 5050-5052. (b) den Blaauwen, T.; Canters, G. W. *J. Am. Chem. Soc.* **1993**, *115*, 1121-1129.

(72) Barrick D. *Curr. Opin. Biotech.* **1995**, *6*, 411-418.

Table 1.1 Properties that define blue copper compared to those of normal copper (represented by $[Cu(NH_3)_4]^{2+}$) (data from ref 3).

	Blue (Type 1)	Normal (Type 2) $([Cu(NH_3)_4]^{2+})$
1. ε_{max} ($M^{-1}cm^{-1}$) (λ_{max} = ~600 nm)	2000 - 6000	53
2. $A_{\|\|}$ (x 10^{-4} cm^{-1}) (EPR hyperfine coupling constant)	20 - 90	211
3. E° (mV *vs.* NHE) ($Cu^{II} \rightarrow Cu^{I}$)	180 - 790	0

Figure 1.1 Electronic absorption spectra of Cu^{II} (**A**) and Cu^{I} (**B**) WT *P. aeruginosa* azurins.

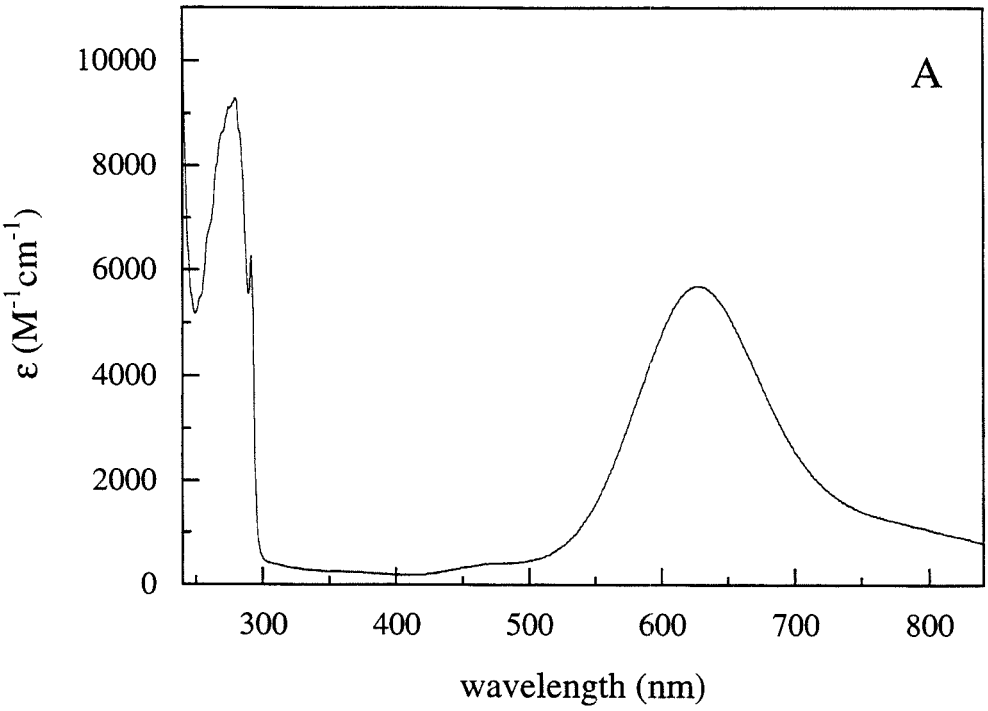
A
10000
8000
6000
4000
2000
0
ε (M-1cm-1)
300
400
500
600
700
800
wavelength (nm)

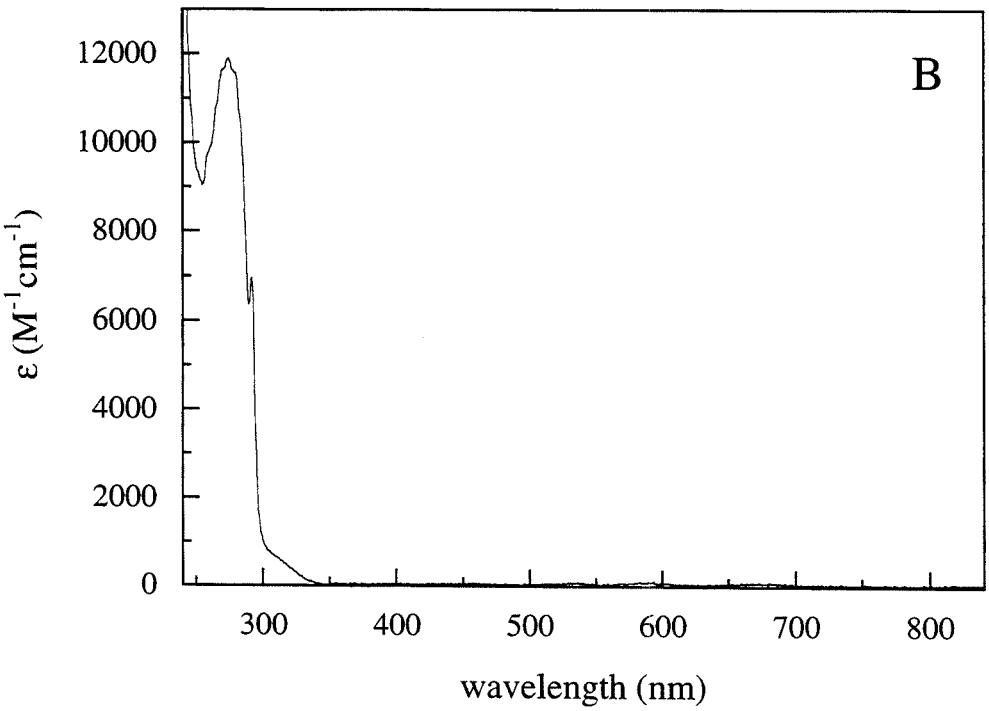
B
12000
10000
8000
6000
4000
2000
0
ε (M-1cm-1)
300
400
500
600
700
800
wavelength (nm)

Figure 1.2 EPR spectrum of Cu^{II} WT *P. aeruginosa* azurin (adapted from ref 66).

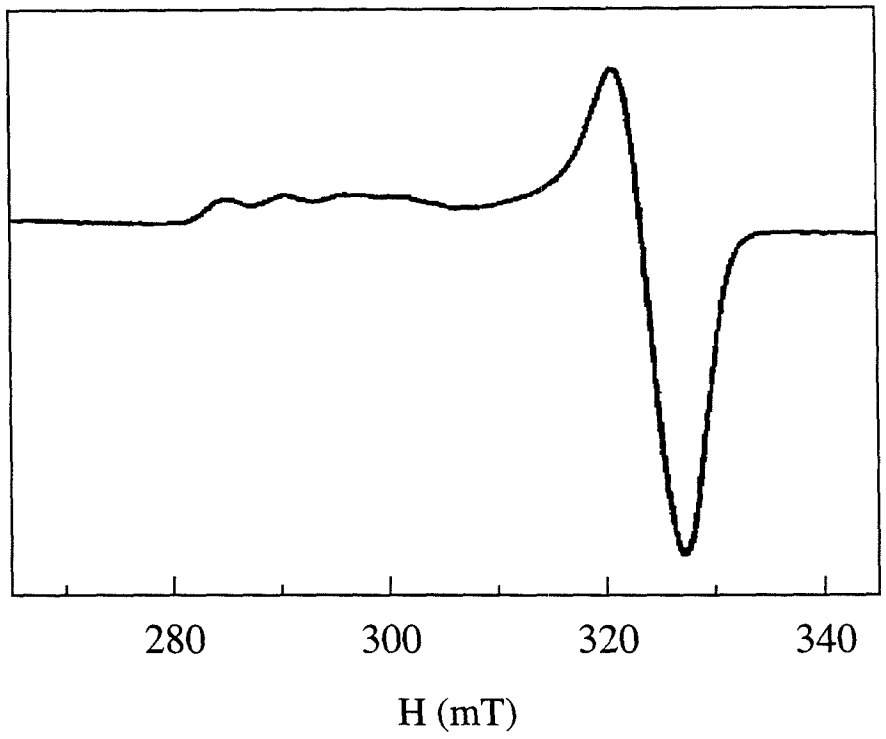
280
300
320
340
H (mT)

Figure 1.3 Ribbon diagram of *P. aeruginosa* azurin showing explicitly the location of the copper site and the Cys3-Cys26 disulfide bond (adapted from ref 41).

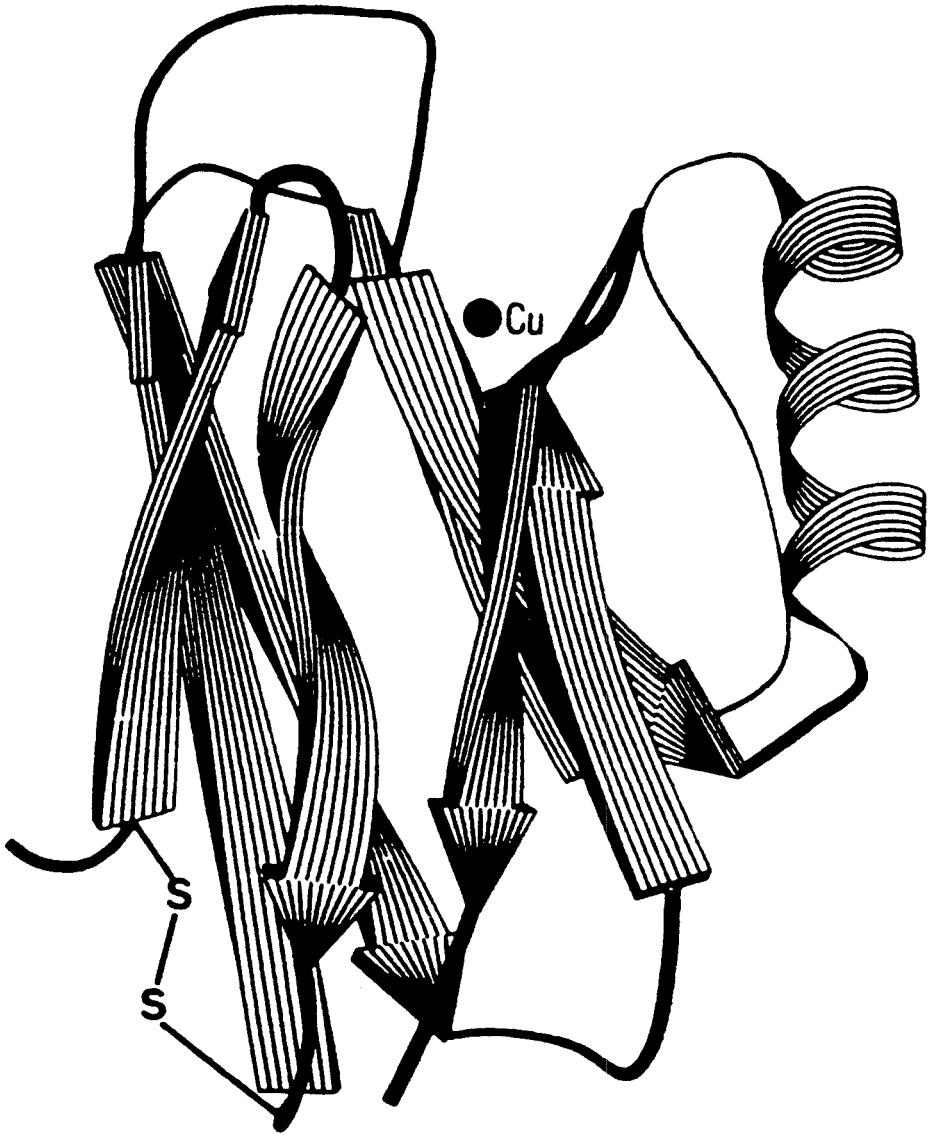
Cu
S
S

Figure 1.4 Schematic representation of the active-site structure of native WT *P. aeruginosa* azurin. The labeled distances (ref 32) are applicable to both oxidized and reduced forms of the protein.

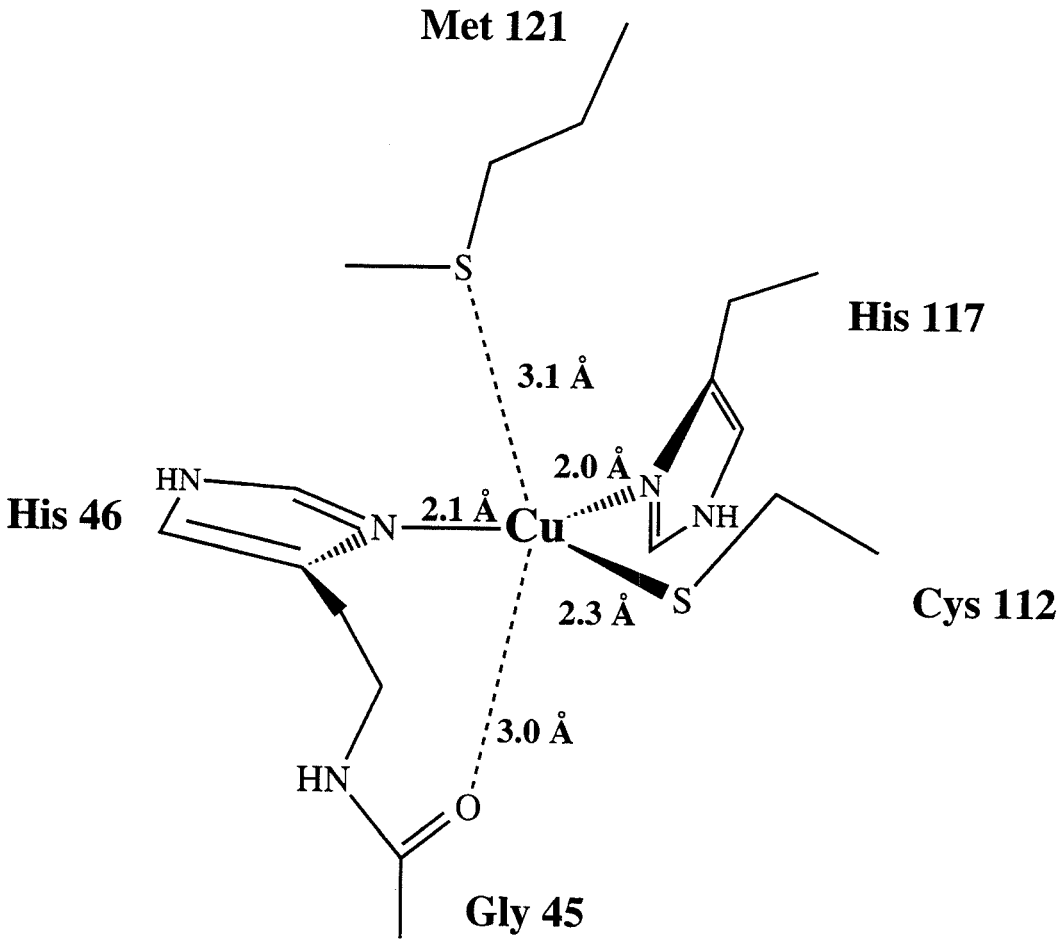
Met 121
S
3.1 Å
His 117
2.0 Å
N
NH
HN
His 46
N
2.1 Å
Cu
S
2.3 Å
Cys 112
3.0 Å
HN
O
Gly 45

Chapter 2

Obtaining Azurin

Introduction

The detailed study of proteins using experimental techniques usually requires that they be available in pure form and in relatively large (> mg) quantities. Given enough biomass, such amounts of naturally occurring proteins can, in principle, be isolated, but this approach is often not very practical. Furthermore, proteins with specifically introduced mutations are usually difficult to obtain from native sources as changes in the primary structure of a protein often lead to compromised function that can ultimately be detrimental to the survival of the host organism. And although the synthesis of polypeptides using chemical and *in vitro* translation methods can lead to novel proteins, these techniques are currently hampered by both low yields and high cost. Therefore, the development of simple biological systems that express high levels of proteins and that ideally do not require them to be functional remains a very important goal in protein chemistry.

In the case of *P. aeruginosa* azurin, three expression systems were reported independently within a span of two years.[1] Since then, site-directed mutagenesis has become a relatively common strategy to study the structure-function relationship of the protein (see Chapter 1). All of the expression systems are related in that the azurin gene is incorporated into a plasmid and the protein expressed in *Escherichia coli*. As in *P. aeruginosa*,[2] the nascent azurin polypeptide in *E. coli* is also processed so that the signal sequence is cleaved and the mature protein secreted into the periplasmic space of the bacterium. A simple osmotic shock protocol[3] is employed to rupture selectively the outer cell wall of *E. coli* (Figure 2.1), thereby requiring only centrifugation to remove most of the offending contaminants.

Here we describe the expression of the *P. aeruginosa* azurin protein using the T7 RNA polymerase expression system[4] and an updated purification protocol that results in the isolation of pure apo protein in yields of ~30 mg per liter of culture. A description of

the mutagenesis protocol used to make the Cys112Asp mutant azurin gene is also presented.

Materials and Methods

Standard molecular biology techniques were employed throughout this work.[5]

DNA. Oligonucleotides were synthesized on 0.2 μmole scales by the Caltech Microchemical Facility using an Applied Biosystems automated DNA synthesizer and were subsequently cleaned by two phenol:chloroform extractions followed by ethanol precipitations. Oligonucleotides used as mutagenesis primers were required to be 5' phosphorylated prior to use.

Plasmid DNA for preparative and sequencing purposes was isolated using the QIAGEN Plasmid Kit (QIAGEN). DNA restriction fragments were isolated from agarose gels using the QIAEX Gel Extraction Kit (QIAGEN). Fragments were eluted twice from the QIAEX beads, yielding a final volume of ~40 μL. An additional centrifugation step was added at the end of the protocol to remove any remaining QIAEX particles.

Mutagenesis. The Cys112Asp mutant azurin gene was made by oligonucleotide-directed mutagenesis using the Muta-Gene phagemid *in vitro* mutagenesis kit (Bio-Rad). A plasmid containing a synthetic WT azurin gene[1c] in the multiple cloning region of pTZ18U was used to make the single-stranded uracil-containing DNA template containing the sense strand of the azurin gene. *Nde* I and *Bgl* II restriction sites have been added at the beginning (the ATG start codon plus the 3 adjacent upstream nucleotides) and end (the 6 nucleotides downstream from the TAG stop codon) of the gene, respectively (Figure 2.2). The following primer was used to introduce the Cys112-to-Asp mutation:

$^{5'}$ CGG GAA AGT **GTC** GAA GAA CAT $^{3'}$
anti-codon for Asp112

Gene sequences were determined by the chain-termination method using primers complementary to the sense strand of the azurin gene. DNA fragments were labeled using either ^{35}S-dATP or fluorescent ddNTP analogs.

Protein Expression and Purification. Azurin was expressed in *E. coli* using the pET System (Novagen). Azurin genes in pTZ18U were excised with *Nde* I/*Bgl* II. The *Nde* I/*Bgl* II azurin gene-containing restriction fragments were then subcloned into the pET-9a expression vector between its *Nde* I/*Bam*H I restriction sites. Note that this ligation step destroys the downstream restriction site. The resultant azurin gene-containing pET-9a plasmids were introduced into competent *E. coli* expression strain BL21(DE3) by heat shock.

A typical protein preparation was started by growing a ~20 mL overnight culture of transformed BL21(DE3) in LB media containing 50 mg/L kanamycin at 37 °C. This preculture was used to inoculate 4 L 2xYT media containing 50 mg/L kanamycin. The culture was grown at 30 °C, and protein synthesis was induced with the addition of 0.75% IPTG once the optical density at 600 nm reached ~1.5, after which the culture was incubated at 30 °C for another 5 to 6 hours. The cells were harvested by repeated centrifugation (4000 x *g*) at 4 °C in 6 x 250 mL centrifuge bottles. The cell paste was resuspended in 6 x 60 mL 20% sucrose/30 mM Tris-HCl/1 mM EDTA (pH 8) with gentle shaking at room temperature. The cell paste was reisolated by centrifugation (10000 x *g*) at 4 °C, and the periplasmic fraction was released into solution by osmotic shock[3] with the addition of and resuspension in 6 x 60 mL ice-cold 4 mM NaCl. These suspensions were shaken gently at 4 °C for 8 to 12 hours. This mixture was centrifuged (4000 x *g*) at 4 °C, and the supernatant collected without concern with contamination from some cellular debris. To the murky supernatant was added slowly 1/10 volume of 0.5 M sodium acetate (pH 4.1) with stirring at 4 °C. The resulting white precipitate was removed by centrifugation (10000 x *g*)

at 4 °C, and the clarified supernatant containing crude azurin was saved for further purification.

The protein solution was concentrated using a stirred ultrafiltration unit fitted with a YM3 membrane (Amicon) and the pH increased to ~9 with an amine (diethanolamine (DEA) or ammonium chloride) buffer. Some precipitation was observed during concentration, but the precipitate redissolved at pH ~9. Azurin was purified by FPLC on a Mono Q (strong anion-exchange) column (Pharmacia) using a NaCl gradient in 10 mM amine buffers (pH ~9). The low salt buffer (Buffer A) contained no additional NaCl; the high salt buffer (Buffer B) was supplemented with 200 mM NaCl. Protein was detected by UV absorption at 280 nm. Fractions containing azurin were identified easily by the presence of a sharp absorption band at 292 nm.[6] Repurification was often necessary to obtain baseline separation of FPLC peaks.

Zn^{II} azurins were made by the addition of excess $ZnCl_2$ to solutions containing apo protein. Meanwhile, Zn^{II} azurins were demetallated by incubation in 0.1 M sodium acetate/0.1 M thiourea/10 mM EDTA (pH 4.5) for several days at room temperature. Pure Zn^{II} and apo azurins were isolated by FPLC, as described above.

Azurin expression was confirmed by SDS-PAGE (15%) under reducing conditions. Gels were stained using colloidal Brilliant Blue G (Sigma).

Spectroscopy. High-resolution absorption spectra were recorded on a modified Cary 14 spectrophotometer.

Results and Discussion

DNA and Mutagenesis. The mutagenesis experiments were accomplished in a routine fashion, resulting in synthetic azurin genes with the desired mutations. Aside from the expected changes in DNA sequence, sequencing using radioactive nucleotide analogs resulted in three regions that were inconsistent with the published synthetic gene sequence

of WT *P. aeruginosa* azurin.[1c] Two of these undesired mutation sites occurred at areas of the gene spanning the amino acid codons for either positions -6 to -4 or 25 to 26. However, as sequencing reactions using inosine in place of guanine eradicated these two problems, the apparent mutations have been rationalized as arising from DNA sequencing compression artifacts.[5] In addition, DNA sequencing experiments using fluorescent dideoxynucleotide terminators showed only the expected sequences at these two sites. The third inconsistency was reproducible using both the radioactive and fluorescent detection methods: the expected Ala1 codon (GCA) was changed to GCT. But as GCT also codes for alanine, this silent mutation was not corrected, and this gene (Figure 2.2) was used as our source of azurin.

Protein Expression and Purification. SDS-PAGE of the crude osmotic shock fluid (Figure 2.3) shows clearly that azurin is the predominant protein isolated from the periplasm. The protein gel also shows that acidification of the crude fluid is enough to remove nearly all of the remaining protein contaminants. Nevertheless, the acidified solution was slightly viscous and colored (light yellow) with an absorption maximum ~260 nm, suggesting the presence of non-proteinaceous material. Therefore, azurin was purified further by FPLC.

FPLC purification of the crude azurin solution revealed two different colorless azurin-containing fractions and a few miscellaneous peaks corresponding to residual unidentified contaminants (Figure 2.4). It was clear, especially from the purification of WT azurin, that only the later fraction (corresponding to Peak B in Figure 2.4) could be reconstituted readily with exogenously added metal ions. A "non-reconstitutable" azurin (corresponding to Peak A in Figure 2.4) has been described[1b] for the WT protein and was determined[7] to be the Zn^{II}-bound form of WT azurin. Therefore, Zn^{II} azurin elutes before apo azurin. This order is consistent with the explanation that the 2+ charge of a Zn^{II} ion makes Zn^{II} azurin overall more positively charged at pH ~9 than the apo protein and thereby

less tightly associated with the anion-exchange resin (regardless of whether the position 112 (Cys or Asp) side chain is protonated in the apo protein).

The source of Zn^{II} has not been determined, although the culture media would be a likely candidate. Since it seemed unlikely that all of the exogenous Zn^{II} could be sequestered during protein expression, we concentrated on separating the Zn^{II} azurin from the apo azurin. The isolated Zn^{II} azurin could then be treated to remove unwanted Zn^{II} ions. FPLC purification of the demetallation reaction again showed the same two peaks: one for residual Zn^{II} azurin and another for apo azurin. The absorption spectra of pure Zn^{II} and apo azurins (Figure 2.5) are practically superposable. But as pure apo azurin is essential for assuring that solutions are free of Zn^{II} contamination during reconstitution of holo azurin with other metals, anion-exchange FPLC offers a convenient and effective method of separating these two forms of azurin.

References

(1) (a) Karlsson, B. G.; Pascher, T.; Nordling, M.; Arvidsson, R. H. A.; Lundberg, L. G. *FEBS Lett.* **1989**, *246*, 211-217. (b) van de Kamp, M.; Hali, F. C.; Rosato, N.; Finazzi Agro, A.; Canters, G. W. *Biochim. Biophys. Acta* **1990**, *1019*, 283-292. (c) Chang, T. K.; Iverson, S. A.; Rodrigues, C. G.; Kiser, C. N.; Lew, A. Y. C.; Germanas, J. P.; Richards, J. H. *Proc. Natl. Acad. Sci. USA* **1991**, *88*, 1325-1329.

(2) Wood, P. M. *FEBS Lett.* **1978**, *92*, 214-218.

(3) Neu, H. C.; Heppel, L. A. *J. Biol. Chem.* **1965**, *240*, 3685-3692.

(4) Studier, F. W.; Rosenberg, A. H.; Dunn, J. J.; Dubendorff, J. W. In *Methods in Enzymology*; Goeddel, D. V., Ed.; Academic Press: San Diego, 1990; Vol. 185, pp 60-89.

(5) Sambrook, J.; Fritsch, E. F.; Maniatis, T. *Molecular Cloning: A Laboratory Manual*, 2nd ed.; Cold Spring Harbor Laboratory: Cold Spring Harbor, 1989.

(6) Yamanaka, T.; Kijimoto, S.; Okunuki, K. *J. Biochem.* **1963**, *53*, 256-259.

(7) Nar, H.; Huber, R.; Messerschmidt, A.; Filippou, A. C.; Barth, M.; Jaquinod, M.; van de Kamp, M.; Canters, G. W. *Eur. J. Biochem.* **1992**, *205*, 1123-1129.

Figure 2.1 Schematic representation of *E. coli* depicting mature azurin in the periplasmic space (between the inner and outer cell walls) and the result of osmotic shock treatment in which only the periplasmic contents are released into solution.

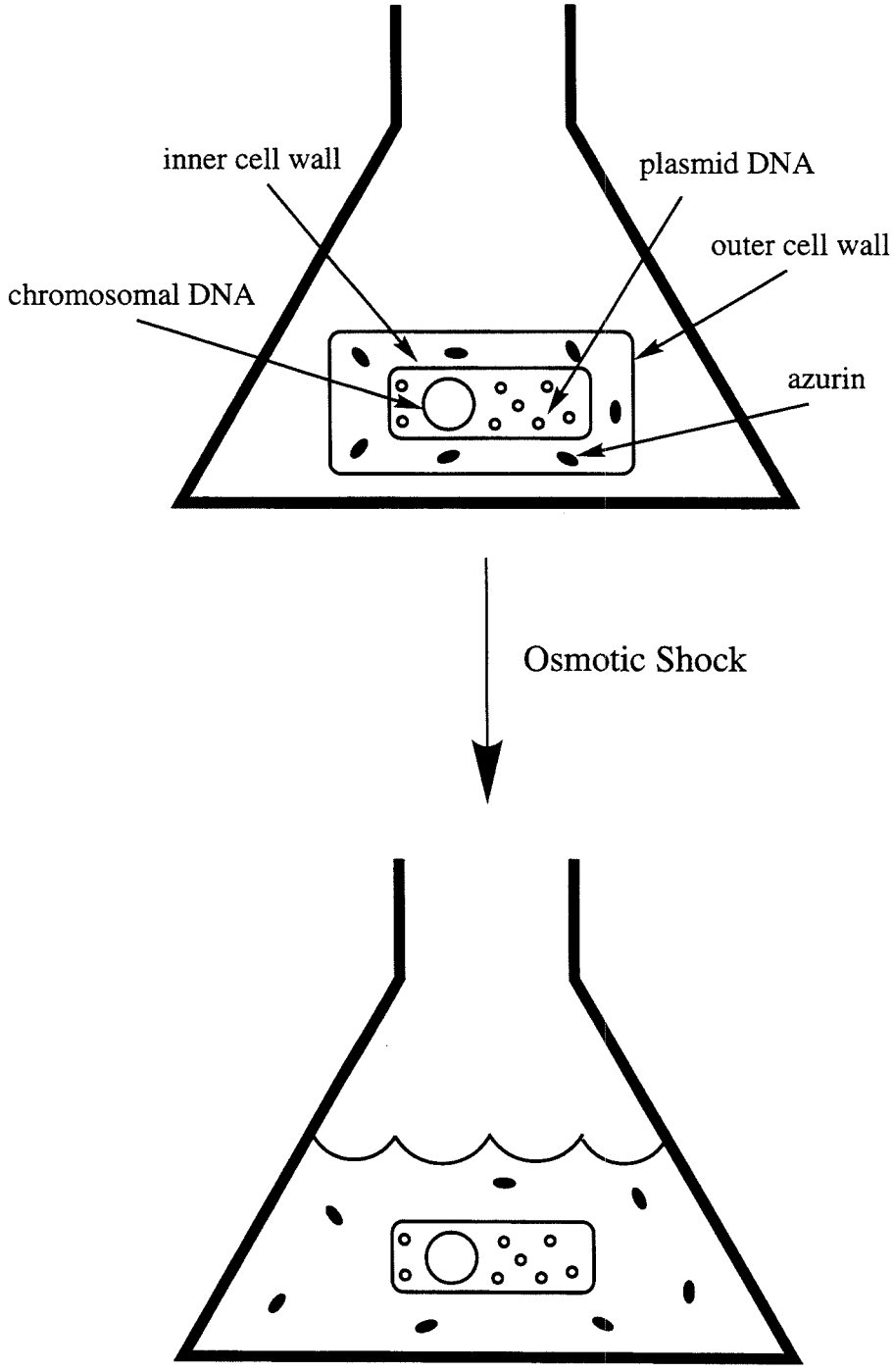
inner cell wall
plasmid DNA
outer cell wall
chromosomal DNA
azurin
Osmotic Shock

Figure 2.2 DNA sequence of the synthetic gene for WT *P. aeruginosa* azurin as found in pTZ18U (*Nde* I/*Bgl* II fragment) and the corresponding amino acid sequence of the azurin preprotein. The boundary between the signal sequence and the mature azurin polypeptide is represented by the vertical bar. The positions of certain residues are noted above their three-letter amino acid codes.

```
    Met Leu Arg Lys Leu Ala Ala Val Ser Leu Leu Ser Leu Leu
CAT ATG CTG CGT AAG CTG GCT GCA GTG TCT CTG CTG TCT CTG CTG
 Nde I
                              1
Ser Ala Pro Leu Leu Ala|Ala Glu Cys Ser Val Asp Ile Gln Gly
TCT GCT CCG CTG CTG GCT|GCT GAA TGC TCC GTT GAT ATC CAG GGT

Asn Asp Gln Met Gln Phe Asn Thr Asn Ala Ile Thr Val Asp Lys
AAT GAT CAG ATG CAG TTC AAC ACC AAC GCC ATC ACC GTC GAC AAG

Ser Cys Lys Gln Phe Thr Val Asn Leu Ser His Pro Gly Asn Leu
AGC TGC AAG CAG TTC ACT GTT AAC CTG TCT CAC CCA GGT AAC CTG

                              83
Pro Lys Asn Val Met Gly His Asn Trp Val Leu Ser Thr Ala Ala
CCG AAG AAC GTT ATG GGT CAC AAC TGG GTT CTG TCC ACC GCG GCT

Asp Met Gln Gly Val Val Thr Asp Gly Met Ala Ser Gly Leu Asp
GAC ATG CAA GGC GTT GTC ACT GAC GGT ATG GCT AGC GGT CTG GAT

Lys Asp Tyr Leu Lys Pro Asp Asp Ser Arg Val Ile Ala His Thr
AAA GAC TAC CTG AAG CCG GAT GAC TCT CGA GTT ATC GCC CAC ACC

Lys Leu Ile Gly Ser Gly Glu Lys Asp Ser Val Thr Phe Asp Val
AAG CTG ATC GGA TCC GGT GAA AAA GAC TCC GTT ACT TTC GAC GTT
            BamH I
                                                  112
Ser Lys Leu Lys Glu Gly Glu Gln Tyr Met Phe Phe Cys Thr Phe
TCC AAG CTT AAA GAA GGT GAA CAG TAC ATG TTC TTC TGC ACT TTC

                                  122
Pro Gly His Ser Ala Leu Met Lys Gly Thr Leu Thr Leu Lys Trm
CCG GGT CAC TCC GCA CTG ATG AAA GGT ACC CTG ACT CTG AAA TAG
Xma I

AGA TCT
 Bgl II
```

Figure 2.3 SDS-PAGE of WT *P. aeruginosa* azurin expressed using the pET-9a expression vector in the *E. coli* expression strain BL21(DE3) (lane 1: 10 μL crude osmotic shock fluid *before* acidification; lane 2: 10 μL crude osmotic shock fluid *after* acidification; lane 3: sample of FPLC purified WT azurin).

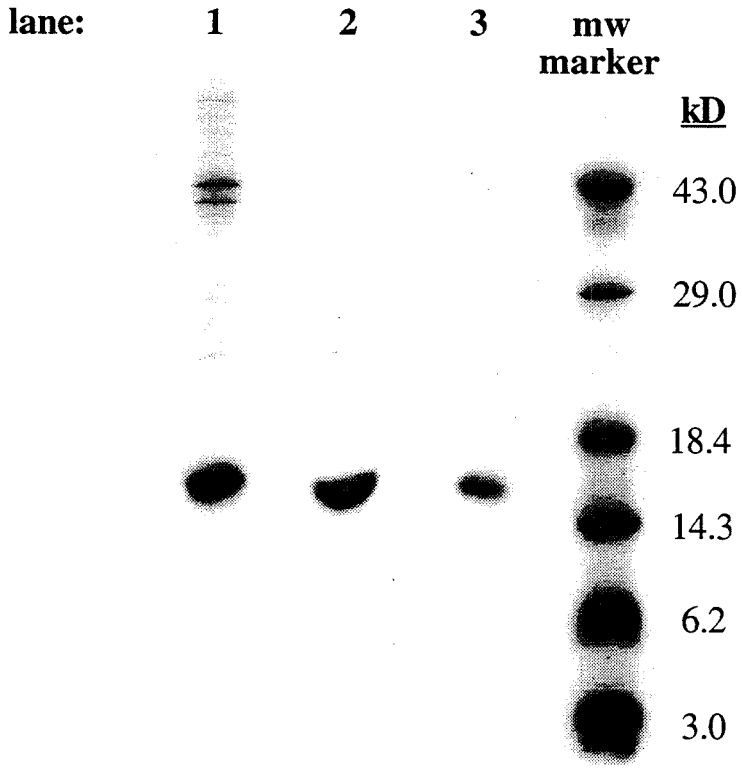
lane:
1
2
3
mw marker
kD
43.0
29.0
18.4
14.3
6.2
3.0

Figure 2.4 FPLC chromatogram (solid trace) from the purification of crude Cys112Asp *P. aeruginosa* azurin (buffer: 10 mM DEA·HCl (pH 8.8); column: Mono Q HR 10/10; flow rate: 1 mL/min; chart speed: 0.25 cm/mL; gradient held at 23% B after 15 min). The dashed trace represents the percentage of Buffer B (starting at 0% and increasing to a maximum of 100%) of the eluant. Peak A corresponds to Zn^{II} Cys112Asp azurin, while Peak B to apo Cys112Asp azurin. FPLC purification of crude WT azurin results in a similar looking chromatogram.

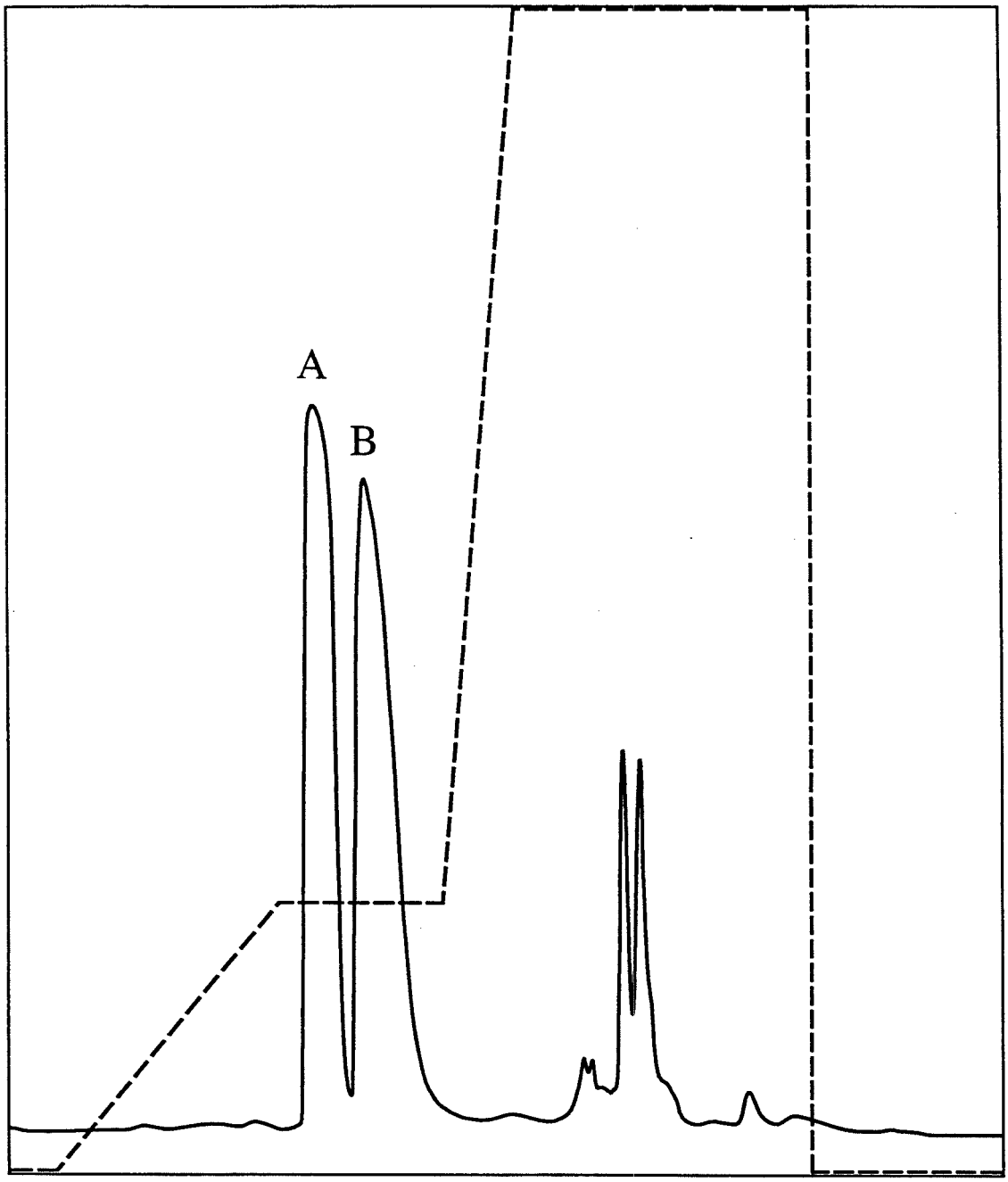
A
B

Figure 2.5 Electronic absorption spectra of apo (**A**) and Zn^{II} (**B**) Cys112Asp *P. aeruginosa* azurins in 10 mM DEA·HCl/~40 mM NaCl (pH ~8.8) at room temperature.

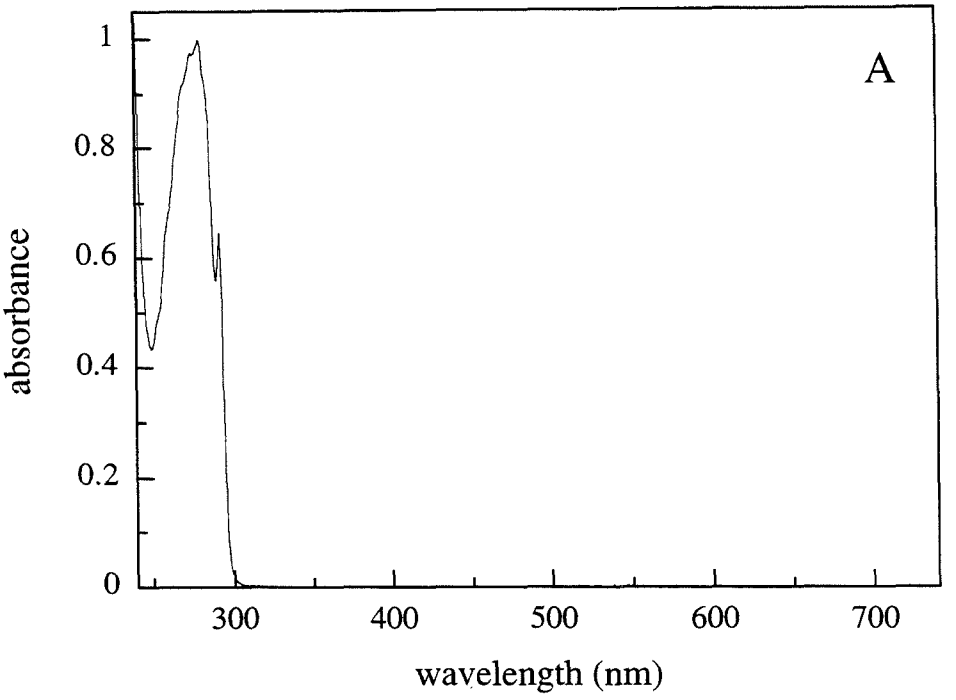
A
absorbance
1
0.8
0.6
0.4
0.2
0
300
400
500
600
700
wavelength (nm)

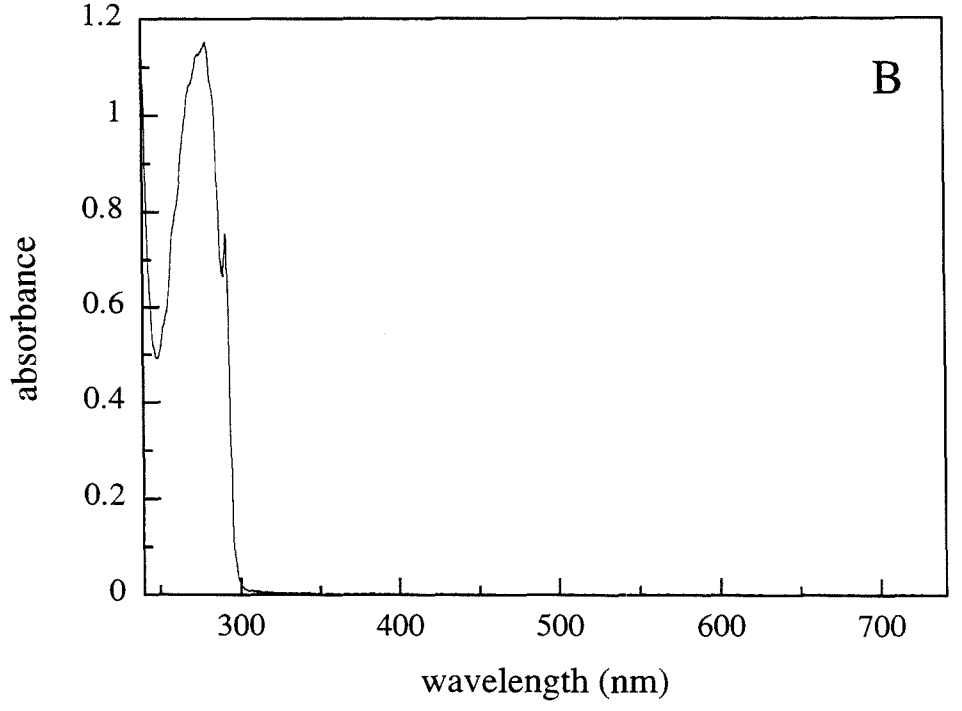
B
absorbance
1.2
1
0.8
0.6
0.4
0.2
0
300
400
500
600
700
wavelength (nm)

Chapter 3

Copper(II) and Copper(I) Cys112Asp Azurins

Introduction[1]

Of the five invariant residues (2His, Cys, Met, Gly) that surround the copper ion in azurins,[2] the bonding interaction between Cu^{II} and the thiolate of the ligand cysteine at position 112 (Cys112) has been shown to be particularly important in accounting for the unusual electronic absorption and EPR properties of the blue copper center[3] (see Chapter 1). The active-site cysteine has also been suggested to provide a well-coupled bridge to the copper center with respect to electron transfer.[4,5] It is striking that mutagenesis studies of Met121,[6] His46,[6,7] and His117[8] have shown that their side chains are not strictly required for maintaining a blue copper site, thereby reinforcing the essential role played by Cys112. While others[9] have used site-directed mutagenesis as a means to understand blue copper sites in proteins by creating an artificial blue copper site, we have probed directly the importance of the copper-thiolate interaction to the spectroscopy, active-site structure, and electron-transfer function of azurin from *P. aeruginosa* by the destroying the native blue copper site. Studies of the copper derivative of a mutant azurin in which the Cys112 ligand is replaced by an Asp is reported.

Materials and Methods[10]

Metal Titration. Molar extinction coefficients of the absorption bands of Cu^{II} Cys112Asp azurin were determined from titration experiments. To an appropriately concentrated solution of known volume of pure recombinant apo Cys112Asp *P. aeruginosa* azurin in 10 mM DEA·HCl/~40 mM NaCl (pH ~8.5) was added aliquots of a standardized solution of aqueous $CuSO_4$ (ε_{810} = 12.7 $M^{-1}cm^{-1}$) in a 1-cm pathlength quartz cuvette. Absorption changes were monitored using a Hewlett-Packard 8452A Diode Array Spectrophotometer and were allowed to stabilize after each addition. The data at a given wavelength were plotted as (observed absorbance) *vs.* (concentration Cu^{II} added). The data were not corrected for volume changes as the maximum change was < 5%. The resulting

titration plot was fit using KaleidaGraph 3.0 (Abelbeck Software) to two lines that best describe the data points in order to determine the point at which the azurin active site was saturated with Cu^{II}.

Protein Preparation. For general purposes, Cu^{II} WT and Cys112Asp azurins were made by the addition of a moderate excess of aqueous $CuSO_4$ to a buffered solution (pH ~9) of the appropriate apo protein. The resultant solutions were allowed to stand for at least 1 hour to assure complete reconstitution. Excess Cu^{II} was chelated with the addition of EDTA, and Cu^{II} WT and Cys112Asp azurins were then purified by FPLC on a Mono Q (strong anion-exchange) column (Pharmacia) using a NaCl gradient in 10 mM DEA·HCl (pH 8.8) or NH_4Cl (pH 9.3). The low salt buffer (Buffer A) contained no additional NaCl; the high salt buffer (Buffer B) was supplemented with 200 mM NaCl. Protein was detected by UV absorption at 280 nm. Concentrated azurin samples were obtained using Centricon-10 concentrator units (Amicon).

Cytochrome c_{551} from *P. aeruginosa* was purchased from Sigma. The cytochrome was concentrated using Centricon-3 concentrator units (Amicon) and purified by FPLC as described for azurin in solutions buffered by 10 mM DEA·HCl (pH 8.8). The reduction potential of cytochrome c_{551} ($E°_{cyt}$) in $\mu = 0.1$ M sodium phosphate (pH 7.0) was determined by cyclic voltammetry in the laboratory of Dr. Michael Hill (Occidental College) using a gold electrode whose surface was modified by Pyridine-4-AldehydeThio-Semicarbazone.[11]

Chemical Reduction. Cu^{I} azurins and Fe^{II} cytochrome c_{551} were made by reduction of concentrated solutions of oxidized protein with either an unbuffered aqueous solution containing $[Ru^{III}(NH_3)_6]Cl_3$/ascorbic acid and sodium dithionite, respectively. (Dithionite reduction of azurins was often accompanied by protein precipitation.) Excess reductant and its oxidized byproducts were removed by gel filtration through a PD-10

column (Pharmacia). Note that $[Ru^{III}(NH_3)_6]^{3+}$ decomposes rapidly at pH > ~8, turning the solution intense orange.

Steady-State Spectroscopic Measurements. High-resolution absorption spectra were recorded on a modified Cary 14 spectrophotometer. EPR spectra were recorded with the assistance of Dr. David B. Goodin (Scripps Research Institute).

Computer Modeling. The active-site structure of Cu^{II} Cys112Asp azurin was modeled using the 2.7-Å resolution structure of Cu^{II} WT *P. aeruginosa* azurin[12] (PDB code 1azu). The Cys112 side chain of WT azurin was replaced by an aspartate side chain using Biograf (Version 2.20) (BIODESIGN). The backbone atoms were fixed while the C_β and C_γ atoms of the aspartate side chain atoms were superimposed on the positions of the C_β and S_γ atoms of cysteine. The Asp112 carboxylate group was rotated about the C_β-C_γ bond to make a pseudosquare planar base defined by the imidazole (N^δ) nitrogens of His46 and His117 and the carboxylate oxygens of Asp112.

Redox Titration. The reduction potential of Cu^{II} Cys112Asp azurin was determined from a redox titration experiment with cytochrome c_{551}. To a 2.5 mL solution (V_i) containing 8.5 μM Fe^{II} cytochrome c_{551} ($[Fe^{II}$ cytochrome $c_{551}]_i$) in μ = 0.1 M sodium phosphate (pH 7.0) was added 4 x 50 μL aliquots of a 4.7 mM Cu^{II} Cys112Asp azurin ($[Cu^{II}$ Cys112Asp azurin$]_{conc}$) under aerobic conditions. The solution was allowed to equilibrate according to:

$$Fe^{II} \text{ cytochrome } c_{551} + Cu^{II} \text{ Cys112Asp azurin} \rightleftharpoons Fe^{III} \text{ cytochrome } c_{551} + Cu^{I} \text{ Cys112Asp azurin}$$

for ~15 minutes after the addition of each aliquot. The absorption spectra of equilibrated solutions were recorded on a modified Cary 14 spectrophotometer. Extinction coefficients of Fe^{II} (ε_{520} = 1.73 x 10^4, ε_{551} = 3.0 x 10^4 $M^{-1}cm^{-1}$) and Fe^{III} (ε_{520} = 1.06 x 10^4, ε_{551} = 9.28 x 10^3 $M^{-1}cm^{-1}$) cytochrome c_{551} were taken from the literature.[13] The amount of Fe^{III}

cytochrome c_{551} in solution was calculated from the ratio of absorbances at 551 and 520 nm; absorption at these wavelengths due to Cu^{II} Cys112Asp azurin was negligible under the conditions of the experiment. The data were plotted as ([Fe^{III} cytochrome c_{551}]) *vs.* (volume Cu^{II} Cys112Asp azurin added) and fit using KaleidaGraph 3.0 (Abelbeck Software) to the following function:

$$[Fe^{III}] = \left(\frac{1}{2(K_{eq}-1)}\right)x$$
$$\left[K_{eq}([Cu]_{tot}+[Fe]_{tot}) - \sqrt{\left(K_{eq}{}^2([Cu]_{tot}+[Fe]_{tot})^2 - 4(K_{eq}-1)(K_{eq}[Cu]_{tot}[Fe]_{tot})\right)}\right] \quad (3.1)$$

where:
[Fe^{III}] ≡ [Fe^{III} cytochrome c_{551}] in solution

$$K_{eq} = \frac{[Fe^{III}\text{ cytochrome } c_{551}][Cu^{I}\text{ Cys112Asp azurin}]}{[Fe^{II}\text{ cytochrome } c_{551}][Cu^{II}\text{ Cys112Asp azurin}]} \quad (3.2)$$

$$[Cu]_{tot} = \left(\frac{V}{V_i+V}\right)[Cu^{II}\text{ Cys112Asp azurin}]_{conc} \quad (3.3)$$

$$[Fe]_{tot} = \left(\frac{V}{V_i+V}\right)[Fe^{II}\text{ cytochrome } c_{551}]_i \quad (3.4)$$

V ≡ volume Cu^{II} Cys112Asp azurin added

K_{eq} was determined from the fit. The reduction potential of Cu^{II} Cys112Asp azurin ($E°_{az}$) was calculated by using the following relationships:

$$E°_{rxn} = -\frac{RT}{nF}\ln K_{eq} \quad (3.5)$$

$$E°_{rxn} = E°_{az} - E°_{cyt} \quad (3.6)$$

where:
$E°_{rxn}$ ≡ potential of the equilibrium between Cys112Asp azurin and cytochrome c_{551}

X-Ray Crystallography. Cu^{II} Cys112Asp azurin crystals were grown by vapor diffusion. 3.0 μL protein (~20 mg/mL) was mixed with 3.0 μL reservoir solution, which contained 0.1 M Tris·HCl (pH 8.0), 25% PEG-4000, 20 mM $CuCl_2$, and 0.1 M $LiNO_3$. The system was allowed to equilibrate at room temperature. Crystals grew over a few days, reaching a final size of approximately 0.3 x 0.1 x 0.1 mm. The space group was determined to be *C*2 with unit cell dimensions of a = 56.5, b = 48.9, c = 95.5 Å, and β = 94.0°. Diffraction data were collected on a Siemans area detector at room temperature. The data were then processed using the program XENGEN. The data set used for the structure determination contained 8392 unique reflections to 2.4 Å (83% complete), merged from a total of 19,753 observations with a merging R of 0.078.

The structure was solved by molecular replacement techniques. A self-rotation function showed a two-fold non-crystallographic axis along the *x* direction. The XPLOR package was used for the molecular replacement and refinement of the structure. Two molecules were found in the asymmetric unit. Non-crystallographic symmetry restraints were used at intermediate stages of the refinement, which was later released to allow different monomers to refine independently. Model building was performed using the TOM/FRODO graphics program. The structure refined to R = 0.20 for data between 8.0 Å and 2.4 Å with $F > F(\sigma)$ with rms deviation from ideal values for bond distances and angles of 0.016 Å and 2.66°, respectively. A total of 980 atoms assembled from 976 protein atoms, 2 copper atoms, and 2 water molecules per monomer are found in the current azurin model.

His83Gln/Cys112Asp/Lys122His Azurin. The His83Gln/Cys112Asp/Lys122His triple mutant azurin gene was constructed using a "cut-and-paste" approach between plasmids containing the Cys112Asp azurin gene in pET-9a (see Chapter 2) and the His83Gln/Lys122His azurin gene in pET-3a (ref 7) (provided by Dr. Ralf Langen) (Figure 3.1). The His83Gln/Cys112Asp/Lys122His azurin gene was excised from pET-3a with *Nde* I/*Eco*R I, and the resultant azurin gene-containing restriction fragment was subcloned

between the *Nde* I/*Eco*R I restriction sites of the pET-9a expression vector. The His83Gln/Cys112Asp/Lys122His azurin protein was expressed, isolated, and purified as described previously in Chapter 2. A higher salt concentration was required to elute both Zn^{II} and apo forms of the His83Gln/Cys112Asp/Lys122His mutant than WT or Cys112Asp azurin. This observation is explained by a simple charge argument: under the purification conditions (pH ~9), what would have been a positively charged surface Lys (pK_a ~11) at position 122 is replaced by a neutral His (pK_a ~6), making the triple mutant protein less positively charged and more tightly associated with the anion-exchange resin. Nevertheless, His83Gln/Cys112Asp/Lys122His azurin was found to be spectroscopically indistinguishable from Cys112Asp azurin.

Ruthenium Labeling. To a solution containing ~0.1-0.2 mM Cu^{II} azurin in 0.3 M sodium carbonate buffer (pH ~7.6) was added ~1 equivalent of $Ru^{II}(2,2'\text{-bipyridyl})_2(CO_3)$ (provided by Gary Mines). The resulting solution was incubated overnight at room temperature and subsequently purified by FPLC as described above using 10 mM NH_4Cl (pH 9.3). The aquo ligand of the purified aquoruthenium-labeled azurin was replace by an imidazole by incubation in 0.5 M imidazole/10 mM NaCl/10 mM $CuSO_4$ (pH 8) for several days. Pure $Ru^{II}(2,2'\text{-bipyridyl})_2$(imidazole)(His)azurin was isolate by FPLC after EDTA treatment to remove excess Cu^{II}. Ruthenium-labeled Cu^{I} azurin was obtained using the chemical reduction protocol described above. Labeled protein concentrations were estimated using $\varepsilon_{492} = 8 \times 10^3\ M^{-1}cm^{-1}$.

Laser Spectroscopy. Laser samples generally contained ~20 μM protein in μ = 0.1 M sodium phosphate (pH 7.0) in a 1-cm pathlength quartz fluorescence cuvette. Solutions were deoxygenated by pump-filling under argon. Samples for flash-quench experiments also contained either $[Ru^{III}(NH_3)_6]Cl_3$ or methyl viologen (MV^{2+}) dichloride as reversible oxidative quencher, which was dissolved into the protein solution after deoxygenation. All laser experiments were performed at the Caltech Beckman Institute

Laser Resource Center. Emission lifetime and electron-transfer experiments were initiated with a ~20 ns pulse of 480-nm light at ~1 mJ/pulse using a XeCl excimer-pumped dye laser (Lambda Physik LPX-210i, FL-3002). Emission was observed at 650 nm. Transient absorption traces were collected at 500 (corresponding to a large absorption difference between the Ru^{II} and Ru^{III} oxidation states of the label) and 600 (corresponding to a large absorption difference between MV^{2+} and $MV^{\cdot+}$) nm.

Stopped-Flow Spectroscopy. Electron-transfer reactions between copper WT and Cys112Asp azurins were studied using stopped-flow techniques in the laboratory of Dr. Paul Saltman (University of California, San Diego). Reduction of azurin was accomplished as described above. Experiments were performed under aerobic conditions in $\mu = 0.1$ M sodium phosphate (pH 7.0) at room temperature. Complications due to air oxidation was avoided by completing experiments within 15 minutes of sample reduction. Transient absorption traces were collected through a 1-cm pathlength sample chamber at 628 and 310 nm. The absorption changes of the system at 310 nm derives from differences in absorption between the Cu^{II} and Cu^{I} states of both Cys112Asp (see Figure 3.5) and WT (see Figures 1.1) azurins, while absorption changes at 628 nm can be considered to reflect solely changes in the concentration of Cu^{II} WT azurin. Therefore, kinetic analyses were performed using data collected at 628 nm, which were modeled using KINSIM[14] to estimate rate constants. Protein concentrations were determined using $\varepsilon_{628} = 5.7 \times 10^3$ for Cu^{II} WT, $\varepsilon_{276} = 11.8 \times 10^3$ for Cu^{I} WT, $\varepsilon_{310} = 2.0 \times 10^3$ for Cu^{II} Cys112Asp, and $\varepsilon_{276} = 10.3 \times 10^3$ $M^{-1}cm^{-1}$ for Cu^{I} Cys112Asp azurins.

Results and Discussion

Metal Titration and Protein Purification. Titration of apo Cys112Asp with Cu^{II} is accompanied by absorption changes that make the solution appear green (indicating formation of Cu^{II} Cys112Asp azurin) (Figure 3.2); then, after ~1 equivalent of Cu^{II} has

been added, the solution turns blue with a clear red-shift in λ_{max} of the visible/near-IR absorption band (Figure 3.2B). A plot of (observed absorbance) *vs.* (concentration Cu^{II} added) shows apparently two separate linear phases (Figure 3.3). The data are consistent with the first linear phase corresponding to increasing and exclusive occupation of the active site of apo Cys112Asp azurin with increasing Cu^{II} addition, while the second phase to the generation of some protein surface-bound Cu^{II} complex (*vide infra*) beyond the addition of 1 equivalent of Cu^{II}. According to this interpretation, the intersection of the two lines that describe a given titration curve denotes the point at which all of the active sites of azurin have been filled by Cu^{II}, and the value of the *x*:*y* ratio of the Cartesian coordinates of the intersection point represents the molar extinction coefficient at that wavelength. In this way, ε_{310} and ε_{754} for Cu^{II} Cys112Asp azurin were calculated to be 2.0×10^3 and 1.0×10^2 $M^{-1}cm^{-1}$, respectively. The error in these values is estimated to be $< \pm 10\%$. The calculated molar extinction coefficients of the 310- and 754-nm bands of Cu^{II} Cys112Asp azurin are significantly greater than previously published.[10] This discrepancy probably arose from contamination by the colorless Zn^{II} derivative in previous protein preparations which did not employ the purification protocol described in Chapter 2.

FPLC purifications of azurin solutions containing excess Cu^{II} in solution resulted generally in very complicated chromatograms with multiple overlapping holo azurin-containing peaks. Absorption spectra of the fractions indicated contamination by non-active-site-bound Cu^{II} ions. Since ultrafiltration of similar solutions also suggested some retention of Cu^{II} by the protein, we conclude that a moderately stable binding site for Cu^{II} exists on the surface of azurin. Treatment with EDTA, however, is enough to remove the exogenously bound Cu^{II} ions and restore normal chromatographic behavior, as shown in Figure 3.4. Cu^{II} Cys112Asp azurin is stable to metal loss for months under the purification conditions.

Electronic and EPR Spectroscopies. The intense charge-transfer band in the 600-nm region characteristic of a blue copper site is conspicuously absent in the absorption spectrum of Cu^{II} Cys112Asp azurin (Figure 3.5A). Furthermore, an absorption band not seen in Cu^{II} WT azurin (Figure 1.1A) is observed as a shoulder to the red of the near-UV protein band. This band ($\varepsilon_{310} = 2.0 \times 10^3\ M^{-1}cm^{-1}$) is attributable to an imidazole-to-Cu^{II} charge-transfer transition in a tetragonal coordination site,[15] and is blue-shifted considerably from a related ligand-to-metal charge-transfer absorption at 481 nm in Cu^{II} WT azurin.[16] A very broad and much weaker absorption centered at 754 nm ($\varepsilon_{754} = 1.0 \times 10^2\ M^{-1}cm^{-1}$) is also observed and is assigned to the ligand-field (d-d) transitions of the d^9 Cu^{II} ion, which are also substantially blue-shifted from the d-d bands found in the native protein.[16] The inferred tetragonal structure of Cu^{II} in the Cys112Asp protein is confirmed in the EPR spectrum (Figure 3.6), which is attributable to a normal type 2 copper center.[17] The EPR spectrum of the isotopically (^{63}Cu) enriched Cu^{II} Cys112Asp azurin exhibits superhyperfine structure in the lowest hyperfine line (Figure 3.6, Inset), indicating the presence of two equivalent equatorial nitrogen ligands[17d] (presumably from His46 and His117).

The absorption spectrum of Cu^{I} Cys112Asp azurin (Figure 3.5B) is very similar to that of Cu^{I} WT azurin (Figure 1.1B), sharing identical absorption maxima at 275 nm. Both reduced proteins are colorless, while gaining near-UV absorptions that have been attributed to Cu^{I} centered transitions.[18] The absorption spectrum of the equally colorless apo Cys112Asp azurin (Figure 2.5A), however, is noticeably different from that of Cu^{I} Cys112Asp azurin (Figure 3.5B), thereby confirming the involvement of Cu^{I} in the near-UV transition of reduced azurins. The spectrum of Cu^{I} Cys112Asp azurin differs from that of the reduced WT protein in that it does not exhibit the absorption shoulder red of the 275-nm protein band. As this band may be indicative of the trigonal planar structure of the WT Cu^{I} site[19] (tentatively assigned as a 3d-to-4p transition based on work on Au^{I}-substituted

azurins[20]), the lack of a similar band in Cu^{I} Cys112Asp azurin suggests a different Cu^{I} geometry for the mutant.

Although the absence of the intense Cys112(thiolate)-to-Cu^{II} charge-transfer transition in Cu^{II} Cys112Asp azurin was expected, we have, nonetheless, demonstrated that Cys112 of *P. aeruginosa* azurin is not obligatory for strong copper binding. Since Cys112 is an internal residue,[12,21] its substitution is unlikely to create a new strong metal-binding site that is not located at the WT active site. Of the possible tetragonal coordination geometries (square planar, square pyramidal, and octahedral), a square planar geometry is doubtful as square planar Cu^{II} complexes with similar potential donor atoms generally exhibit larger hyperfine coupling constants ($A_{\|} > \sim 200 \times 10^{-4}$ cm^{-1}).[22] Although an octahedral Cu^{II} geometry is possible, we believe the spectroscopic properties of Cu^{II} Cys112Asp azurin, in conjunction with those of the Co^{II} derivative of Cys112Asp azurin (see Chapter 4), are most consistent with a distorted square pyramidal geometry. Qualitative computer modeling was undertaken to assess possible copper coordination structures within the active-site of Cys112Asp azurin.

Computer Modeling. Inspection of the crystal structure of WT azurin[12,21] reveals that only the sulfur atom of Cys112 protrudes into the active-site cavity. Replacement of the Cys112 sulfur atom with a carboxylate group (an operation that corresponds to a Cys-to-Asp mutation) can be accomplished apparently without introducing steric clashes with neighboring atoms of the polypeptide chain. A square pyramidal Cu^{II} structure can be envisioned by utilizing the imidazole nitrogens of the native histidine ligands (His46, His117), a bidentate Asp112 carboxylate, and an axially positioned carbonyl oxygen of Gly45. The possibly, however, of axial coordination by the thioether of Met121 or a water molecule can not be excluded with certainty.

With respect to the possible bonding interactions between Cu^{II} and Asp112, the modeling suggests that the formation of a normally encountered planar bidentate copper-

carboxylate bond[23] would require substantial rearrangement of the protein structure due to geometrical constraints imposed by the aspartate side chain. Therefore, since a large distortion of the protein structure is energetically unfavorable, it is likely that the copper is displaced significantly from the plane of the Asp112 carboxylate group in forming the $Cu^{II}N_2O_2(O)$ structure. The idea of the polypeptide scaffold stabilizing an unusual coordination geometry is not inconceivable as it is well established as evidenced in the unusual distorted trigonal (pseudotetrahedral) coordination geometry of blue copper itself.[24]

The active-site structure of Cu^I Cys112Asp azurin remains more speculative, but it is worth noting that a ~90° twist of the Asp112 carboxylate group can convert the distorted square pyramidal metal-binding site of the Cu^{II} active-site model into a distorted tetrahedral site defined by His46, His117, Gly45, and a monodentate Asp112 without causing any steric conflicts. As tetrahedral Cu^I complexes are common (while square pyramidal Cu^I complexes are not),[22] it is conceivable that metal reduction is accompanied by such a change in coordination geometry. Furthermore, a tetrahedral Cu^I ion would not exhibit a 3d-to-4p electronic transition, in accord with our interpretation of the electronic absorption data of Cu^I WT and Cys112Asp azurins (*vide supra*).

Redox Titration. The direct electrochemistry of WT azurin has been documented,[25] but analogous experiments with Cys112Asp azurin did not result in satisfactory signals. Therefore, since crude preliminary experiments had shown that Cys112Asp azurin could exchange electrons with cytochrome c_{551} from *P. aeruginosa*, a redox titration experiment was performed to determine the $Cu^{II/I}$ Cys112Asp azurin reduction potential. Purification of commercial cytochrome c_{551} revealed two major along with a few small peaks in the FPLC chromatogram (Figure 3.7). Although both Peaks A and B produced superposable absorption spectra indicative of Fe^{III} cytochrome c_{551} (data not shown), the larger peak (Peak B) was used in subsequent experiments owing to its greater availability. The

reduction potential of the purified cytochrome ($E°_{cyt}$) was determined in the redox titration buffer to be 255 mV *vs.* NHE by cyclic voltammetry (see Figure 3.8).

Addition of oxidized Cys112Asp azurin to a solution of reduced cytochrome c_{551} is accompanied by absorption changes in the Q-band region of the cytochrome absorption spectrum (Figure 3.9). Furthermore, isosbestic behavior was preserved during the titration experiment (after correcting for volume changes) at wavelengths (504, 528, 542, 558 nm) known to be isosbestic points between Fe^{II} and Fe^{III} cytochrome c_{551},[13] thereby indicating not only the production of oxidized cytochrome c_{551} but also that the Q-band region of the spectrum can be considered transparent with respect to absorption from Cu^{II} Cys112Asp azurin. Although the experiment was performed in air, severe complications due to air oxidation were not encountered as < 10% of a control solution containing a similar concentration of reduced cytochrome c_{551} was oxidized during the time of the redox titration experiment. Furthermore, the possibility of azurin-catalyzed air oxidation of the cytochrome is discounted since only partial oxidation was observed.

Upon transforming the absorption data into a titration plot (Figure 3.10A), a fit to eq 3.1 yielded $K_{eq} = 0.049$. Subsequent application of eq 3.5 and 3.6 results in $E°_{az} = 179$ mV *vs.* NHE. The sensitivity of the calculated $E°_{az}$ to K_{eq} was assessed qualitatively by generating simulated titration plots according to eq 3.1 with K_{eq} defined as either 0.04 (translating to $E°_{az} = 173$ mV *vs.* NHE) or 0.06 (translating to $E°_{az} = 183$ mV *vs.* NHE) (Figure 3.10B). The two simulated plots envelop the observed data while differing in potential by only 10 mV. The simulated plot with $K_{eq} \equiv 0.04$ may, in fact, represent a better description of the cytochrome c_{551}-Cys112Asp azurin equilibrium if the small amount of Fe^{III} cytochrome c_{551} that is produced from air oxidation is considered. Regardless, 180 mV *vs.* NHE remains a reasonable estimate of the reduction potential of Cu^{II} Cys112Asp azurin at pH 7.0. Interestingly, this value still falls within the range of observed reduction potentials for blue copper sites in proteins (Table 1.1).

Crystal Structure: General. The unit cell of the Cu^{II} Cys112Asp *P. aeruginosa* azurin crystal is composed of four asymmetric units, each of which contains a dimer of holo azurin molecules (Figure 3.11). Furthermore, owing to the use of Cu^{II} in the crystallization buffer, there is a copper ion that links each azurin molecule to another in a neighboring asymmetric unit. The non-active-site copper center is coordinated by the amino nitrogen and carbonyl oxygen atoms of Ala1, N^{ε}(His83) from a different azurin molecule, and a solvent water molecule (H_2OA) in a distorted square planar geometry (Figure 3.12, Table 3.1). The metal is displaced ~0.6 Å from the square plane toward a patch of electron density that has been modeled as a second water molecule (H_2OB). The H_2OB(O)-metal distances are 3.2 Å in molecule A and 3.7 Å in molecule B of the asymmetric unit. The magnitude of these distances as well as their 0.5 Å difference indicates that H_2OB is not coordinated to the metal center. Regardless, Cu^{II} ions can apparently mediate the oligomerization of azurin molecules, and this process is probably related to the surface-bound copper form of azurin that had been proposed to exist in solution from observations made from the Cu^{II} titration and FPLC purification experiments (*vide supra*).

The two non-crystallographically related Cys112Asp azurin molecules are nearly identical as reflected in the 0.3 Å rms deviation between their main chain atom positions. The interface between the two azurin molecules is lined on either side by the residues (Met13, Leu39, Pro40, Val43, Met44, Phe114, Pro115, Gly116, Ala119, Leu120) that define the hydrophobic patch of *P. aeruginosa* azurin[26] (Figure 3.11). Interprotein contacts between hydrophobic patches have also been observed in the crystal structures of WT[21] as well as a number of mutant azurins.[26,27] Variations in the relative orientation of the individual molecules in the hydrophobic azurin dimer structure have been noted,[26] and the Cys112Asp azurin dimer structure is distinct from all the other reported structures. This difference may result indirectly from structural requirements imposed by the surface-bound copper ions. Meanwhile, in the middle of the hydrophobic patch, the His117 side chain,

which is thought to mediate electron transfer between the active-site copper and physiological redox partners,[28] remains partially solvent exposed. Water molecules have been identified within the hydrophobic dimer crevice of certain azurin structures[27a,26] and have been implicated to be important in promoting the observed facile electron self-exchange kinetics by providing a hydrogen-bonded bridge between opposing His117 N^{ε} atoms,[29] which are ~6.6 Å apart in the WT dimer. The corresponding distance in the Cys112Asp azurin structure is ~9.7 Å, and some electron density that has yet to be accounted for is detected between the Cys112Asp azurin dimer.

The crystal structures of the low (5.5) and high (9.0) pH forms of WT azurin showed that the Pro36-Gly37 peptide bond undergoes significant structural rearrangements between the two pH values.[21] A hydrogen bond is present in the low pH structure between the Pro36-Gly37 peptide carbonyl group and a protonated N^{ε} of His35. At high pH, this hydrogen bond is destroyed as the carbonyl group flips out, and the His35 side chain becomes deprotonated. Interestingly, the Pro36-Gly37 peptide carbonyl group of the current Cys112Asp azurin structure is oriented intermediate between those of the low and high pH forms of the WT protein. The existence of a hydrogen bond between the carbonyl group and His35 in the mutant structure is, nonetheless, clearly discounted. Therefore, we have chosen to use the Cu^{II} WT azurin structure at pH 9.0 (PDB code 5azu) to make quantitative comparisons with that of Cu^{II} Cys112Asp azurin.

Despite major differences in the arrangement of molecules between WT and Cys112Asp azurins within their respective crystal lattices, the main chain atoms of the azurin monomers are nearly superposable, except at the N-termini (Figure 3.13). A localized disparity in structure at this region is not surprising as the positional errors are generally greater at the termini of proteins and, more significantly, the non-active-site Cu^{II} ion is coordinated at this location in the Cys112Asp azurin structure. In the WT azurin structure, the Ala1 amino group is hydrogen bonded to the backbone carbonyl oxygen of

Ser4, while the Ala1 backbone carbonyl group is hydrogen bonded to NH(Ser4). But, in Cys112Asp azurin, the terminal amino group, in addition to coordinating the copper ion, is hydrogen bonded to O^{γ}(Ser25), while the Ala1 carbonyl oxygen is involved in bonding interaction with only the exogenous copper ion. When Ala1 and Glu2 are excluded in an rms deviation calculation (main chain atoms), the value decreases from 0.9 Å to only 0.5 Å.

Crystal Structure: Active Site. The distorted square pyramidal active-site coordination structure of Cu^{II} Cys112Asp azurin that was proposed from spectroscopic and computer modeling studies (*vide supra*) is confirmed in the crystal structure (Figure 3.14, Table 3.1). The metal is coordinated by both carboxylate oxygens of Asp112, N^{δ} of His46 and His117, and the backbone carbonyl oxygen of Gly45 and is displaced slightly from the pseudosquare base defined by the side chains of His46, Asp112, and His117 towards Gly45. Meanwhile, the ~4.0 Å distance between the thioether sulfur of Met121 and the copper center precludes the existence of any bonding interaction. The Asp112 carboxylate group[23] coordinates the metal asymmetrically such that one of the metal-oxygen bonds is ~0.6 Å longer than the other (Figure 3.15A). In addition, the Cu^{II} ion is positioned ~1 Å out of the plane defined by the carboxylate group of Asp112 (Figure 3.15B).

Aside from the introduction of two extra carboxylate oxygen atoms from the Asp112 side chain, many small perturbations to the native active-site structure have occurred to accommodate the Cu^{II} ion in Cys112Asp azurin (Figure 3.16). While the position of the His46 side chain has not moved considerably, the entire His117 side chain has translated in toward the active-site cavity and also closer to the Gly45 carbonyl group, thereby withdrawing the solvent-exposed part of the His117 imidazole ring away slightly from the bulk solvent. Like the active-site structures of Zn^{II} (ref 30) and Ni^{II} (ref 31) azurins, both the metal and Gly45 carbonyl group of Cu^{II} Cys112Asp azurin have moved closer to each other. The relatively long Met121 side chain has rearranged itself so that the thioether sulfur atom is located farther from the active site core. Finally, the entire Asp112 side chain

is pulled away from the active-site cavity, perhaps to lessen the severity of the out-of-plane binding of the copper. The two WT Cys112 side chain-to-main chain hydrogen bonds, however, are preserved in the mutant active site. But, instead of two hydrogen bonds to a single sulfur atom (S^{γ}(Cys112)-NH(Asn47) and S^{γ}(Cys112)-NH(Phe114)), they are split one each to either of the Asp112 carboxylate oxygens ($O^{\delta 1}$(Asp112)-NH(Asn47) and $O^{\delta 2}$(Asp112)-NH(Phe114)). The structure of apo Cys112Asp azurin is required to assess the degree to which the metal is responsible for the observed structural rearrangements, but it is apparent that ideal planar metal-carboxylate binding would require much more drastic alterations. Therefore, the overriding stability of the polypeptide fold of azurin can be considered to form a rack[32] that is rigid enough to force the unusual and strained bent metal-bidentate carboxylate bonding interaction.

Electron Transfer: Laser.[33] Attempts were made to observe high-driving force laser-induced intramolecular electron-transfer reactions between the copper center of either Cys112Asp or His83Gln/Cys112Asp/Lys122His azurin and a ruthenium complex attached covalently to the protein surface at His83 (metal-metal distance ~15 Å) or His122 (~12 Å), respectively. Unlike experiments with azurins that retain blue copper centers,[34] however, we were limited to being able to observe absorption changes related to the Ru label only (and not the Cu center). The technically simple photoinduced experiment (Figure 3.17A), which requires only labeled oxidized protein, did not result in any detectable formation of Ru^{III}. In other words, the lifetime of Ru^{II*} (τ = ~100 ns) is apparently too short to allow for excited-state electron-transfer to the oxidized copper center to occur. (Some luminescence quenching is observed, which can be ascribed to excited-state energy transfer due to spectral overlap between emission of the Ru^{II} label and absorption (d-d) of Cu^{II} Cys112Asp or His83Gln/Cys112Asp/Lys122His azurin.)

The more sophisticated oxidative flash-quench experiment[35] (Figure 3.17B), which requires labeled reduced protein, circumvents the limited lifetime of Ru^{II*} by reacting it with

an exogenous quencher to make Ru^{III} bimolecularly. Then, in principle, the intramolecular electron-transfer reaction between Cu^{I} and Ru^{III} can be observed. As experiments with Cys112Asp azurin produced results that were uninterpretable, we focused our efforts on the His83Gln/Lys122His azurin system. The Ru^{III} label formed using this scheme was observed to decay exponentially (Figure 3.18), as would be expected for a first-order reaction. However, the electron-transfer rate constant was found to be dependent on protein concentration, a property that is inconsistent with a unimolecular process. There are two likely bimolecular electron-transfer reactions that can lead to the reduction of Ru^{III} in competition with the desired intramolecular reaction:

$$Ru^{III} - Cu^{I} + Q^{-} \longrightarrow Ru^{II} - Cu^{I}$$

$$Ru^{III} - Cu^{I} + Ru^{II} - Cu^{I} \longrightarrow Ru^{II} - Cu^{I} + Ru^{II} - Cu^{II}$$

The first reaction corresponds to the thermal electron-transfer reaction between the products of the quenching reaction. Control experiments using labeled oxidized protein showed that this reaction can be minimized (for up to ~1 ms) by lowering the concentration of quencher used. The second reaction corresponds to the bimolecular electron-transfer reaction between Cu^{I} of one protein with the Ru^{III} label of another, a reaction that is pseudo first order under the conditions of the flash-quench experiment. (< 5% of the irradiated sample leads to Ru^{III} formation.)

We conclude, therefore, that intramolecular electron transfer can not compete effectively against the latter bimolecular side reaction with second-order rate constant ~2 x 10^{8} $M^{-1}s^{-1}$. At the very least, however, we can assign an upper limit of ~10^{3} s^{-1} to the intramolecular electron-transfer rate constant for the Cu^{I}-to-Ru^{III} reaction involving His83Gln/Cys112Asp/Lys122His azurin. The electron-transfer rate constant for His83Gln/ Lys122His azurin system, in which the blue copper center is preserved, has been measured under the same conditions to be 7.1 x 10^{6} s^{-1}.[34a] To understand the origins of

this large discrepancy in rate constants between blue (Cys112) and normal (Asp112) azurins, we turn to the theory of electron transfer developed by Marcus.[36]

The semiclassical Marcus expression for the rate constant (k_{et}) of a nonadiabatic electron-transfer reaction between rigidly fixed donor and acceptor groups is described by:[36]

$$k_{et} = \left(\frac{4\pi^3}{h^2 \lambda k_B T}\right)^{\frac{1}{2}} (H_{AB})^2 \exp\left(\frac{-(\Delta G^\circ + \lambda)^2}{4\lambda k_B T}\right) \tag{3.7}$$

where:
$\Delta G^\circ \equiv$ thermodynamic driving force of the reaction
$H_{AB} \equiv$ electronic coupling matrix element
$\lambda \equiv$ reorganization energy

Although ΔG° of the intramolecular electron-transfer reaction involving His83Gln/ Cys112Asp/Lys122His azurin (~-0.87 eV) is close to that involving His83Gln/Lys122His azurin (~-0.75 eV), our inability to measure a discrete electron-transfer rate constant for the His83Gln/ Cys112Asp/Lys122His azurin system precludes any quantitative discussion of the effect of the Cys-to-Asp mutation on H_{AB} and λ. We can conclude, however, that the substitution has altered significantly one or both of these parameters. To determine whether the difference in the rate constants can be ascribed solely to λ, we considered the bimolecular electron-transfer reaction between WT and Cys112Asp azurins.

Electron Transfer: Stopped-Flow. Results from the redox titration experiment between Cys112Asp azurin and cytochrome c_{551} (*vide supra*) had demonstrated that relatively efficient protein-protein electron-transfer reactions involving Cys112Asp azurin was possible. Indeed, we found that Cys112Asp azurin will also transfer electrons with WT azurin. To quantitate this reaction, we examined by stopped-flow spectrophotometry the reaction between Cu^{II} WT and Cu^{I} Cys112Asp azurins:

$$Cu^{II}\ WT\ azurin + Cu^{I}\ Cys112Asp\ azurin \underset{k_{21}}{\overset{k_{12}}{\rightleftharpoons}} Cu^{I}\ WT\ azurin + Cu^{II}\ Cys112Asp\ azurin$$

($\Delta G° = \sim -0.13$ eV $\Rightarrow K_{eq} = k_{12}/k_{21} = \sim 160$)

An important feature of this system is that changes in concentrations of both reactants can be observed during the course of the reaction as both WT and Cys112Asp azurins exhibit significant absorption differences between oxidation states at 628 and 310 nm, respectively (see Figures 1.1 and 3.5). Upon mixing the reactants, absorption changes are observed that indicate depletion of Cu^{II} WT azurin (Figure 3.19A) with concomitant formation of Cu^{II} Cys112Asp azurin (Figure 3.19B) due to electron transfer between Cu^{II} WT and Cu^{I} Cys112Asp azurins. The kinetics at 628 and 310 nm are superposable (Figure 3.20), indicating that electron transfer occurs directly between the copper sites of WT and mutant proteins without formation of an intermediate species.

Attempts to model the data to second-order kinetics were unsuccessful so long as the first time point was included. However, when that one point is excluded, the rest of the data can be modeled well with k_{12} and k_{21} set to 1.60×10^4 and 1.00×10^2 $M^{-1}s^{-1}$, respectively (Figure 3.21). Our inability to model the entire data set suggested initially that the problem with the time point may be due to an instrument-derived artifact. However, a similar problem point is mirrored in the data collected at 310 nm (Figure 3.19B), and examination of the reaction kinetics at shorter time bases revealed the presence of a faster kinetic phase that was complete within the first ~0.1 s of the reaction (Figure 3.22). Based on the observed change in absorbance after these first ~0.1 s, the reaction is already ~25% complete. In fact, if the simulated kinetic trace (Figure 3.21) is extrapolated to the initial concentration of Cu^{II} WT azurin before any reaction has occurred, ~2.4 s would have had to elapsed before ~25% of the reaction was complete. As 2.4 s is well within the deadtime of

the stopped-flow instrument, we believe that this fast phase is a non-artifactual phenomenon. Its significance to electron transfer in our system, however, is currently not well understood.

The reverse reaction between Cu^{I} WT and Cu^{II} Cys112Asp azurins was also examined. Upon mixing, an increase in absorption at 628 nm is observed (Figure 3.23A), indicating the formation of Cu^{II} WT azurin. A fast kinetic phase similar to that observed in the reaction between Cu^{II} WT and Cu^{I} Cys112Asp azurins is seen in this reaction as well. As a result, attempts to model the kinetics of this reaction also proved unsuccessful without excluding the first data point (Figure 3.23B). Nevertheless, the remaining data points were modeled with k_{12} and k_{21} set to 1.40×10^4 and 1.75×10^2 $M^{-1}s^{-1}$, respectively. These values agree reasonably well with those used to model the forward reaction.

Electron Transfer: Is It All in λ? The reason for the multiphasic transient absorption kinetics observed in the reactions between WT and Cys112Asp azurins may result from the known pH-dependent conformational heterogeneity of *P. aeruginosa* azurin,[21] suggesting that we may be observing at least two separate and kinetically resolved reactions. Regardless, the kinetics of the slower phases can be used to place estimated lower limits on the bimolecular electron-transfer rate constants: $k_{12} \geq \sim 1.4 \times 10^4$ and $k_{21} \geq \sim 1.8 \times 10^2$ $M^{-1}s^{-1}$. Meanwhile, NMR techniques have been used to determine the rate constant of the electron self-exchange reaction of WT *P. aeruginosa* azurin:[37]

$$Cu^{II}\text{ WT azurin} + Cu^{I}\text{ WT azurin} \overset{k_{11}}{\rightleftharpoons} Cu^{I}\text{ WT azurin} + Cu^{II}\text{ WT azurin}$$

k_{11} has been estimated to be $\sim 10^5$ $M^{-1}s^{-1}$ at 25 °C.[35] With values of k_{12} (or k_{21}) and k_{11} in hand, an estimate of k_{22}, the electron self-exchange rate constant for Cys112Asp azurin, can be made using the following approximated form of the Marcus cross relation:[36]

$$k_{12}^2 \approx k_{11}k_{22}K_{eq} \qquad (3.8)$$

Thus, k_{22} is calculated to be at least 20 $M^{-1}s^{-1}$. As $\Delta G°$ of the self-exchange reaction is 0, the nearly four orders of magnitude difference between k_{11} and k_{22} must be a reflection of significant differences in H_{AB} and/or λ between the WT and mutant systems. Classical Marcus theory can be used to estimate the maximum possible change in reorganization energy that is caused by the Cys-to-Asp mutation.

The rate constant of a bimolecular electron-transfer reaction (k) is given by:[36]

$$k = \kappa A\sigma^2 \exp\left(\frac{-\Delta G^{\ddagger}}{RT}\right) \tag{3.9}$$

where:
$\kappa \equiv$ transmission coefficient (probability of electron transfer of the transition-state complex)
$A\sigma^2 \equiv$ measure of collision frequency
$\Delta G^{\ddagger} \equiv$ free energy of activation

Crystallographic studies have shown that the Cys-to-Asp mutation does not drastically perturb the surface structure of the hydrophobic patch that is thought to be important in the electron self-exchange reaction of azurin.[38] Therefore, it is reasonable to assume that both WT and Cys112Asp azurins react with themselves and with each other through a very similar encounter complex structures. If we assume further that the electronic coupling (H_{AB}) between the copper centers in the encounter complex is unaltered by the mutation, the pre-exponential factor in eq 3.9 can be considered the same for the electron self-exchange reactions of both WT and Cys112Asp azurins. By taking the ratio of k_{11} and k_{22}, we obtain:

$$\frac{k_{11}}{k_{22}} = \exp\left(\frac{\Delta\Delta G^{\ddagger}}{RT}\right) \tag{3.10}$$

where:

$$\Delta\Delta G^{\ddagger} = \Delta G^{\ddagger}_{22} - \Delta G^{\ddagger}_{11} \tag{3.11}$$

$\Delta\Delta G^{\ddagger}$ is calculated to be ~21 kJ/mol (or ~0.22 eV).

Since the reactants and products of an electron self-exchange reaction are identical, the work needed to bring both the reactants (w^r) and products (w^p) to form encounter complexes are also identical,. As a result, $\Delta G^{\ddagger}$ of an electron self-exchange reaction is related to λ (which contains both inner- and outer-sphere contributions to the reorganization energy) by:[36]

$$\Delta G^{\ddagger} = \frac{\lambda}{4} \tag{3.12}$$

By extension, $\Delta\Delta G^{\ddagger}$ can be related to $\Delta\lambda$ by:

$$\Delta\Delta G^{\ddagger} = \frac{\Delta\lambda}{4} \tag{3.13}$$

where:

$$\Delta\lambda = \lambda_{Cys112Asp} - \lambda_{WT} \tag{3.14}$$

Therefore, $\Delta\lambda$ is calculated to be ~0.87 eV (or ~84 kJ/mol), assuming no change in electronic coupling.

The reorganization energy of the ruthenium-labeled WT azurin system described above has been estimated to be ~0.8 eV.[34a] Furthermore, the self-exchange reorganization energies of the ruthenium label and WT azurin can be estimated to be ~0.6 and 1.0 eV, respectively.[33] By using another manifestation of the Marcus cross relation (related to eq 3.8):[36]

$$\lambda_{tot} = \frac{1}{2}(\lambda_d + \lambda_a) \tag{3.15}$$

where:

$\lambda_d \equiv$ self-exchange reorganization energy of the electron donor group

$\lambda_a \equiv$ self-exchange reorganization energy of the electron acceptor group

the reorganization energy of the ruthenium-labeled Cys112Asp azurin system is estimated to be ~1.3 eV. Then, by assuming that the electronic coupling application of eq 3.7 predicts that the rate constant of intramolecular electron transfer in the ruthenium-modified Cys112Asp azurin should be smaller by a factor of ~3.6 from that of the Cys112 azurin system (k_{et} = 7.1 x 10^6 s^{-1} (ref 34a)). Therefore, theory predicts that the electron-transfer rate constant for ruthenium-labeled His83Gln/Cys112Asp/Lys122His azurin should be *at least* ~2 x 10^6 s^{-1}; the experimental value of this rate constant was determined to be *at most* ~10^3 s^{-1}. It is clear from these calculations that our assumption that the Cys-to-Asp mutation has not affected H_{AB} is untenable in the intramolecular electron-transfer reaction between Cu^I and the Ru^{III} label at position 122. For the same reason, H_{AB} between Cu^I and the Ru^{III} label at position 83 (k_{et} = 1.1 x 10^6 s^{-1} for WT azurin[34b]) is altered significantly by the Cys-to-Asp mutation.

This conclusion leads us to consider what has changed between WT and Cys112Asp azurin structures to cause such dramatic decreases in electronic coupling in the intramolecular systems. As the overall structure of Cys112Asp azurin was determined to be very similar to that of the WT protein (*vide supra*), the coupling provided by the β-sheet structure of azurin[34] is most likely preserved. Since theoretical studies suggest that electron-transfer between the copper and ruthenium centers occurs through the ligand thiolate sulfur atom in the Cys112 azurin systems,[34b] it is reasonable to assume that whatever change has occurred in electronic coupling is localized at or near the mutation site. Unlike Cys112 azurins, we would expect some structural rearrangements to occur between the Cu^{II} and Cu^I oxidation states of Cys112Asp azurins. Unfortunately, we do not have a good handle on the active-site structure of Cu^I Cys112Asp azurin. Although computer modeling suggests that pseudotetrahedral coordination utilizing a monodentate Asp112

carboxylate is possible (*vide supra*), it is also possible that the Asp112 side chain is detached completely from the metal center in the reduced state, thereby providing no bonded coupling to the Cu^{I} center at all through the position 112 side chain. (Partial ligand detachment has been documented in the crystal structure of Cu^{I} Met121Gln azurin from *A. denitrificans*.[39]) On the other hand, the fact that bimolecular electron-transfer reactions between Cys112Asp azurin and both cytochrome c_{551} and WT azurin can be observed indicates that the copper center of Cys112Asp azurin is still coupled to external reactants through His117.

References

(1) For a more detailed general introduction, see: Chapter 1.

(2) Adman, E. T. *Adv. Protein Chem.* **1991**, *42*, 145-197.

(3) Gewirth, A. A.; Solomon, E. I. *J. Am. Chem. Soc.* **1988**, *110*, 3811-3819.

(4) (a) Solomon, E. I.; Baldwin, M. J.; Lowery, M. D. *Chem. Rev.* **1992**, *92*, 521-542. (b) Solomon, E. I.; Lowery, M. D. *Science* **1993**, *259*, 1575-1581.

(5) Regan, J. J.; Di Bilio, A. J.; Langen, R.; Skov, L. K.; Winkler, J. R.; Gray, H. B.; Onuchic, J. N. *Chem. Biol.* **1995**, *2*, 489-496.

(6) (a) Karlsson, B. G.; Aasa, R.; Malmström, B. G.; Lundberg, L. G. *FEBS Lett.* **1989**, *253*, 99-102. (b) Karlsson, B. G.; Nordling, M.; Pasher, T.; Tsai, L. C.; Sjölin, L.; Lundberg, L. G. *Protein Eng.* **1991**, *4*, 343-349. (c) Chang, T. K.; Iverson, S. A.; Rodrigues, C. G.; Kiser, C. N.; Lew, A. Y. C.; Germanas, J. P.; Richards, J. H. *Proc. Natl. Acad. Sci. USA* **1991**, *88*, 1325-1329.

(7) Germanas, J. P.; Di Bilio, A. J.; Gray, H. B.; Richards, J. H. *Biochemistry* **1993**, *32*, 7698-7702.

(8) (a) den Blaauwen, T.; van de Kamp, M.; Canters, G. W. *J. Am. Chem. Soc.* **1991**, *113*, 5050-5052. (b) den Blaauwen, T.; Canters, G. W. *J. Am. Chem. Soc.* **1993**, *115*, 1121-1129.

(9) (a) Lu, Y.; Gralla, E. B.; Roe, J. A.; Valentine, J. S. *J. Am. Chem. Soc.* **1992**, *114*, 3560-3562. (b) Lu, Y.; LaCroix, L. B.; Lowery, M. D.; Solomon, E. I.; Bender, C. J.; Peisach, J.; Roe, J. A.; Gralla, E. B.; Valentine, J. S. *J. Am. Chem. Soc.* **1993**, *115*, 5907-5918.

(10) Parts of the work described in this chapter have been published: Mizoguchi, T. J.; Di Bilio, A. J.; Gray, H. B.; Richards, J. H. *J. Am. Chem. Soc.* **1992**, *114*, 10076-10078.

(11) Hill, H. A. O.; Page, D. J.; Walton, N. J. *J. Electroanal. Chem.* **1987**, *217*, 129-140.

(12) Adman, E. T.; Jensen, L. H. *Isr. J. Chem.* **1981**, *21*, 8-12.

(13) Rosen. P.; Pecht, I. *Biochemistry* **1976**, *15*, 775-786.

(14) Barshop, B. A.; Wrenn, R. F.; Frieden, C. *Anal. Biochem.* **1983**, *130*, 134-145.

(15) (a) Bernarducci, E.; Schwindinger, W. F.; Hughey, J. L.; Krogh-Jespersen, K.; Schugar, H. J. *J. Am. Chem. Soc.* **1981**, *103*, 1686-1691. (b) Knapp, S.; Keenan, T. P.; Zhang, X.; Fikar, R.; Potenza, J. A.; Schugar, H. J. *J. Am. Chem. Soc.* **1990**, *112*, 3452-3464.

(16) Solomon, E. I.; Hare, J. W.; Dooley, D. M.; Dawson, J. H.; Stephens, P. J.; Gray, H. B. *J. Am. Chem. Soc.* **1980**, *102*, 168-178.

(17) (a) Vänngård, T.; Malmström, B. G. *J. Mol. Biol.* **1960**, *2*, 118-124. (b) Malmström, B. G.; Reinhammar, B.; Vänngård, T. *Biochim. Biophys. Acta* **1968**, *156*, 67-76. (c) Malkin, R.; Malmström, B.G.; Vänngård, T. *FEBS Lett.* **1968**, *1*, 50-54. (d) Vänngård, T. In *Biological Applications of Electron Spin Resonance*, Swartz, H. M.; Bolton, J. R.; Borg, D. C., Eds.; Wiley: New York, 1972; pp 411-447. (e) Peisach, J.; Blumberg, W. E. *Arch. Biochem. Biophys.* **1974**, *165*, 691-708.

(18) Tamilarasan, R.; McMillan, D. R. *Inorg. Chem.* **1986**, *25*, 2037-2040.

(19) Shepard, W. E. B.; Anderson, B. F.; Lewandoski, D. A.; Norris, G. E.; Baker, E. N. *J. Am. Chem. Soc.* **1990**, *112*, 7817-7819.

(20) McCleskey, T. M.; Mizoguchi, T. J.; Richards, J. H.; Gray, H. B., submitted.

(21) Nar, H.; Messerschmidt, A.; Huber, R.; van de Kamp, M.; Canters, G. W. *J. Mol. Biol.* **1991**, *221*, 765-772.

(22) Hathaway, B. J. In *Comprehensive Coordination Chemistry*; Wilkinson, G.; Gillard, R. D.; McCleverty, J. A., Eds.; Pergamon: Oxford, 1987; Vol. 5, pp 533-774.

(23) For a discussion of metal binding to isolated carboxylate groups in proteins, see: Glusker, J. P. *Adv. Protein Chem.* **1991**, *42*, 1-76.

(24) Lippard, S. J.; Berg, J. M. *Principles of Bioinorganic Chemistry*; University Science Books: Mill Valley, 1994; Chapter 12, pp 359-360.

(25) For example, see: (a) Dhesi, R.; Cotton, T. M.; Timkovich, R. *J. Electroanal. Chem.* **1983**, *154*, 129-139. (b) Armstrong, F. A.; Hill, H. A. O.; Oliver, B. N.; Walton, N. J. *J. Am. Chem. Soc.* **1984**, *106*, 921-923.

(26) Tsai, L.-C.; Sjölin, L.; Langer, V.; Pascher, T.; Nar, H. *Acta Crystallogr., Sect. D* **1995**, *51*, 168-176.

(27) (a) Nar, H.; Messerschmidt, A.; Huber, R.; van de Kamp, M.; Canters, G. W. *J. Mol. Biol.* **1991**, *218*, 427-447. (b) Sjölin, L.; Tsai, L.-C.; Langer, V.; Pascher, T.; Karlsson, G.; Nordling, M.; Nar, H. *Acta Crystallogr., Sect. D* **1993**, *49*, 449-457. (c) Tsai, L.-C.; Sjölin, L.; Langer, V.; Bonander, N.; Karlsson, B. G.; Vänngård, T.; Hammann, C.; Nar, H. *Acta Crystallogr., Sect. D* **1995**, *51*, 711-717.

(28) (a) van de Kamp, M.; Silvestrini, M. C.; Brunori, M.; Van Beeumen, J.; Hali, F. C.; Canters, G. W. *Eur. J. Chem.* **1990**, *194*, 109-118. (b) Van Pouderoyen, G.; Mazumdar, S.; Hunt, N. I.; Hill, H. A. O.; Canters, G. W. *Eur. J. Biochem.* **1994**, *222*, 583-588.

(29) Mikkelsen, K. V.; Skov, L. K.; Nar, H.; Farver, O. *Proc. Natl. Acad. Sci. USA* **1993**, *90*, 5443-5445.

(30) Nar, H.; Huber, R.; Messerschmidt, A.; Filippou, A. C.; Barth, M.; Jaquinod, M.; van de Kamp, M.; Canters, G. W. *Eur. J. Biochem.* **1992**, *205*, 1123-1129.

(31) Moratal, J. M.; Romero, A.; Salgado, J.; Perales-Alarcón, A.; Jiménez, H. R. *Eur. J. Biochem.* **1995**, *228*, 653-657.

(32) Malmström, B. G. *Eur. J. Biochem.* **1994**, *223*, 711-718.

(33) Winkler, J. R.; Gray, H. B. *Chem. Rev.* **1992**, *92*, 369-379.

(34) (a) Langen, R.; Chang, I-J.; Germanas, J. P.; Richards, J. H.; Winkler, J. R.; Gray, H. B. *Science* **1995**, *268*, 1733-1735. (b) Regan, J. J.; Di Bilio, A. J.; Langen, R.; Skov, L. K.; Winkler, J. R.; Gray, H. B.; Onuchic, J. N. *Chem. Biol.* **1995**, *2*, 489-496.

(35) Chang, I-J.; Gray, H. B.; Winkler, J. R. *J. Am. Chem. Soc.* **1991**, *113*, 7056-7057.

(36) Marcus, R. A.; Sutin, N. *Biochim. Biophys. Acta* **1985**, *811*, 265-322.

(37) Groeneveld, C. M.; Canters, G. W. *Eur. J. Biochem.* **1985**, *153*, 559-564.

(38) (a) van de Kamp, M.; Floris, R.; Hali, F. C.; Canters, G. W. *J. Am. Chem. Soc.* **1990**, *112*, 907-908. (b)

(39) Romero, A.; Hoitink, C. W. G.; Nar, H.; Huber, R.; Messerschmidt, A.; Canters, G. W. *J. Mol. Biol.* **1993**, *229*, 1007-1021.

Table 3.1 Interatomic distances and angles involving the surface- and active-site-bound copper centers of the two non-symmetry-related Cu^{II} Cys112Asp *P. aeruginosa* azurin molecules that define an asymmetric unit (see Figure 3.11) (n/a = not applicable) The average values are also presented. H_2OA is defined as the water molecule with the shorter bond to the exogenous copper atom. $O^{\delta 1}$ of Asp112 is defined as the carboxylate oxygen with the shorter bond to the active-site copper center. Analogous values involving the active-site copper of WT *P. aeruginosa* azurin (pH 9.0)[21] are given for comparison.

Cu^{II} Azurin

	Cys112Asp (molecule A)	Cys112Asp (molecule B)	Cys112Asp (average)	WT (pH 9.0) (average)
1. Exogenous Cu				
Distances (Å)				
Cu–NH_2(Ala1)	2.1	2.1	2.1	n/a
Cu–O(Ala1)	2.6	2.6	2.6	n/a
Cu–N^{ε}(His83)	2.0	1.9	2.0	n/a
Cu–O(H_2OA)	2.4	2.5	2.5	n/a
Cu–O(H_2OB)	3.2	3.7	3.5	n/a
Angles (°)				
NH_2(Ala1)–Cu–O(Ala1)	83	77	86	n/a
NH_2(Ala1)–Cu–N^{ε}(His83)	108	100	104	n/a
NH_2(Ala1)–Cu–O(H_2OA)	141	127	134	n/a
NH_2(Ala1)–Cu–O(H_2OB)	149	161	155	n/a
O(Ala1)–Cu–N^{ε}(His83)	141	155	148	n/a
O(Ala1)–Cu–O(H_2OA)	70	74	72	n/a
O(Ala1)–Cu–O(H_2OB)	84	86	85	n/a
N^{ε}(His83)–Cu–O(H_2OA)	80	89	85	n/a
N^{ε}(His83)–Cu–O(H_2OB)	100	99	100	n/a
O(H_2OA)–Cu–O(H_2OB)	58	53	56	n/a
2. Active-Site Cu				
Distances (Å)				
Cu–S^{γ}(Cys112)	n/a	n/a	n/a	2.3
Cu–$O^{\delta 1}$(Asp112)	1.9	1.9	1.9	n/a
Cu–$O^{\delta 2}$(Asp112)	2.5	2.5	2.5	n/a
Cu–N^{δ}(His46)	2.0	2.0	2.0	2.1
Cu–N^{δ}(His117)	2.1	2.0	2.1	2.0
Cu–O(Gly45)	2.6	2.6	2.6	3.0
Cu–S^{δ}(Met121)	4.0	3.9	4.0	3.1

(Table 3.1, continued)

	Cys112Asp (molecule A)	Cys112Asp (molecule B)	Cys112Asp (average)	WT (pH 9.0) (average)
Angles (°)				
S^{γ}(Cys112)–Cu–N^{δ}(His46)	n/a	n/a	n/a	134
S^{γ}(Cys112)–Cu–N^{δ}(His117)	n/a	n/a	n/a	122
S^{γ}(Cys112)–Cu–O(Gly45)	n/a	n/a	n/a	98
S^{γ}(Cys112)–Cu–S^{δ}(Met121)	n/a	n/a	n/a	110
$O^{\delta 1}$(Asp112)–Cu–$O^{\delta 2}$(Asp112)	58	58	58	n/a
$O^{\delta 1}$(Asp112)–Cu–N^{δ}(His46)	109	86	98	n/a
$O^{\delta 1}$(Asp112)–Cu–N^{δ}(His117)	134	145	140	n/a
$O^{\delta 1}$(Asp112)–Cu–O(Gly45)	112	95	104	n/a
$O^{\delta 1}$(Asp112)–Cu–S^{δ}(Met121)	84	76	80	n/a
$O^{\delta 2}$(Asp112)–Cu–N^{δ}(His46)	166	144	155	n/a
$O^{\delta 2}$(Asp112)–Cu–N^{δ}(His117)	79	100	90	n/a
$O^{\delta 2}$(Asp112)–Cu–O(Gly45)	102	89	96	n/a
$O^{\delta 2}$(Asp112)–Cu–S^{δ}(Met121)	93	96	95	n/a
N^{δ}(His46)–Cu–N^{δ}(His117)	111	113	112	103
N^{δ}(His46)–Cu–O(Gly45)	87	91	89	77
N^{δ}(His46)–Cu–S^{δ}(Met121)	80	77	79	74
N^{δ}(His117)–Cu–O(Gly45)	91	113	102	88
N^{δ}(His117)–Cu–S^{δ}(Met121)	82	80	81	88
O(Gly45)–Cu–S^{δ}(Met121)	162	165	164	149

Figure 3.1 "Cut-and-paste" construction of the pET-3a (His83Gln/Cys112Asp/ Lys122His) plasmid (□ denotes a WT codon; ■ denotes a mutant codon). First, the His83Gln/Cys112Asp double mutant was made by replacing the *Bam*H I/*Eco*R I fragment of pET-3a (His83Gln/Lys122His) containing the position 112 and 122 codons with the analogous fragment from pET-9a (Cys112Asp) (**A**). Subsequently, the *Xma* I/*Eco*R I fragment containing the position 122 codon of the resultant pET-3a (His83Gln/ Cys112Asp) plasmid was substituted by the analogous fragment from pET-3a (His83Gln/ Lys122His) (**B**).

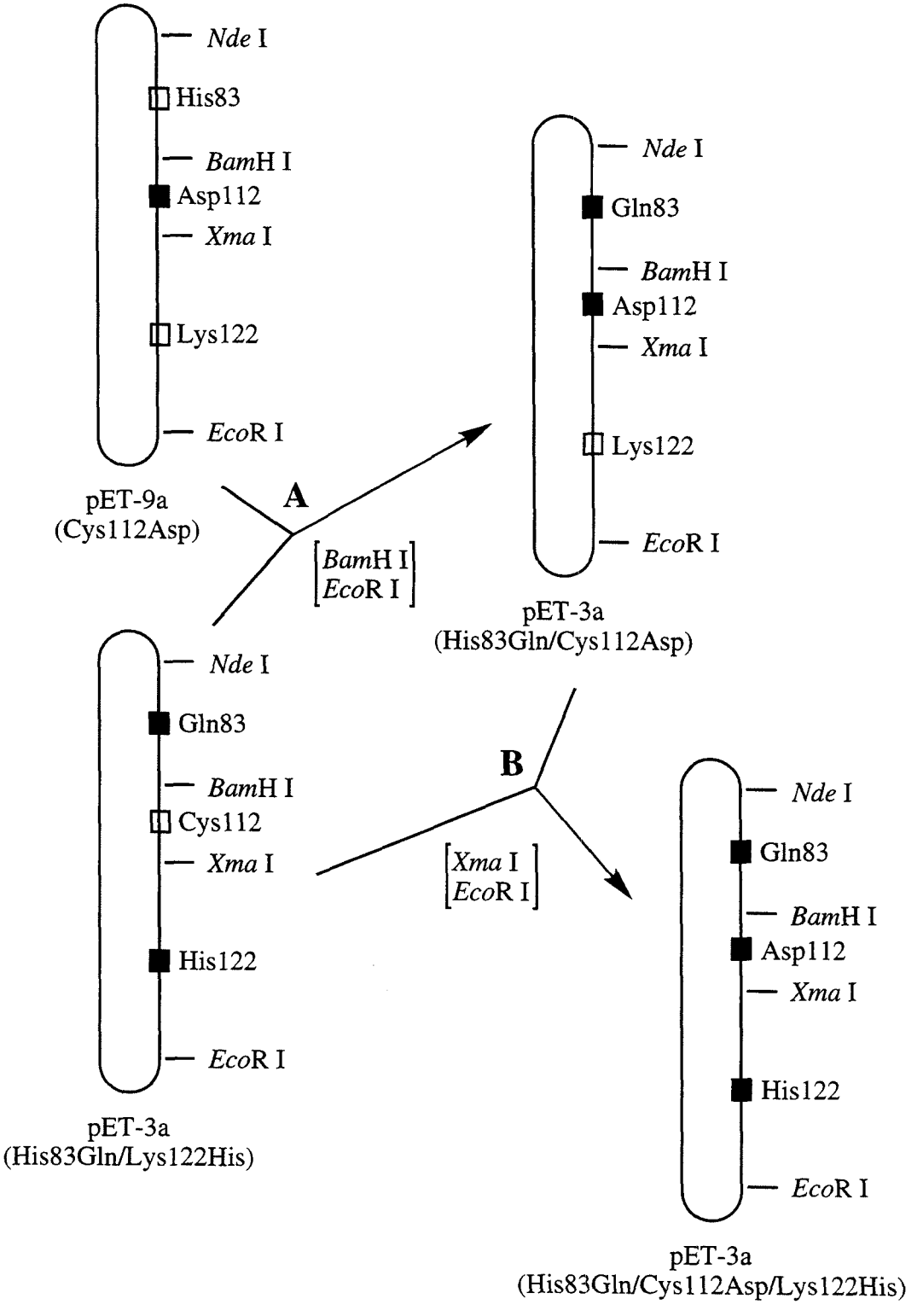
Nde I
His83
BamH I
Asp112
Xma I
Lys122
EcoR I
pET-9a
(Cys112Asp)
A
BamH I
EcoR I
Nde I
Gln83
BamH I
Asp112
Xma I
Lys122
EcoR I
pET-3a
(His83Gln/Cys112Asp)
Nde I
Gln83
BamH I
Cys112
Xma I
His122
EcoR I
pET-3a
(His83Gln/Lys122His)
B
Xma I
EcoR I
Nde I
Gln83
BamH I
Asp112
Xma I
His122
EcoR I
pET-3a
(His83Gln/Cys112Asp/Lys122His)

Figure 3.2 Absorption changes accompanied by the titration of apo Cys112Asp *P. aeruginosa* azurin with Cu^{II} in the near-UV (**A**) and the visible/near-IR (**B**).

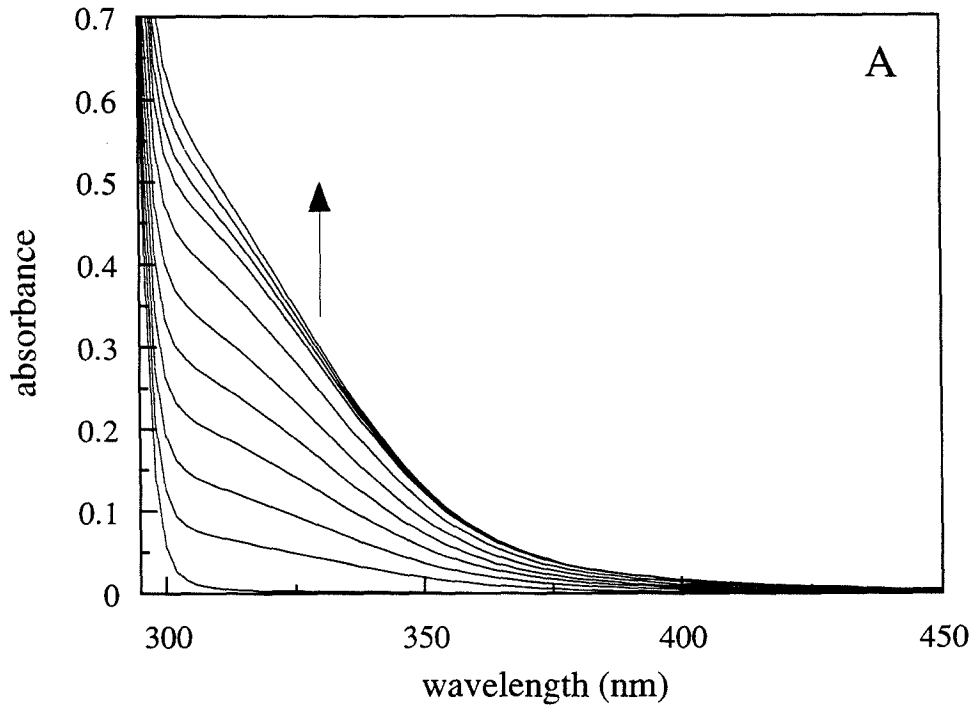
A
absorbance
0.7
0.6
0.5
0.4
0.3
0.2
0.1
0
300
350
400
450
wavelength (nm)

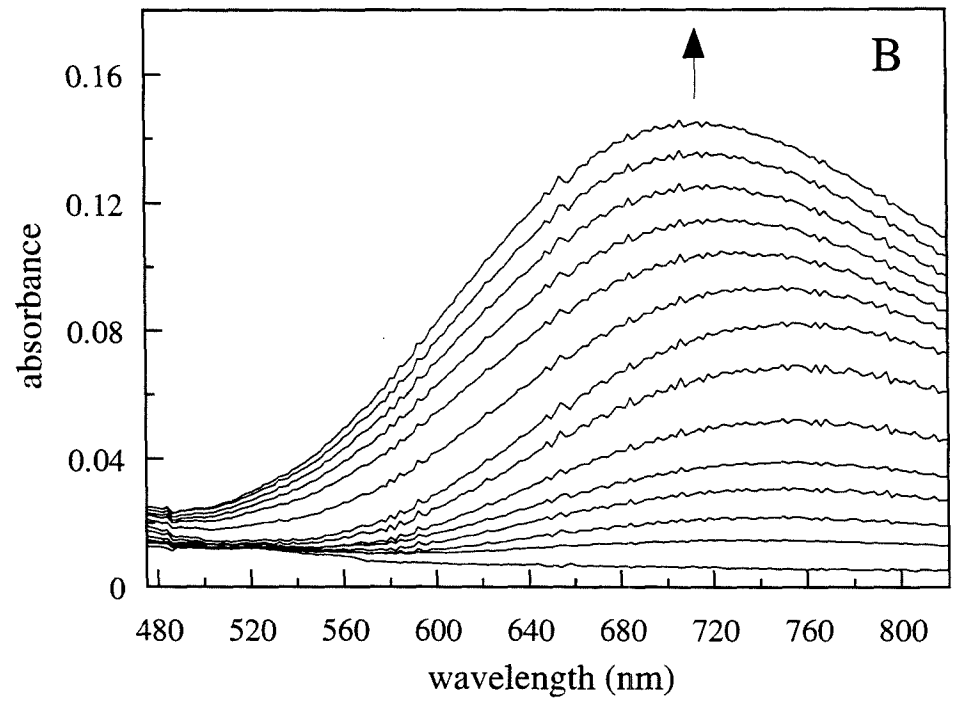
B
absorbance
0.16
0.12
0.08
0.04
0
480
520
560
600
640
680
720
760
800
wavelength (nm)

Figure 3.3 Titration plots derived from the data from Figure 3.2 with accompanying fits to two lines: λ_{obs} = 310 nm (**A**), and λ_{obs} = 754 nm (**B**). The coordinates of the intersection points are noted. (The abscissae of the two intersection points do not coincide as the data from 310 and 754 nm are from separate experiments.)

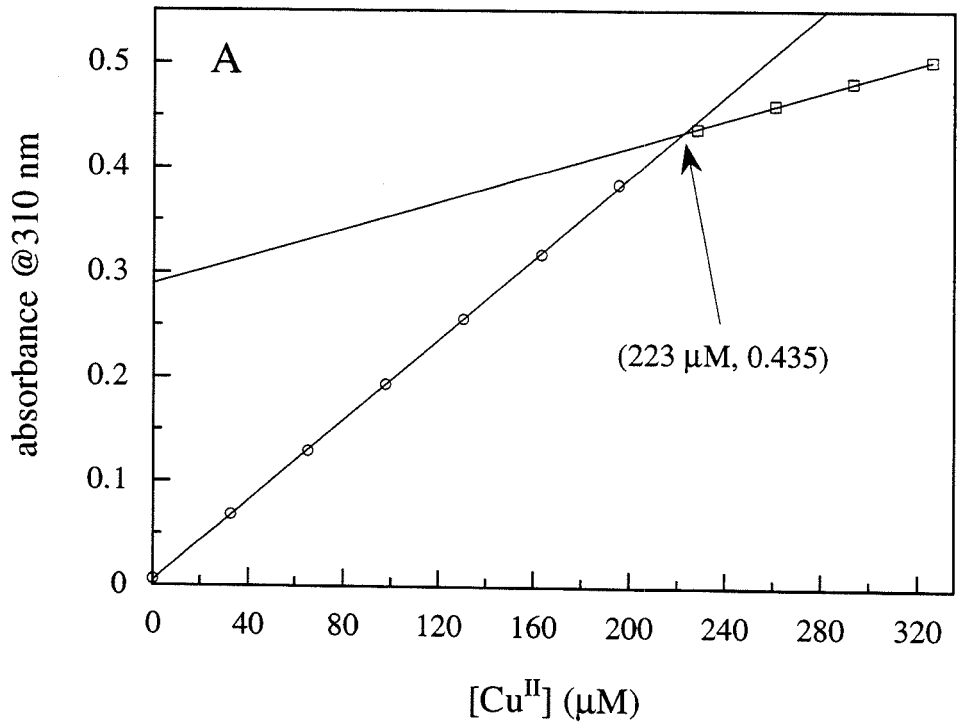
A
absorbance @310 nm
0.5
0.4
0.3
0.2
0.1
0
0
40
80
120
160
200
240
280
320
(223 μM, 0.435)
[Cu^II] (μM)

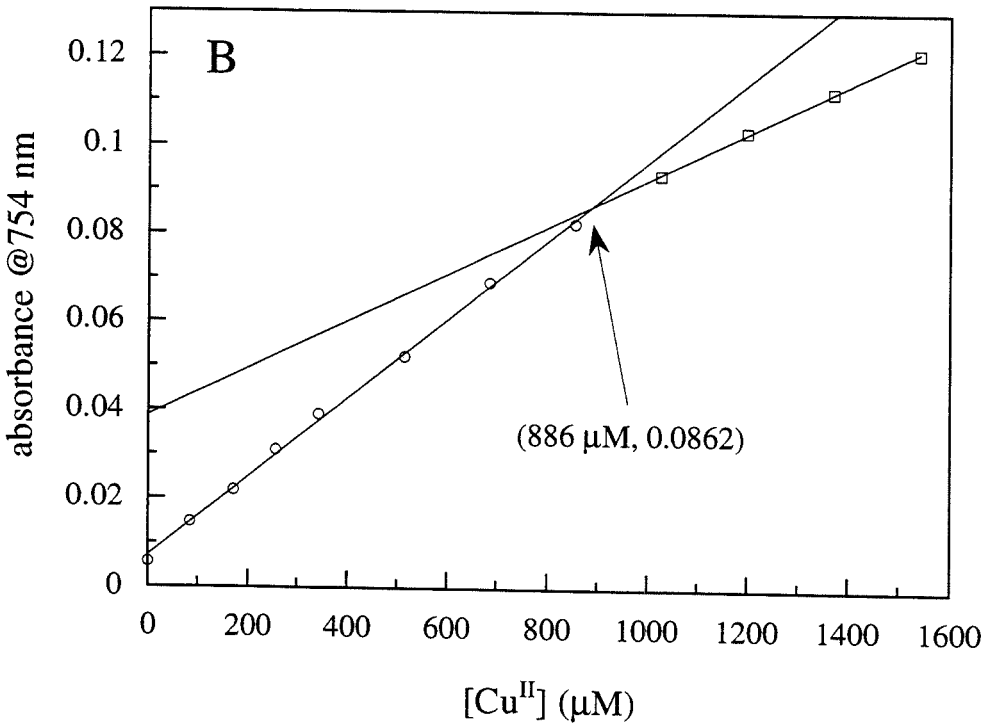
B
absorbance @754 nm
0.12
0.1
0.08
0.06
0.04
0.02
0
0
200
400
600
800
1000
1200
1400
1600
(886 μM, 0.0862)
[Cu^II] (μM)

Figure 3.4 FPLC chromatogram (solid trace) from the purification of Cu^{II}-reconstituted Cys112Asp *P. aeruginosa* azurin (buffer: 10 mM DEA·HCl (pH 8.8); column: Mono Q HR 10/10; flow rate: 1 mL/min; chart speed: 0.25 cm/mL; gradient held at 22% B after 15 min). The dashed trace represents the percentage of Buffer B (starting at 0% and increasing to a maximum of 100%) of the eluant. Peak A corresponds to Cu^{II} Cys112Asp azurin, while Peak B to the Cu^{II} EDTA complex.

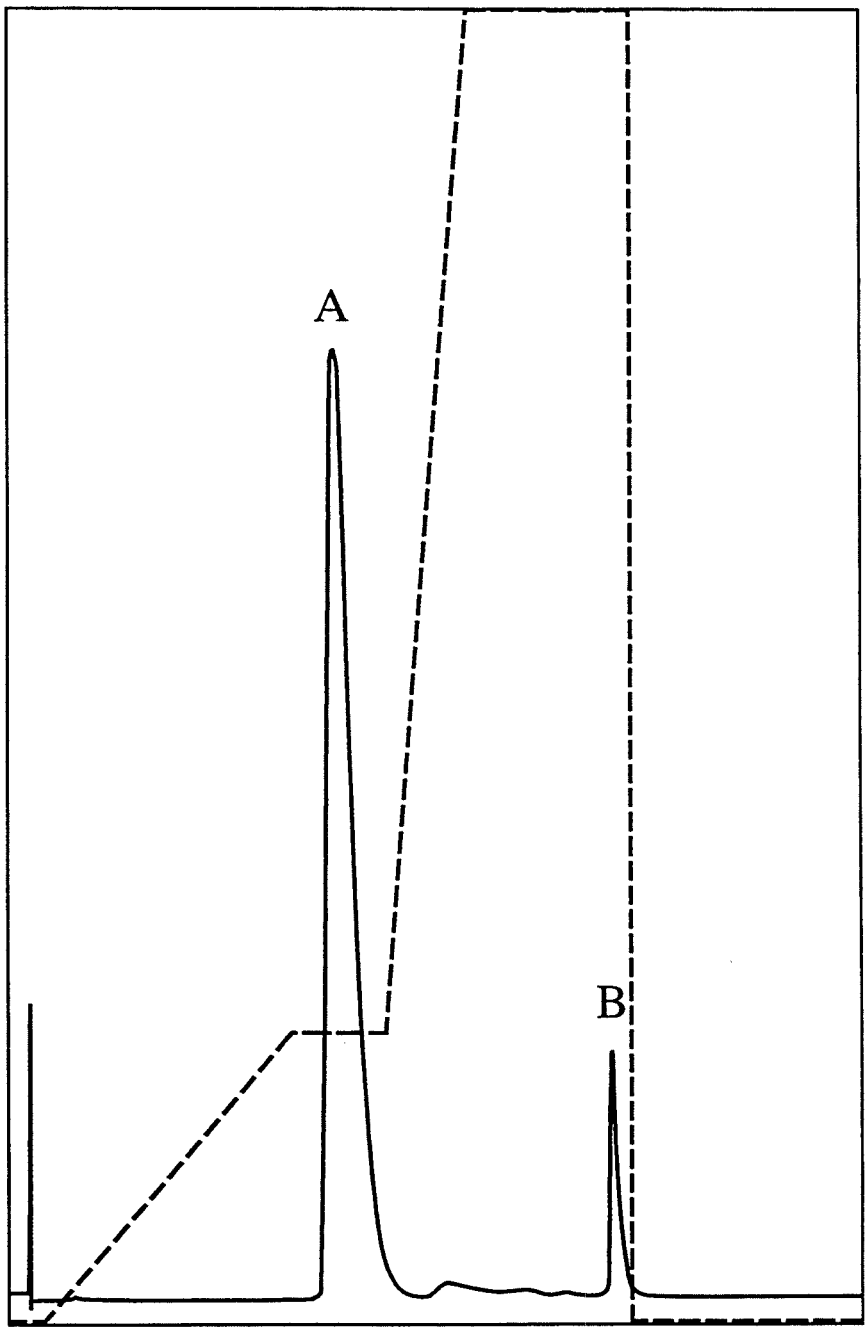
A
B

Figure 3.5 Electronic absorption spectra of Cu^{II} Cys112Asp *P. aeruginosa* azurin in 10 mM DEA·HCl/~40 mM NaCl (pH 8.8) (**A**) and Cu^{I} Cys112Asp azurin in $\mu = 0.1$ M sodium phosphate (pH 7.0) (**B**) at room temperature.

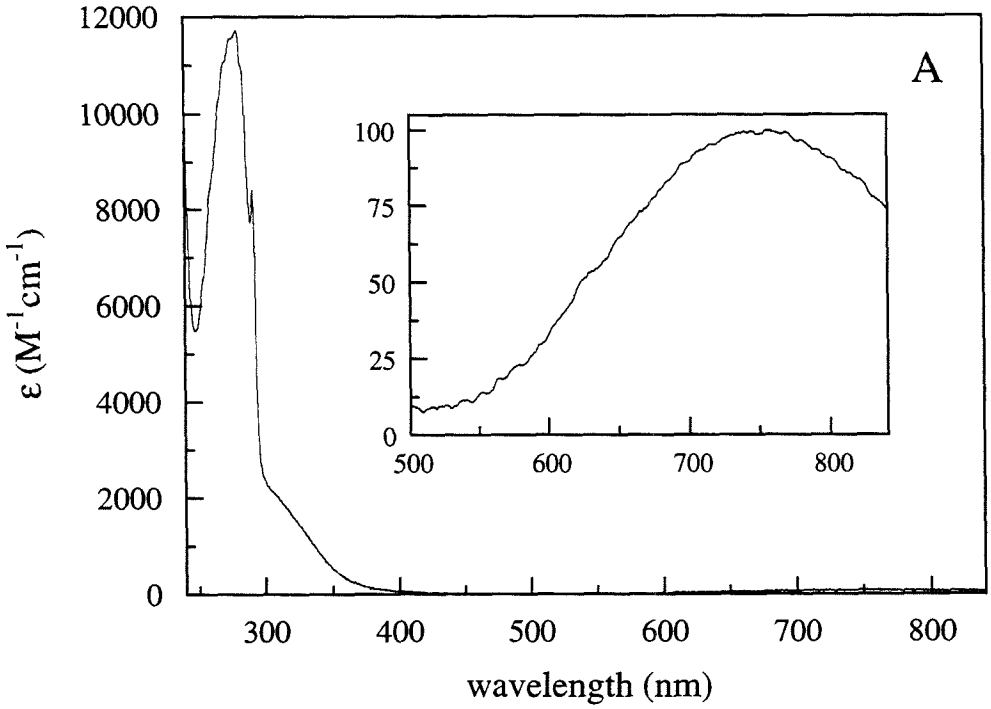
A
12000
10000
8000
6000
4000
2000
0
ε (M-1cm-1)
300
400
500
600
700
800
wavelength (nm)
100
75
50
25
0
500
600
700
800

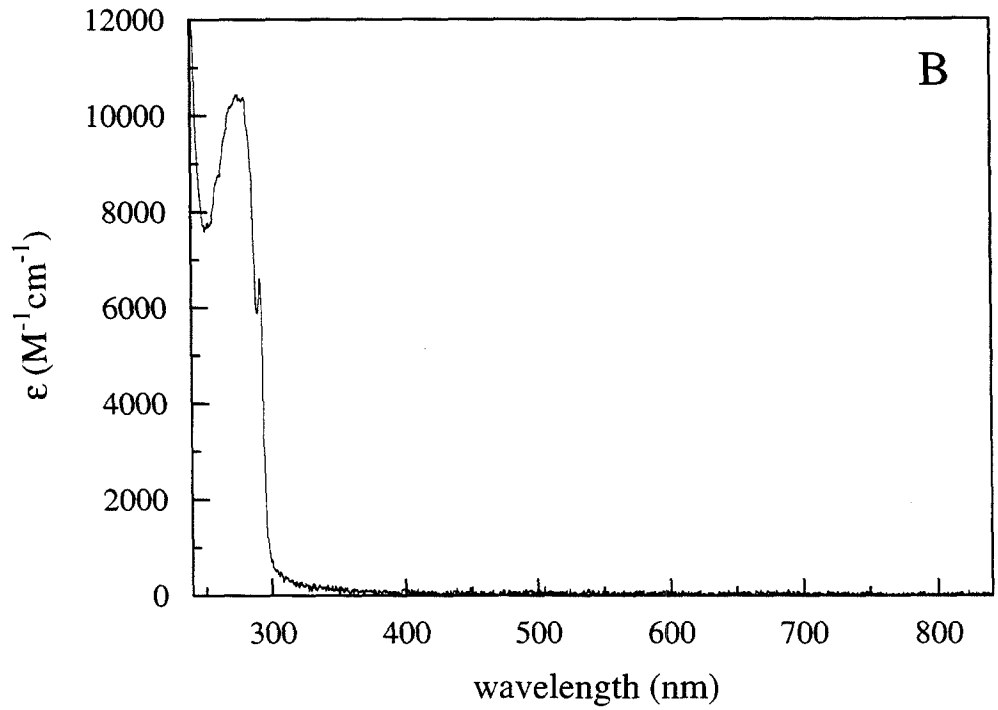
B
12000
10000
8000
6000
4000
2000
0
ε (M-1cm-1)
300
400
500
600
700
800
wavelength (nm)

Figure 3.6 X-band (9.506 GHz) EPR spectrum of a frozen solution of $^{63}Cu^{II}$ Cys112Asp *P. aeruginosa* azurin in 10 mM DEA·HCl buffer (pH 9.0)-glycerol mixture (1:1) at 85 K. The spin-Hamiltonian parameters are: $g_{\|} = 2.315(1)$, $A_{\|} = 152(1) \times 10^{-4}$ cm^{-1}; $g_{\perp} = 2.075(5)$, $A_{\perp} = 10(2) \times 10^{-4}$ cm^{-1}; $A_{\|}^{N} = 10(2) \times 10^{-4}$ cm^{-1}, $A_{\perp}^{N} = 10(1) \times 10^{-4}$ cm^{-1}.

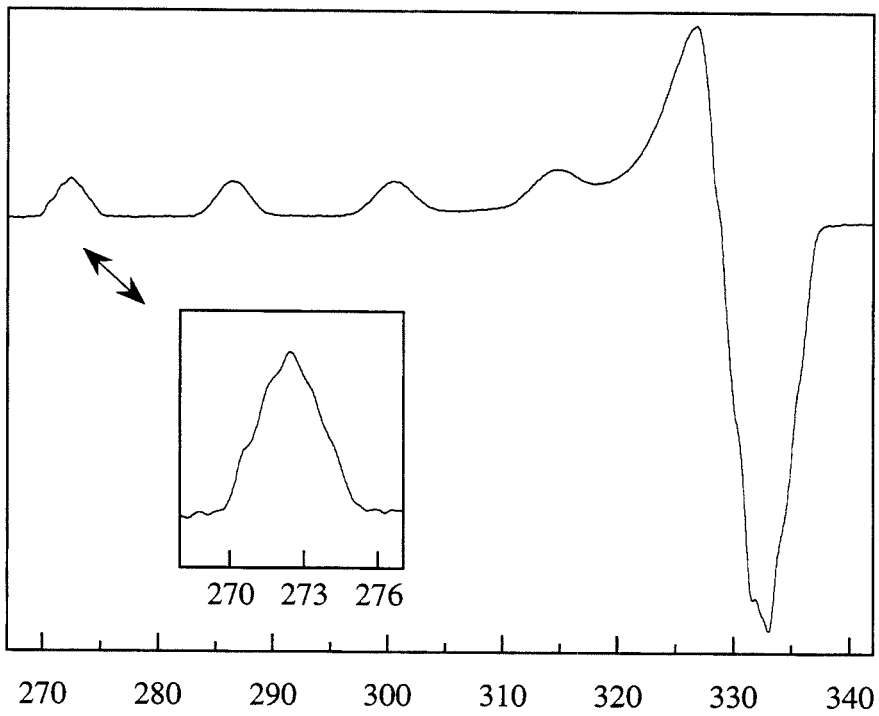
270 273 276
270 280 290 300 310 320 330 340
H (mT)

Figure 3.7 FPLC chromatogram (solid trace) from the purification of Sigma-brand *P. aeruginosa* cytochrome c_{551} (buffer: 10 mM DEA·HCl (pH 8.8); column: Mono Q HR 10/10; flow rate: 1 mL/min; chart speed: 0.25 cm/mL; gradient held at 25% B after 20 min). The dashed trace represents the percentage of Buffer B (starting at 0% and increasing to a maximum of 100%) of the eluant. Protein from Peak B was used in the redox titration experiment.

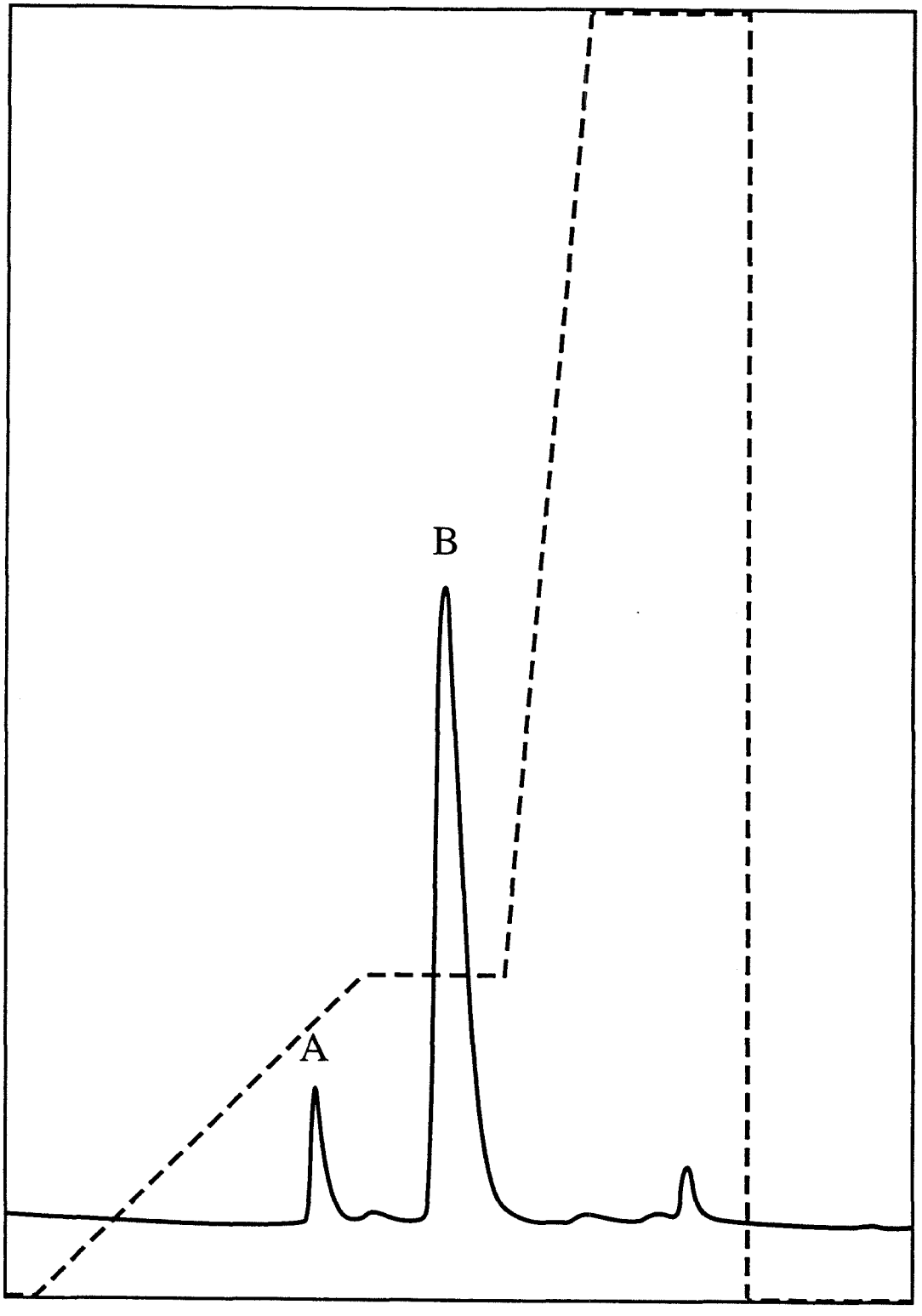
B
A

Figure 3.8 Cyclic voltammogram of Fe^{III} cytochrome c_{551} from *P. aeruginosa* (~0.6 mM) in μ = 0.1 M sodium phosphate (pH 7.0) at room temperature (scan rate = 10 mV/s, $E_{1/2}$ = 14 mV *vs.* SCE (or 255 mV *vs.* NHE)).

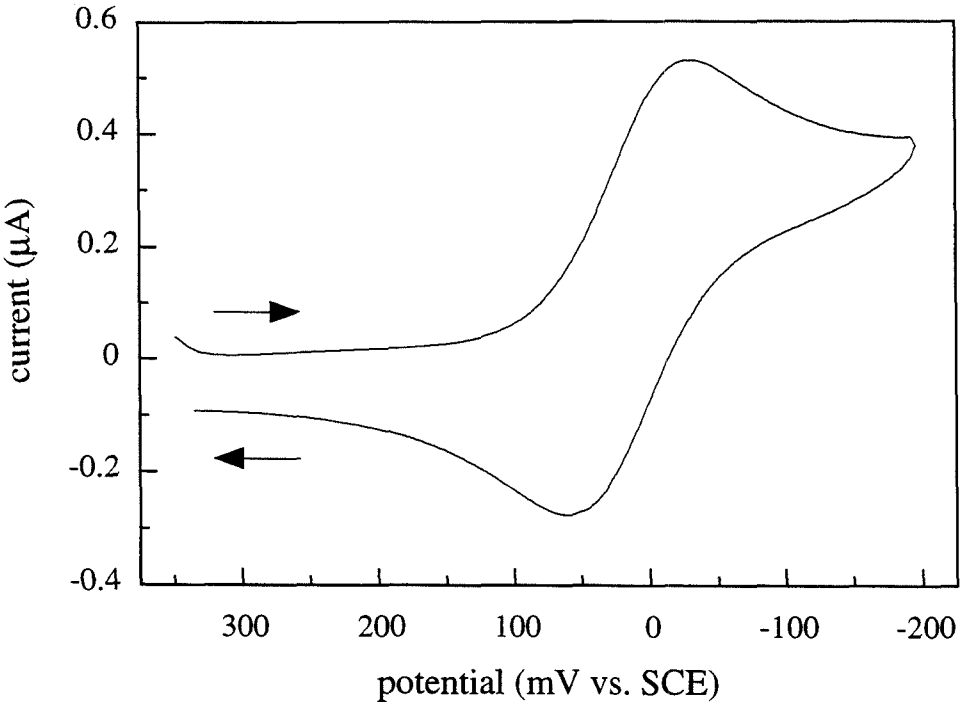
0.6
0.4
0.2
0
-0.2
-0.4
current (μA)
300
200
100
0
-100
-200
potential (mV vs. SCE)

Figure 3.9 Overlay of visible absorption spectra from the titration of Fe^{II} cytochrome c_{551} with Cu^{II} Cys112Asp azurin, both from *P. aeruginosa*. Spectra were not corrected for changes in volume. The numbers in the figure legend represent the volume (μL) of Cu^{II} Cys112Asp azurin added to the solution.

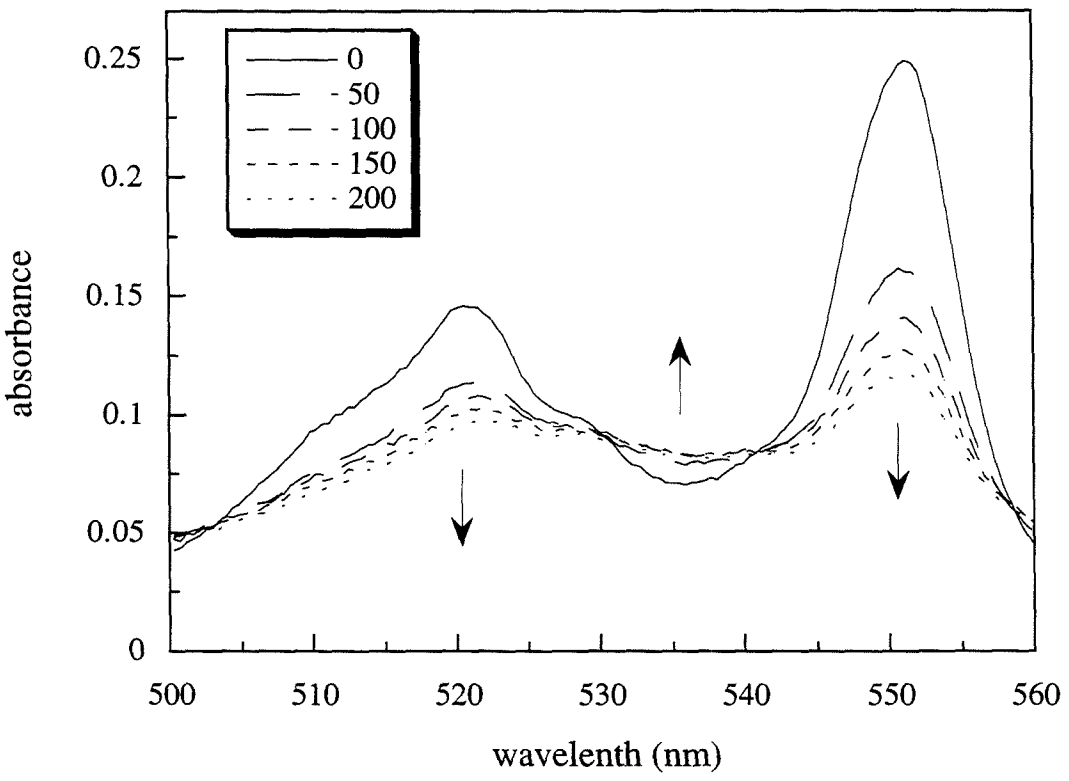
0
50
100
150
200
absorbance
0.25
0.2
0.15
0.1
0.05
0
500
510
520
530
540
550
560
wavelenth (nm)

Figure 3.10 (**A**) Titration plot derived from the data from Figure 3.9 with accompanying fit to eq 3.1. (**B**) Simulated titration plots using eq 3.1 with K_{eq} defined as either 0.04 or 0.06. The experimental points are included for reference.

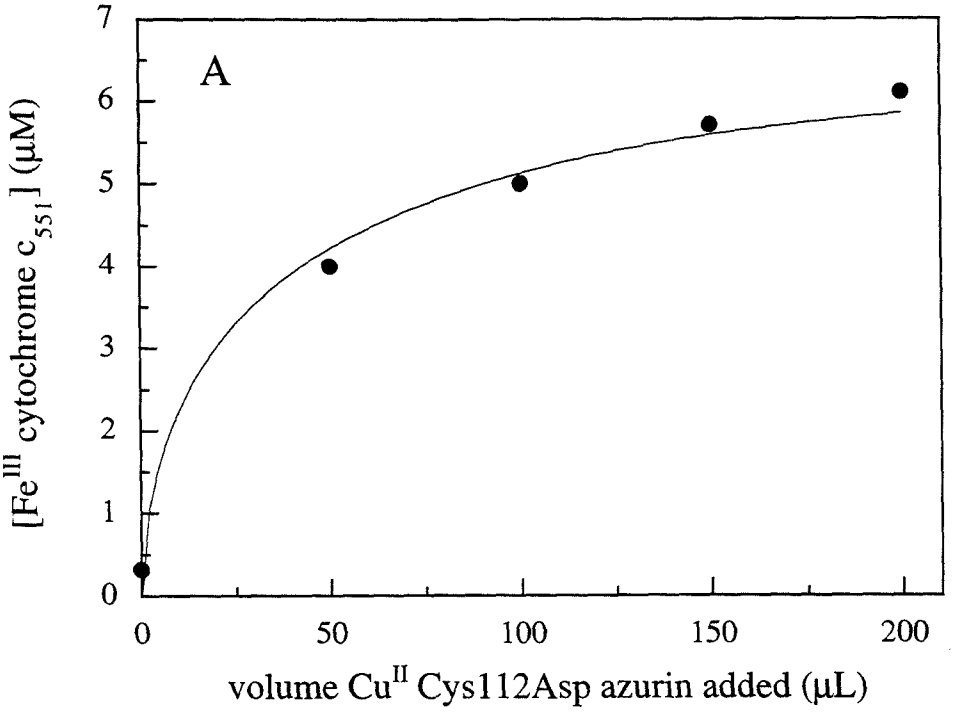
A
[Fe^III cytochrome c551] (μM)
volume Cu^II Cys112Asp azurin added (μL)
0
1
2
3
4
5
6
7
0
50
100
150
200

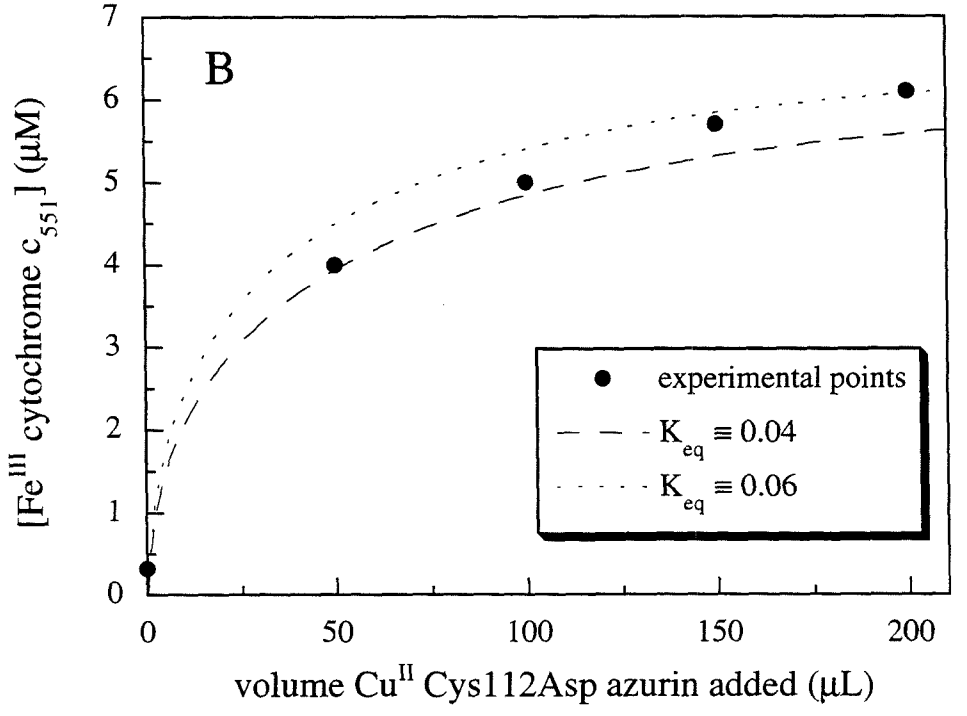
B
[Fe^III cytochrome c551] (μM)
volume Cu^II Cys112Asp azurin added (μL)
experimental points
K_eq ≡ 0.04
K_eq ≡ 0.06
0
1
2
3
4
5
6
7
0
50
100
150
200

Figure 3.11 Main chain trace of the Cu^{II} Cys112Asp *P. aeruginosa* azurin dimer that constitutes an asymmetric unit. The side chains of the residues (Met13, Leu39, Pro40, Val43, Met44, Phe114, Pro115, Ala119, Leu120) that define the hydrophobic patch[26] are also shown.

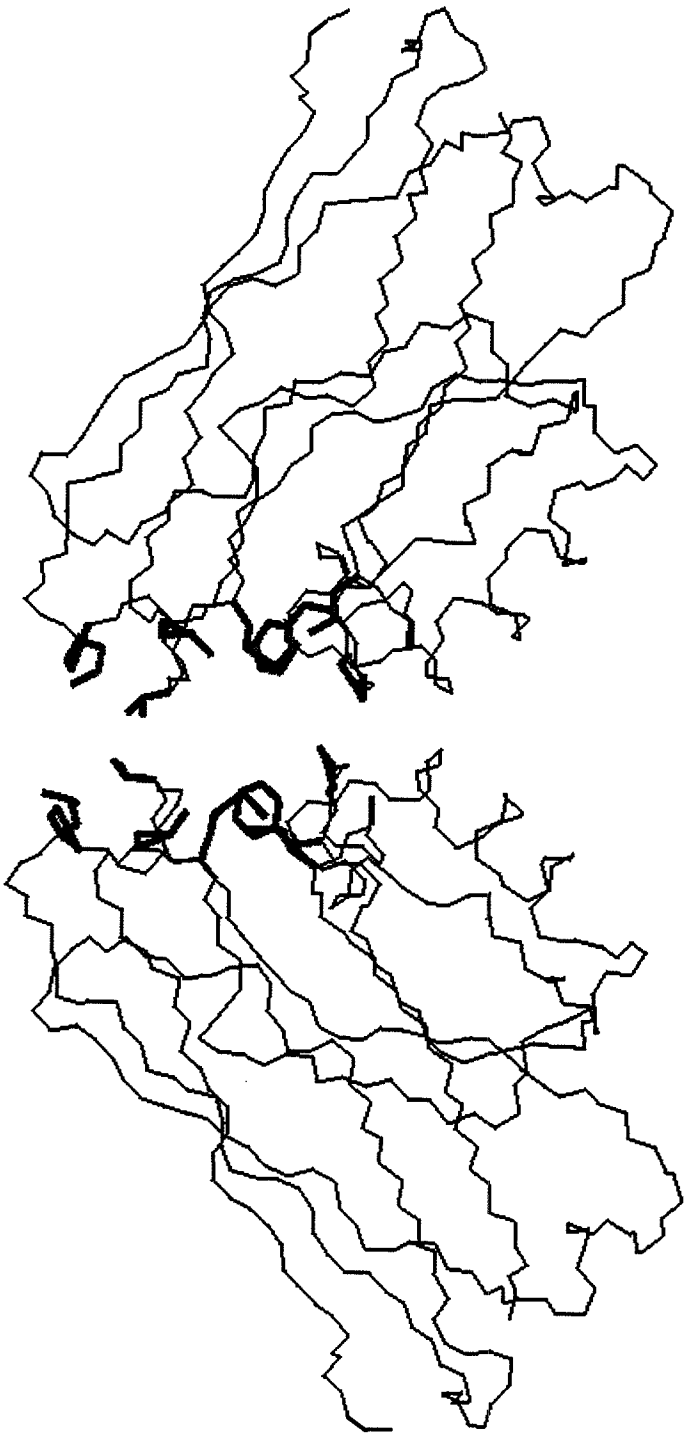

Figure 3.12 Coordination structure of the surface-bound Cu^{II} ion of Cys112Asp *P. aeruginosa* azurin (molecule A). Interatomic distances and angles are given in Table 3.1.

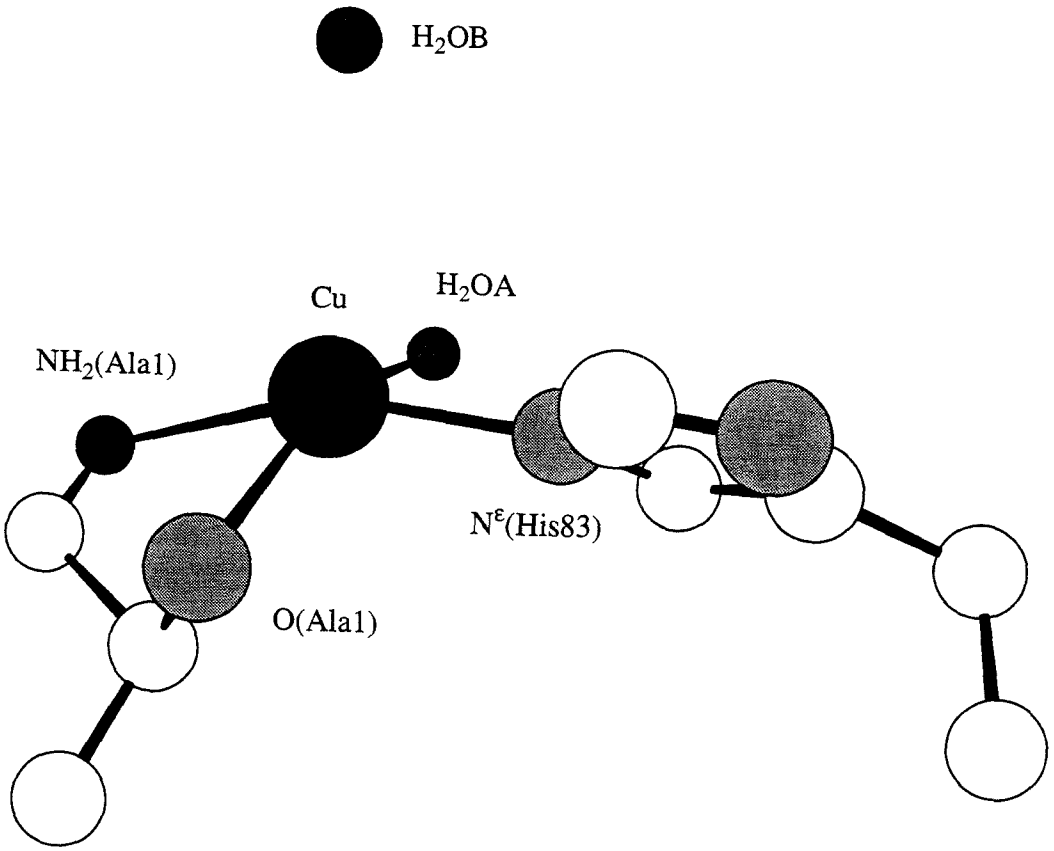
H_2OB
Cu
H_2OA
NH_2(Ala1)
N^{ε}(His83)
O(Ala1)

Figure 3.13 Overlay of the main chain traces of Cu^{II} Cys112Asp (molecule A) and of Cu^{II} WT (pH 9.0, molecule A (ref 21)) *P. aeruginosa* azurins. The two main chain structures exhibit an rms deviation overlap of 0.9 Å; the value decreases to 0.5 Å if the first two residues are ignored.

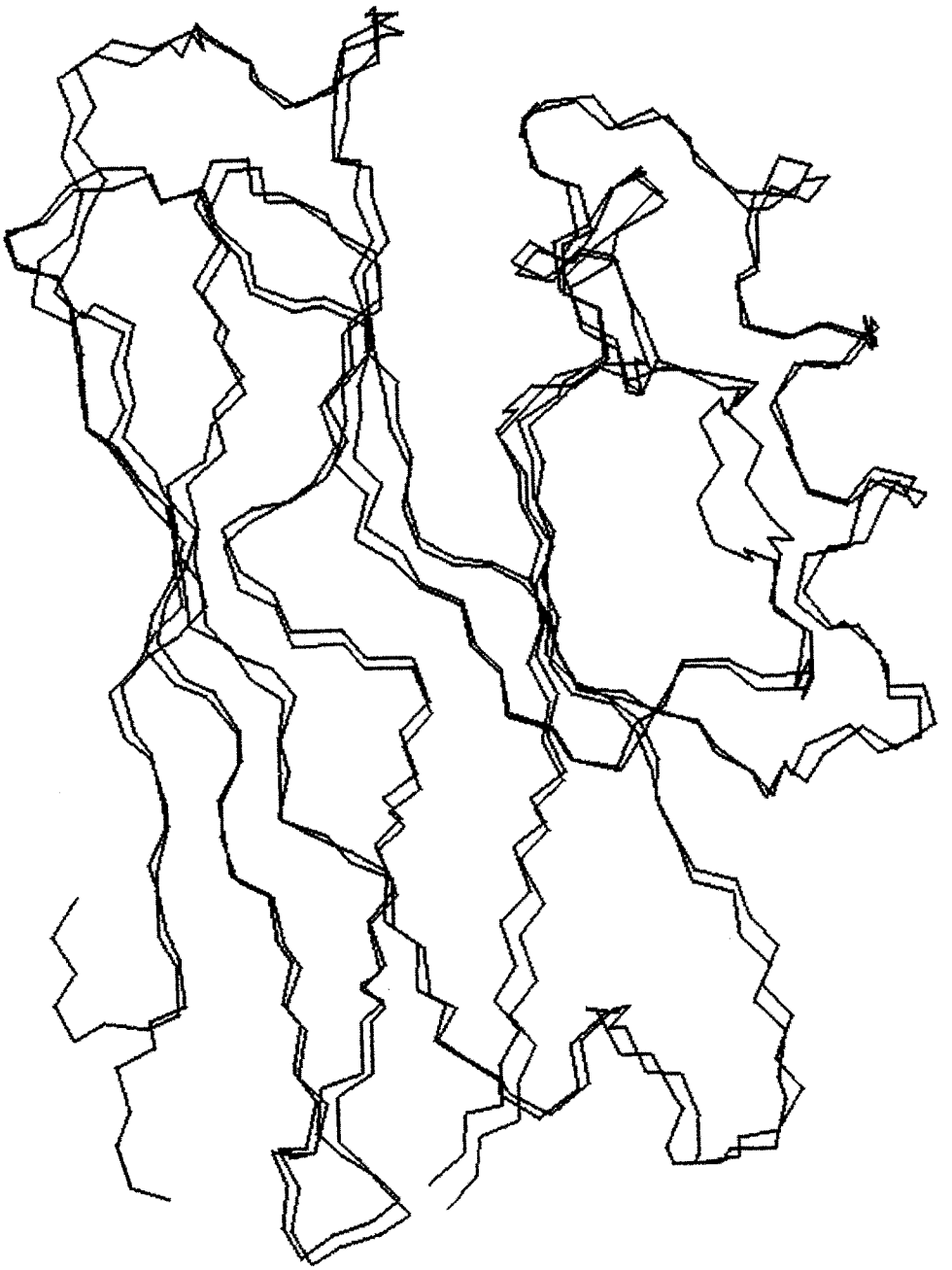

Figure 3.14 Coordination structure of the active-site Cu^{II} ion of Cys112Asp *P. aeruginosa* azurin (molecule A). Interatomic distances and angles are given in Table 3.1.

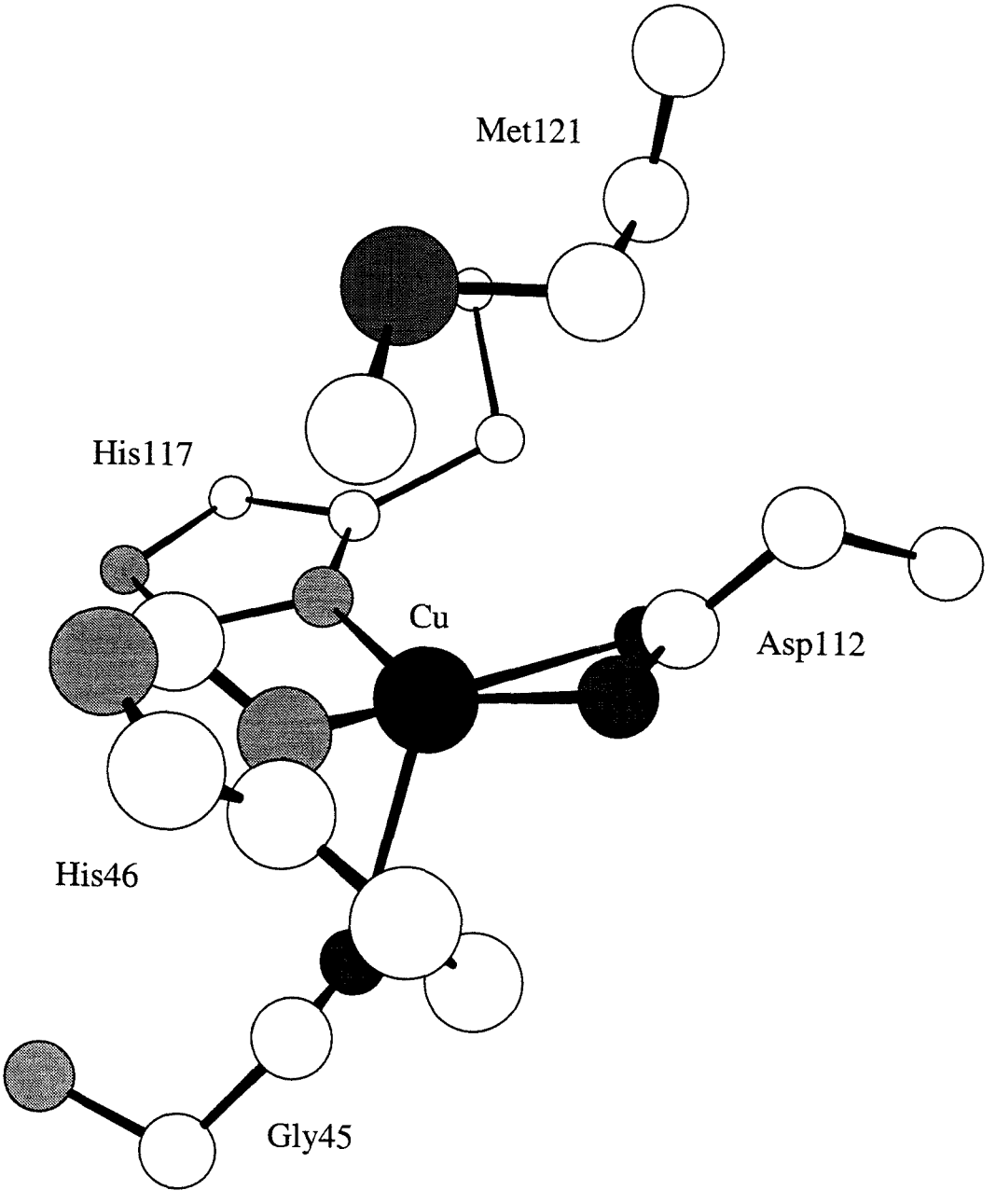
Met121
His117
Cu
Asp112
His46
Gly45

Figure 3.15 Top (**A**) and side (**B**) views of the Asp112 carboxylate group along with the active-site Cu^{II} center of Cys112Asp *P. aeruginosa* azurin (molecule A). The extent to which the metal is displaced from the plane of the carboxylate group can also be gauged by the angle defined by C^{β}(Asp112)-C^{γ}(Asp112)-Cu, which is 148 and 153° for molecules A and B, respectively.

A

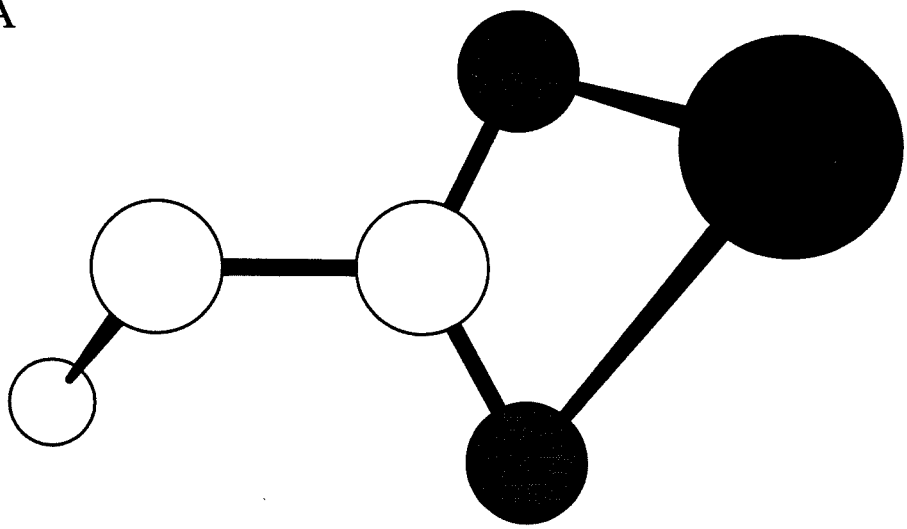

B

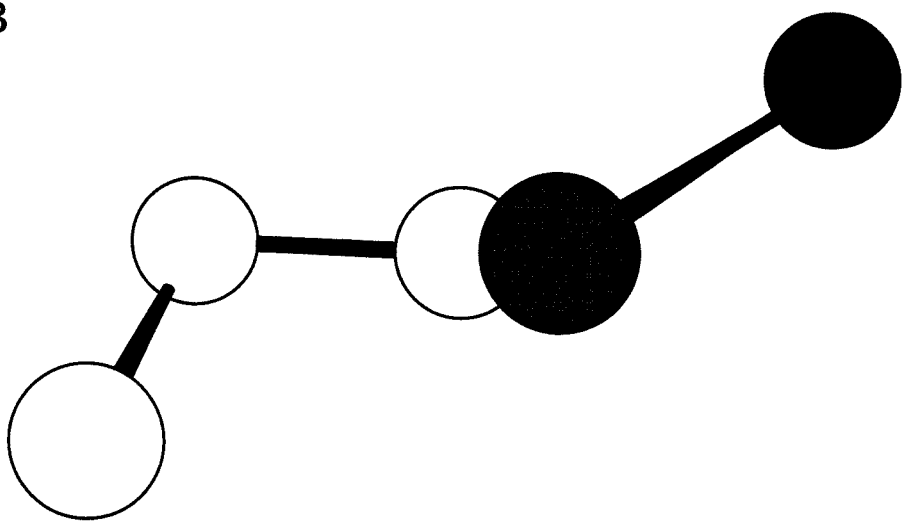

Figure 3.16 Overlay of the active-site Cu^{II} coordination structures of Cys112Asp and WT (pH 9.0, molecule A (ref 21)) *P. aeruginosa* azurins. The atomic coordinates were determined from an overlay of the main chain traces (excluding Ala1 and Glu2).

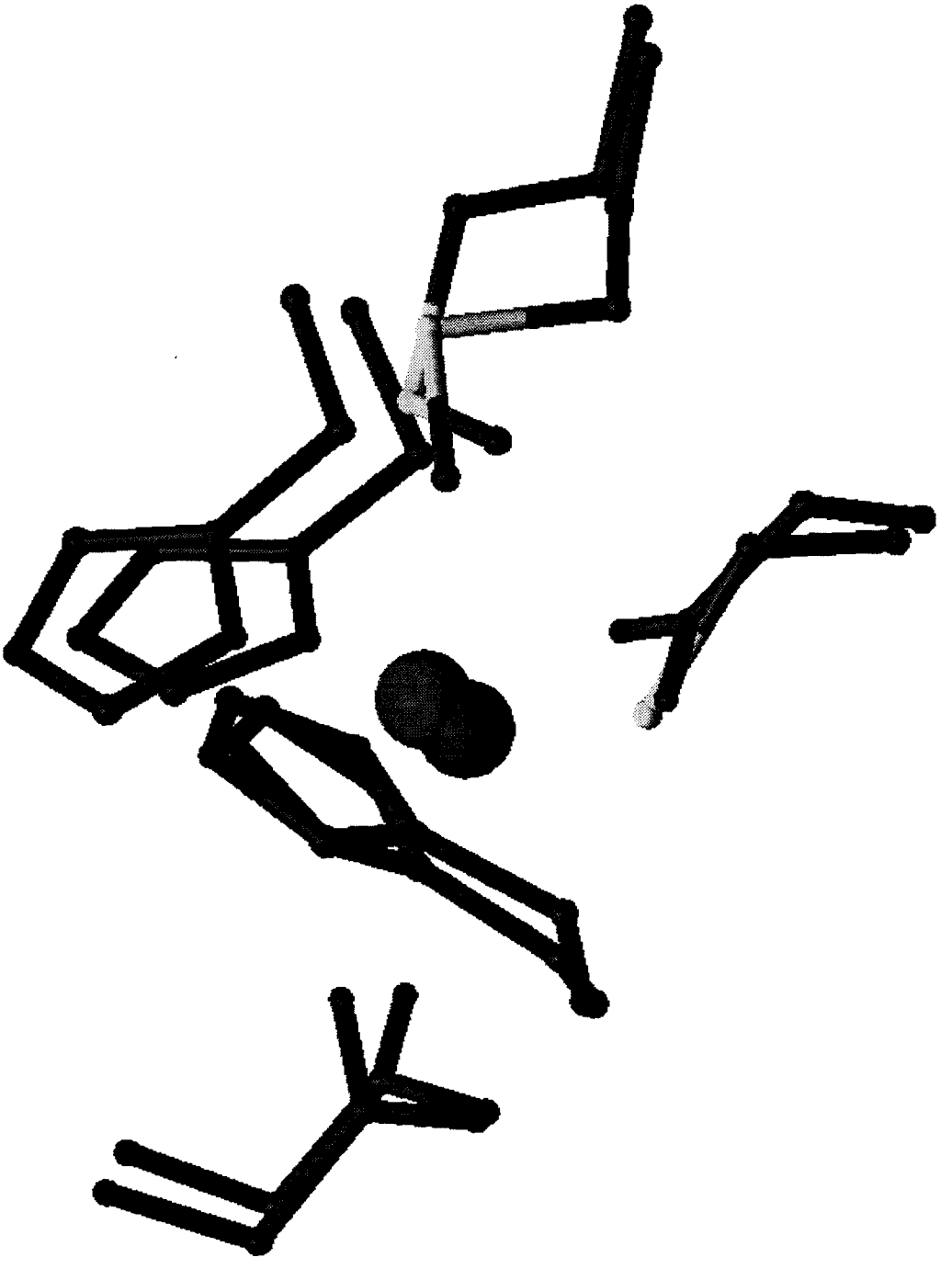

Figure 3.17 Photoinduced (**A**) and flash-quench (**B**) schema for intramolecular electron-transfer reactions involving ruthenium-labeled azurins. Q denotes an exogenously added quencher molecule.

A

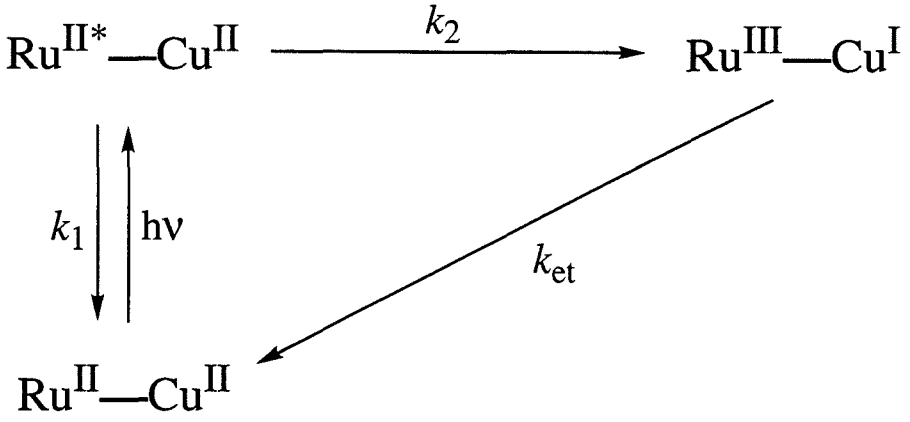
Ru^II*—Cu^II
k2
Ru^III—Cu^I
k1
hν
ket
Ru^II—Cu^II

B

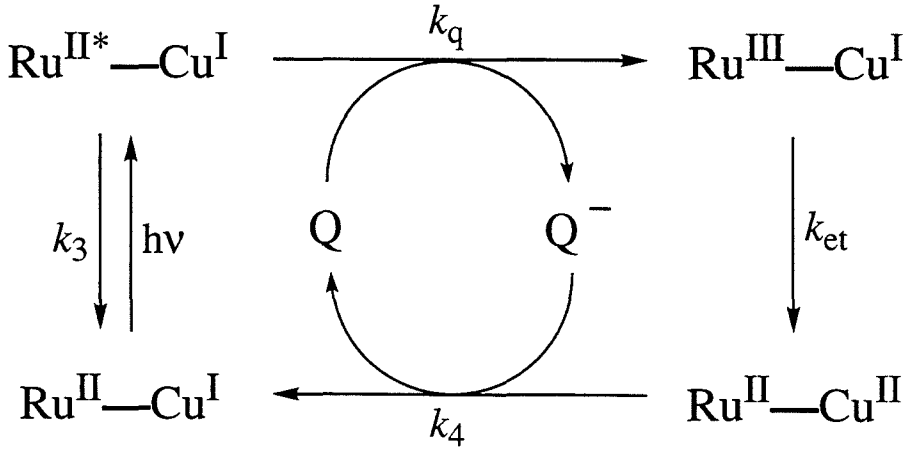
Ru^II*—Cu^I
kq
Ru^III—Cu^I
k3
hν
Q
Q^−
ket
Ru^II—Cu^I
k4
Ru^II—Cu^II

Figure 3.18 Transient absorption trace at 500 nm from a flash-quench experiment using the His83Gln/Cys112Asp/ Lys122His azurin system. The initial negative change in absorbance signifies the "instantaneous" formation of Ru^{III}. The subsequent decay back to zero corresponds to reduction of the Ru^{III} label over time. The data has been fit to a single exponential function (dark line), yielding an apparent first-order rate constant of 5.6 x 10^3 s^{-1}.

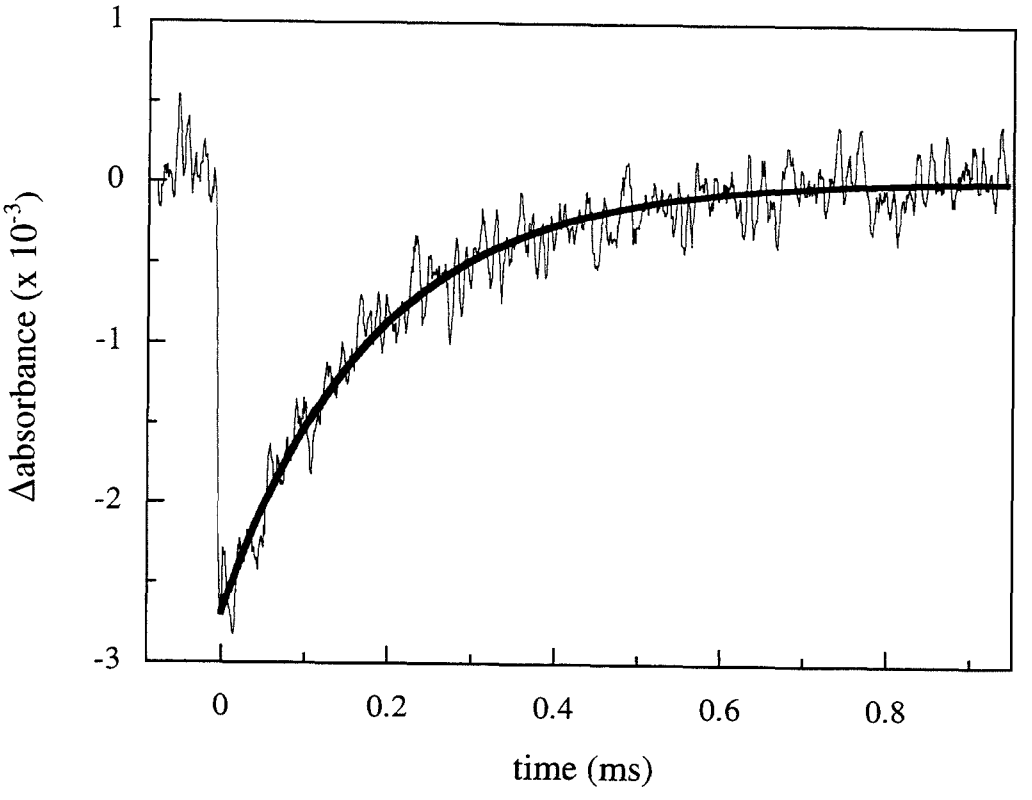
1
0
-1
-2
-3
Δabsorbance (x 10-3)
0
0.2
0.4
0.6
0.8
time (ms)

Figure 3.19 Transient absorption traces (average of 4 runs; 100 data points per run) at 628 (**A**) and 310 (**B**) nm from the reaction between Cu^{II} WT (9.6 μM) and Cu^{I} Cys112Asp (15 μM) *P. aeruginosa* azurins. The recorded absorbance is referenced against the absorbance of the solution after completion of the reaction.

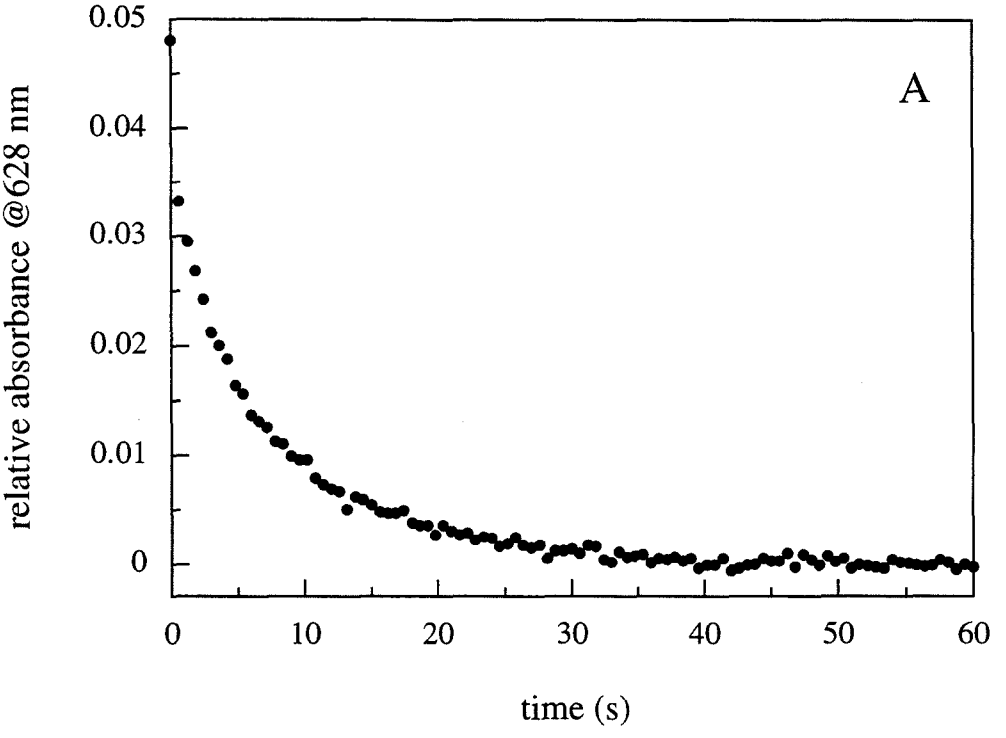
0.05
0.04
0.03
0.02
0.01
0
relative absorbance @628 nm
A
0
10
20
30
40
50
60
time (s)

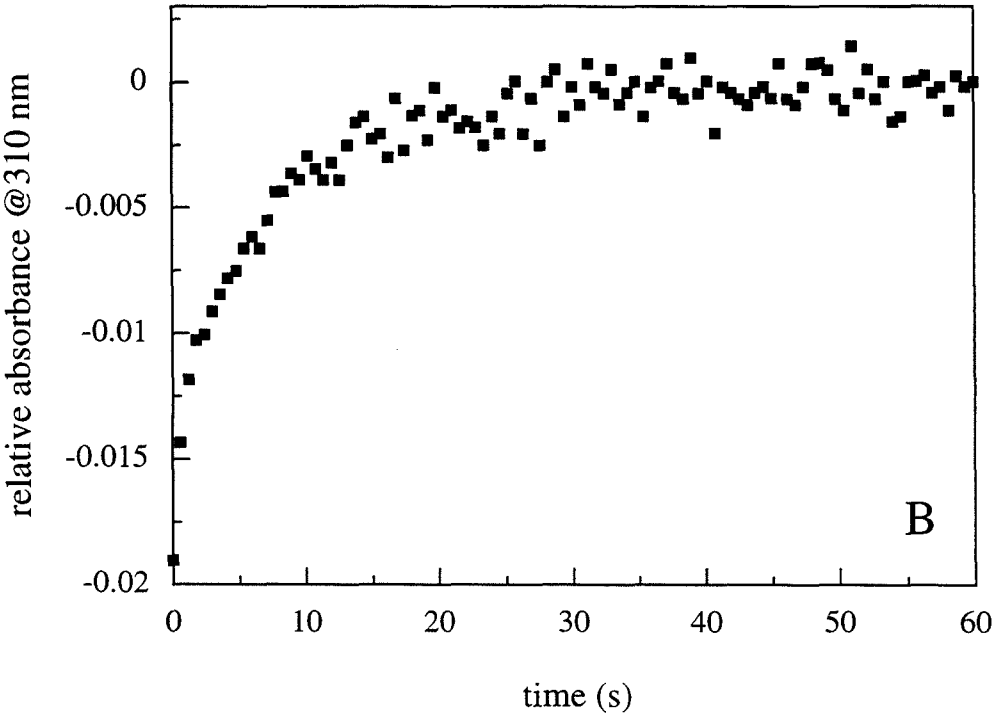
0
-0.005
-0.01
-0.015
-0.02
relative absorbance @310 nm
B
0
10
20
30
40
50
60
time (s)

Figure 3.20 Manual overlay of the transient absorption traces at 628 and 310 nm from Figure 3.19. The 628-nm data was scaled and offset accordingly.

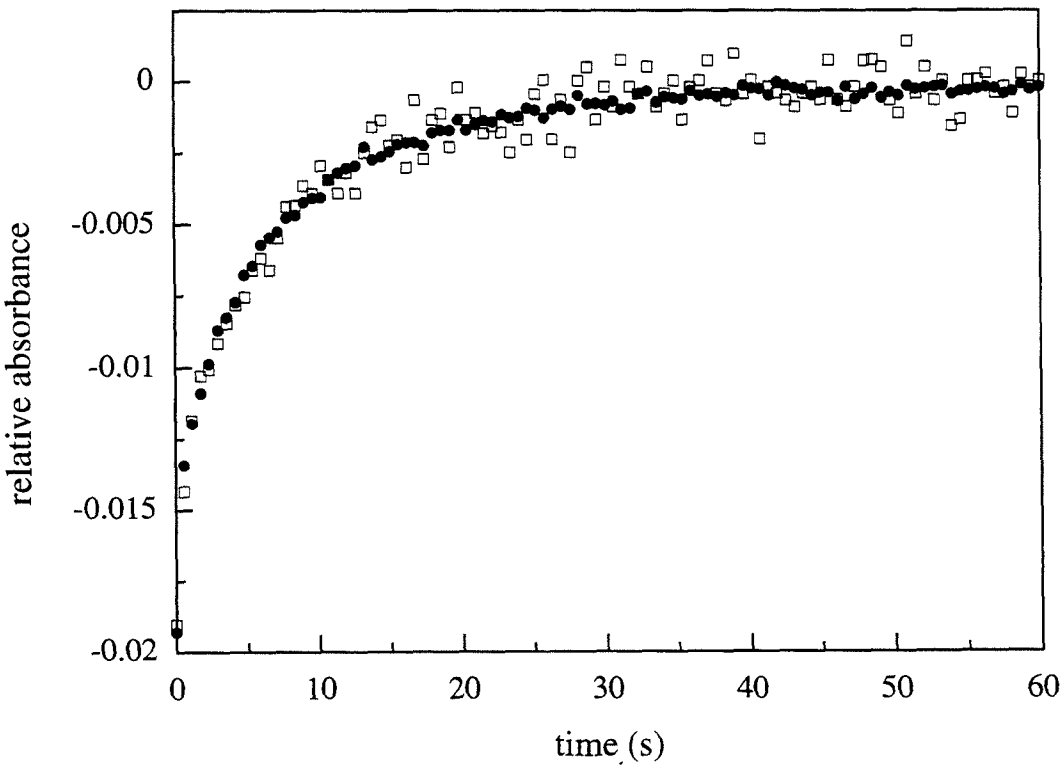
relative absorbance
0
-0.005
-0.01
-0.015
-0.02
0
10
20
30
40
50
60
time (s)

Figure 3.21 Overlay of the transient absorption data collected at 628 nm (derived from Figure 3.19A) (open circles) and a simulated second-order kinetic trace (solid circles) with $k_{12} \equiv 1.60 \times 10^4$ and $k_{21} \equiv 1.00 \times 10^2$ $M^{-1}s^{-1}$ using the following initial azurin concentrations: Cu^{II} WT, 5.9; Cu^{I} WT, 3.7; Cu^{II} Cys112Asp, 3.7; Cu^{I} Cys112Asp, 11.3 μM. The experimental data presented here differ from the raw 628-nm data shown in Figure 3.19A in that the absorbance coordinates are offset by +0.00057 absorbance units (calculated using K_{eq} of the reaction) to correct for the non-zero absorbance of the reference at 628 nm.

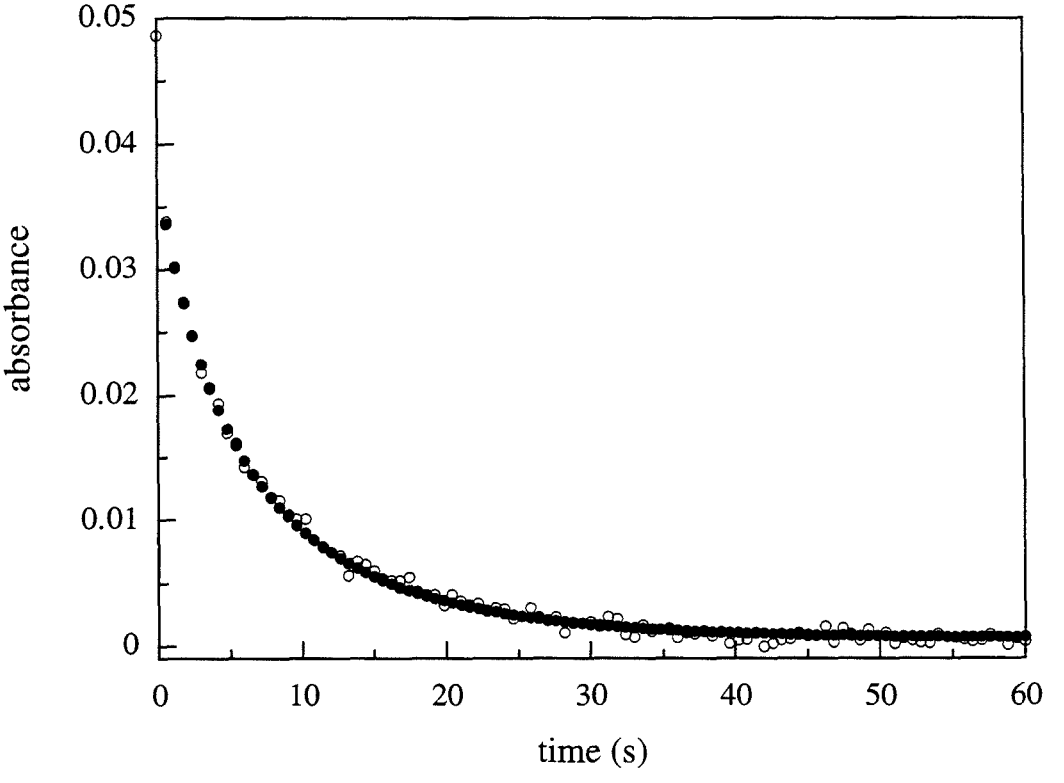
0.05
0.04
0.03
0.02
0.01
0
absorbance
0
10
20
30
40
50
60
time (s)

Figure 3.22 Transient absorption trace (100 data points) at 628 nm of the reaction from Figure 3.19 over a 5-second time base. The recorded absorbance is *not* referenced against the absorbance of the solution after completion of the reaction but rather an undetermined time after the 5-second scan.

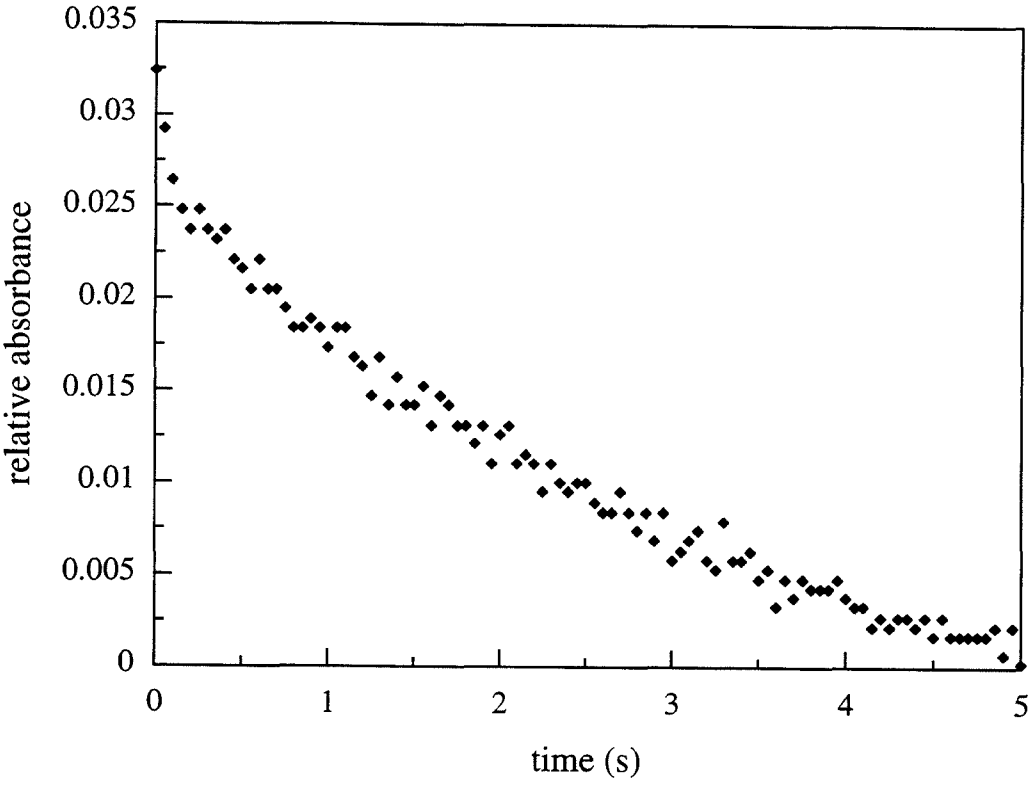
0.035
0.03
0.025
0.02
0.015
0.01
0.005
0
relative absorbance
0
1
2
3
4
5
time (s)

Figure 3.23 (**A**) Transient absorption trace (average of 8 runs; 100 data points per run) at 628 nm from the reaction between Cu^{I} WT (57 μM) and Cu^{II} Cys112Asp (42 μM) *P. aeruginosa* azurins. The recorded absorbance is referenced against the absorbance of the reaction buffer solution. (**B**) Overlay of the transient absorption data from **A** (open circles) and a simulated second-order kinetic trace (solid circles) with $k_{12} \equiv 1.40 \times 10^{4}$ and $k_{21} \equiv 1.75 \times 10^{2}$ $M^{-1}s^{-1}$ using the following initial azurin concentrations: Cu^{II} WT, 1.85; Cu^{I} WT, 40.15; Cu^{II} Cys112Asp, 55.15; Cu^{I} Cys112Asp, 1.85 μM.

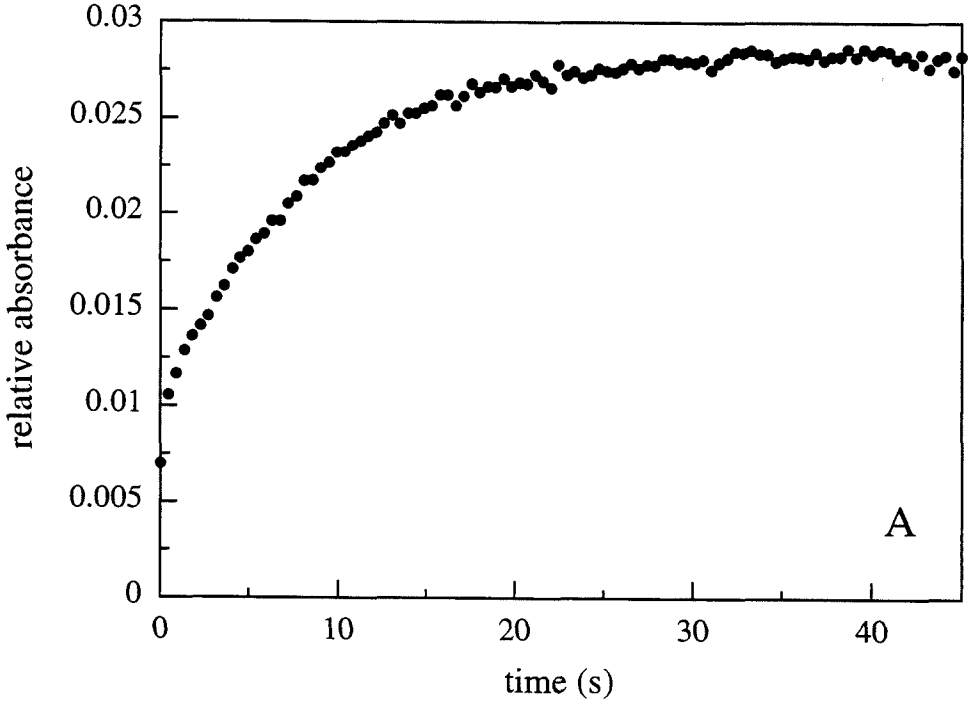
0.03
0.025
0.02
0.015
0.01
0.005
0
relative absorbance
0
10
20
30
40
time (s)
A

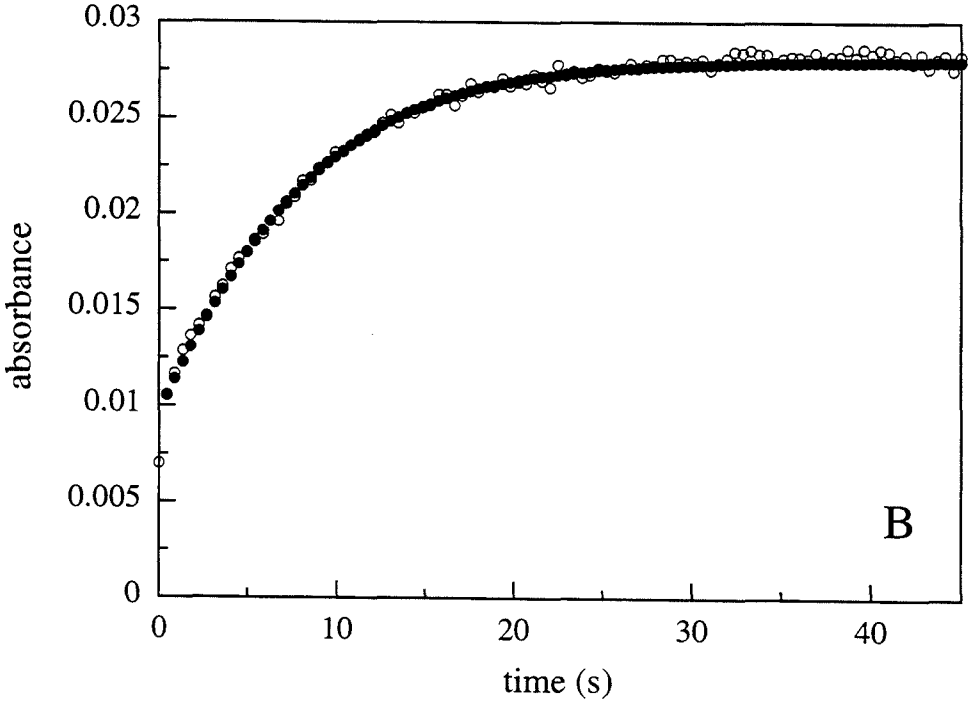
0.03
0.025
0.02
0.015
0.01
0.005
0
absorbance
0
10
20
30
40
time (s)
B

Chapter 4

Cobalt(II) Cys112Asp Azurin

Introduction

Metal substitution studies can provide valuable insights into the coordination chemistry of metalloprotein active sites. For example, the paramagnetic d^7 Co^{II} ion has often been incorporated into the active sites of Zn^{II} proteins as the diamagnetic d^{10} Zn^{II} ion is very difficult to probe using standard spectroscopic methods.[1] Co^{II}-substituted proteins generally exhibit d-d transitions in the visible region that can be analyzed with respect to band positions, shapes, and intensities. By comparing such information to those of Co^{II} compounds of known structure, an educated guess as to the coordination number, the geometry, and even the ligand set[2] of Co^{II} sites can be made, thereby providing information that may be germane to the spectroscopically silent native Zn^{II} sites. Moreover, as Co^{II} sites in proteins are often high-spin, NMR spectroscopic techniques can also be employed toward the elucidation of active-site structures of Co^{II} proteins.[3] Owing to the relatively fast electronic spin-relaxation times of high-spin Co^{II}, NMR resonances associated with nuclei located near the metal center can be observed. As these resonances generally appear well-separated from the other resonances that crowd the main (~0-10 ppm) portion of an NMR spectrum, the hyperfine-shifted signals can be assigned more easily to specific nuclei.

Although blue copper sites in proteins exhibit inherently rich spectroscopy, Co^{II} substitution experiments proved to be instrumental in confirming the assignment of the characteristic 600-nm band of blue copper to a Cys(thiolate)-to-Cu^{II} charge-transfer transition prior to the first structure determination of a blue copper protein.[4] The first Co^{II}-substituted blue copper protein to be reported was that of stellacyanin;[5] the Co^{II} derivatives of plastocyanin and azurin followed soon afterwards.[6] All Co^{II}-substituted blue copper sites in proteins exhibit intense bands in the near-UV and some weaker features in the visible (*e.g.*, see Figure 4.1). The two near-UV bands are Cys(thiolate)-to-Co^{II} charge-transfer transitions that are analogous to the native Cys(thiolate)-to-Cu^{II} charge-transfer transitions centered ~460 and ~600 nm. The positions of these bands are significantly

blue-shifted in the Co^{II} derivatives owing to the increased stability of the 2+ over the 1+ oxidation state of cobalt. Meanwhile, the double-humped d-d bands in the visible region are attributable to Co^{II} in pseudotetrahedral coordination environments.

NMR signals in and around oxidized blue copper active sites can not be observed because of the relatively slow electronic spin-relaxation times of Cu^{II}. (NMR studies of reduced (diamagnetic d^{10} Cu^{I}) blue copper proteins have, however, been reported.[7]) Although NMR spectroscopy of Co^{II}-substituted blue copper sites has not been pursued extensively, NMR spectra of Co^{II}-substituted azurin from *P. aeruginosa*[8] were known to exhibit hyperfine-shifted signals well before the blue copper active-site structure had been revealed by X-ray crystallography. Since completion of our work described below, most of the signals from protons within 10 Å of the Co^{II} center of *P. aeruginosa* azurin have been assigned.[9]

We made the Co^{II} derivative of Cys112Asp *P. aeruginosa* azurin to gain a better understanding of the structural perturbations caused by the Cys-to-Asp mutation. Data from electronic and NMR spectroscopies have been used to construct a computer model of the Co^{II} active site *independent* of the Cu^{II} Cys112Asp azurin structure described in Chapter 2.

Materials and Methods[10]

Metal Titration. Molar extinction coefficients of the absorption bands of Co^{II} WT and Cys112Asp azurins were determined from titration experiments. To an appropriately concentrated solution of known volume of pure recombinant apo WT or Cys112Asp *P. aeruginosa* azurin in 10 mM DEA·HCl/~40 mM NaCl (pH ~8.5) was added aliquots of a standardized solution of aqueous $CoCl_2$ ($\varepsilon_{510} = 4.81\ M^{-1}cm^{-1}$) in a 1-cm pathlength quartz cuvette. Absorption changes were monitored using a Hewlett-Packard 8452A Diode Array Spectrophotometer and allowed to stabilize after each addition. The data at a given

wavelength were plotted as (observed absorbance) *vs.* (concentration Co^{II} added). The data were not corrected for volume changes as the maximum change was < 6%. The resulting titration plot was fit using KaleidaGraph 3.0 (Abelbeck Software) to two lines that best describe the data points in order to determine the point at which the azurin active site was saturated with Co^{II}.

Protein Preparation. For general purposes, Co^{II} WT and Cys112Asp azurins were made by the addition of a moderate excess of aqueous $CoCl_2$ to buffered solutions (pH ~9) of the appropriate apo protein. The resultant solutions were allowed to stand for at least 1 hour to assure complete reconstitution; precipitation of some $Co(OH)_2$ was often observed. Excess Co^{II} was chelated with the addition of EDTA, and the Co^{II} azurins were then purified by FPLC on a Mono Q (strong anion-exchange) column (Pharmacia) using a NaCl gradient in 10 mM DEA·HCl (pH 8.8). The low salt buffer (Buffer A) contained no additional NaCl; the high salt buffer (Buffer B) was supplemented with 200 mM NaCl. Protein was detected by UV absorption at 280 nm. Concentrated protein samples were obtained using Centricon-10 concentrator units (Amicon). The buffer composition of the NMR samples was converted to sodium phosphate by repeated ultrafiltration in either H_2O or D_2O solution.

Spectroscopic Measurements. High-resolution absorption spectra were recorded on a modified Cary 14 spectrophotometer.

NMR spectra were recorded on a Bruker AMX600 spectrometer operating at a magnetic field of 14.1 T or on a Bruker MSL200 at 4.7 T. 1D experiments were performed using the superWEFT pulse sequence (180°-τ-90°).[11] NMR spectra were calibrated by assigning the H_2O or the residual HDO signal a chemical shift of 4.81 ppm from DSS (298 K). 1D NOE difference spectra were recorded using previously reported methodology.[12] 2D NOESY experiments were recorded in phase-sensitive TPPI mode.[13] In order to detect connectivities among hyperfine-shifted, fast-relaxing signals, 1024 x 512

data-point matrices were collected over a 100-kHz spectral width. Mixing and recycle delays were 6 and 120 ms, respectively. To investigate the spectral region between -10 and 20 ppm, NOESY experiments were recorded using 2048 x 1024 data points over a 20-kHz spectral width. Mixing and recycle delays were 15 and 580 ms, respectively. To suppress the strong solvent signal, presaturation was used during both mixing and recycle delays. A COSY experiment, recorded in magnitude mode, was acquired over a 20-kHz spectral width. 2048 x 512 data points were acquired using 480 ms of recycle delay. The same experiment was also performed using 512 x 180 data points with 115 ms of recycle delay. All 2D NOESY data were processed using a shifted ($\pi/2$ or $\pi/3$) sine-squared weighting function in both dimensions prior to Fourier transformation. An unshifted sine-squared weighting function was used in processing 2D COSY data. Reported pH values were not corrected for the deuterium isotope effect.

Computer Modeling. Azurin structures were modeled employing the BIOGRAF simulation package (Molecular Simulations) based on the crystal-structure coordinates of *P. aeruginosa* azurin (PDB code 4azu)[14] in which the copper ion was removed and all hydrogen atoms were added.. All calculations were done using POLARIS AminoLib charges[15] and DREIDING II force-field parameters.[16] Note that the Cys112 thiolate was protonated to the corresponding thiol prior to minimization. The demetallated WT azurin crystal structure was minimized with all atoms moveable by five steps of deepest-descent minimization followed by 200 steps of conjugate-gradient minimization. Thereafter, all mutants that were built converged within 100 steps of conjugate-gradient minimization. Cys112Asp azurin was constructed by replacing the sulfhydryl group of Cys112 in the calculated apo WT azurin structure with a carboxylate group. The metal ion was added manually to the minimized structures.

Results and Discussion

Metal Titration and Protein Purification. Titration of apo WT and Cys112Asp azurins with Co^{II} is accompanied by absorption changes that make the solutions appear blue (indicating formation of Co^{II} WT azurin) and purple (indicating formation of Co^{II} Cys112Asp azurin), respectively (Figure 4.2). In both cases, the absorption increase is linear with respect to added Co^{II} until ~1 equivalent has been added, after which only minimal changes are observed (Figure 4.3). Each titration plot was fit to two lines (Figure 4.3), and, as discussed for the Cu^{II} titration experiments (Chapter 3), the ratio of the Cartesian coordinates of the intersection point of the two lines represents the molar extinction coefficient. In this way, ε_{638} for Co^{II} WT azurin was determined to be 5.1 x 10^2 $M^{-1}cm^{-1}$, while ε_{610} for Co^{II} Cys112Asp azurin to be 2.9 x 10^2 $M^{-1}cm^{-1}$. The error in these values is estimated to be $< \pm 10\%$. The molar extinction coefficients of the d-d bands of Co^{II} Cys112Asp azurin are significantly greater than previously published.[17] This discrepancy probably arose from contamination by the colorless Zn^{II} derivative in previous protein preparations which did not employ the purification protocol described in Chapter 2.

The FPLC elution profiles of Co^{II} WT and Cys112Asp azurins are not only similar to each other but also to those of Cu^{II} and Zn^{II} WT and Cys112Asp azurins, indicating very similar charge distributions among these proteins at pH ~9. The azurin surface, however, does not appear to present as strong of a non-active-site binding site for Co^{II} as for Cu^{II} (see Chapter 3). Co^{II} WT and Cys112Asp azurins are stable to metal loss for months under the purification conditions, but the metal can be removed at low pH using the Zn^{II} extraction protocol described in Chapter 2.

Electronic Spectroscopy. In contrast to the absorption spectrum of Co^{II} WT azurin (Figure 4.1), the spectrum of Co^{II} Cys112Asp azurin (Figure 4.4) shows a clear absence of the intense near-UV bands, reinforcing the importance of the cysteine ligand to these transitions in the Co^{II} WT protein. Meanwhile, a comparison of the Co^{II} d-d transitions

(Figure 4.5) reveals significant differences in band shapes and intensities. Instead of the two broad visible transitions that characterize Co^{II}-substituted blue copper proteins, the transitions of Co^{II} Cys112Asp azurin show better resolved structure. The intensities of the d-d bands of Co^{II} WT azurin fall in the range typical for distorted tetrahedral Co^{II} ($\varepsilon_{max} > 250\ M^{-1}cm^{-1}$).[1,18] Although the d-d bands of Co^{II} Cys112Asp azurin are weaker than those of the Co^{II} WT protein, they are still more intense than those generally found in five-coordinate Co^{II} complexes ($50 < \varepsilon_{max} < 150\ M^{-1}cm^{-1}$),[1,18] being just above the lower limit for distorted tetrahedral species; this observation is suggestive of a geometry perhaps intermediate between four and five coordination.

Based on the metal coordinating properties of amino acids,[2] it is reasonable to assume that both active-site histidines (His46 and His117) and either the cysteine (Cys112) or aspartate (Asp112) contribute donor atoms to the Co^{II} ion. The importance of the backbone carbonyl group of Gly45 and the Met121 side chain to the Co^{II} coordination environment, however, is difficult to predict from electronic absorption data alone. Therefore, we turned to paramagnetic NMR spectroscopy to gain a more complete picture of the active-site coordination structure of Co^{II} WT and Cys112Asp azurins.

NMR Spectroscopy. The 200-MHz ^{1}H-NMR spectra of both the Co^{II}-substituted WT and Cys112Asp azurins show a number of hyperfine-shifted signals (Figure 4.6). Most of the WT azurin signals have been observed and assigned previously.[19] The two WT azurin signals *a* and *b* (Figure 4.6A, B) can be assigned to the β-CH_2 protons of Cys112. β-CH_2 protons of coordinated cysteines are always found far downfield in Co^{II}-substituted metalloproteins.[20] Their large hyperfine shifts confirm regular coordination of Cys112 to the Co^{II} ion. These signals are not present in the Asp112 mutant (Figure 4.6C, D).

The assignment of histidine ring protons was achieved through NOE and NOESY data on H_2O and D_2O samples. Comparison of the H_2O and D_2O NMR spectra of both

the WT and mutant proteins reveals the disappearance of WT signals *e* and *f* (Figure 4.6B, A) and mutant signals *c* and *e* (Figure 4.6D, C), all of which can be assigned to exchangeable imidazole-NH protons. WT signal *f* and mutant signal *e* have fractional intensities due to partial saturation from solvent but gain full intensity at lower pH (data not shown). From NOE and NOESY experiments, WT signal *e* is dipole-coupled to signal *h*, and signal *f* to signal *g* (data not shown), as already reported.[19] Likewise, in the mutant, signal *c* is dipole-coupled to signal *f*, and signal *e* to signal *d*. Figure 4.7 shows the region of the NOESY spectrum performed on the Cys112Asp derivative where the connectivities *c-f* and *d-e* are observed. In line with previous work,[19] the *e-h* and *f-g* pairs in the WT protein are assigned to $H^{\varepsilon 2}$-$H^{\delta 2}$ pairs of two coordinated histidines, and the same assignment is made for the *c-f* and *d-e* pairs in the mutant.

The sequence-specific assignment is facilitated by the observation that the $H^{\varepsilon 2}$ proton of His117 is solvent-exposed while that of His46 is not. The fractional intensity of WT signal *f* and mutant signal *e* at pH 7.0 indicates relatively high solvent-exchange rates. Therefore, WT pair *e-h* and mutant pair *c-f* are assigned to His46 whereas WT pair *f-g* and mutant pair *d-e* are assigned to His117. The chemical shifts of these signals in both systems are all in the range (50-80 ppm) typical of ring protons of regularly coordinated histidines.[21] The $H^{\varepsilon 1}$ protons are expected to yield much broader signals due to their ring positions adjacent to the coordinating $N^{\delta 1}$ nitrogens. Possible candidates for these protons are WT signals *c* and *d* and mutant signals *a* and *j* (Figure 4.6). However, no connectivities could be detected from such broad signals to confirm this assignment. If the assignment is correct, the smaller shift of signal *j* in the mutant would be indicative of some difference in at least the pseudocontact contribution to the shift of this proton in the immediate vicinity of the metal ion.

There is a strong NOESY and COSY cross peak between WT signals *i* and *q* (data not shown), as observed previously.[19] Despite their experiencing hyperfine shifts opposite

in sign, they have been assigned as the α-CH_2 proton pair of Gly45. This assignment is confirmed by an NOE between signal *q* and the slowly exchangeable proton *m* (Figure 4.6B) assigned as the amide NH proton of Gly45. In the mutant protein, no similarly strong connectivities between upfield- and downfield-shifted signals are observed. However, strong NOESY and COSY connectivities typical of a geminal proton pair are detected between mutant signals *b* and *l*, both downfield, although one is much more shifted than the other (Figure 4.8).

Note that the spectrum of Co^{II} Cys112Asp azurin at pH 5.5 (Figure 4.8A) is slightly different from the spectrum at pH 8.0 (Figure 4.6D). Indeed, some signals experience hyperfine-shift changes. In particular, signals *c*, *h*, and *i* move slightly downfield, sizably upfield, and slightly upfield, respectively, on decreasing the pH from 7.0 to 4.5. At intermediate pH values, both "high pH" and "low pH" signals are observed. Signals from the "high pH" form (the minor species at pH 5.5) are labeled with primes. The observation of two sets of signals at intermediate pH values demonstrates the presence of two pH-dependent species in equilibrium. The chemical exchange rate between the two species is slow on the NMR timescale ($k_{ex} \leq 2 \times 10^3\ s^{-1}$).

Figure 4.8B shows the -15 to 20 ppm region of the 1D NOE difference spectrum obtained upon saturation of mutant signal *b* in D_2O. In addition to the strong NOE to signal *l*, an NOE to signal *m* is also observed. Mutant signal *b* experiences additional dipolar connectivities involving hyperfine-shifted signals. Figure 4.8A shows the 1D NOE difference spectra over the entire spectral window obtained upon irradiation of signal *b* in H_2O solution (trace (a)) and D_2O solution (trace (b)). In H_2O, two NOEs are observed with the exchangeable signals *i* and *k*. Inspection of the X-ray crystal structure of azurin[14] confirms that no other reasonable candidate exists for a hyperfine-shifted geminal proton pair close in space to hyperfine-shifted exchangeable protons. Therefore, we conclude that the *b-l* pair in the mutant must be assigned to the α-CH_2 protons of Gly45. Mutant signal *i*

can then be assigned to the amide NH proton of His46 in view of its larger shift and signal *k* to the amide NH proton of Gly45 itself. In contrast to the analogous WT protons, the substantially different hyperfine shifts of some of the above protons indicate that, although coordinated in both cases, some differences may exist in the binding mode of the Gly45 carbonyl group. For example, a slightly shorter carbonyl-Co^{II} bond in the mutant might significantly increase the downfield contact contribution to the shifts of both α-CH_2 protons of Gly45 and the amide NH proton of His46. Alternatively, a reduction in the upfield pseudocontact contribution from WT to mutant is possible.

Of the other hyperfine-shifted signals outside the diamagnetic region (Figure 4.6), we are left with signals *j, k, n, o, p* in WT and signals *g, h, n* in the mutant. There is little analogy between the two derivatives as far as these signals are concerned. Signals *g* and *h* in the mutant have shifts and linewidths typical of β-CH_2 protons of a coordinated carboxylate residue (Figure 4.8A),[22] and hence can be assigned to Asp112 coordinated regularly through *at least* one oxygen.

WT signals *j* and *p* have been assigned tentatively to the γ-CH_2 protons of Met121, with signals *n* and *o* attributed to its β-CH_2 protons.[19] The NOE experiments performed upon saturation of the WT signals *a* and *b* (β-CH_2 protons of Cys112) allowed us to detect an NOE between signal *b* and at least one of the two unresolved signals *n* and *o* (Figure 4.9). Such an NOE is consistent with the proposed assignment[19] of signals *n* and *o* to the β-CH_2 protons of Met121.

A crucial point for the assignment of Met121 signals would be the identification of the ε-CH_3 signal. As can be seen in Figure 4.10, WT signal *l* (of intensity 3), assigned previously as the ε-CH_3 protons of Met121,[19] is dipolarly connected to signal *q* (H^{α} of Gly45). Signal *l* gives rise to three dipolar connectivities (Figure 4.11A, cross peaks 1, 2, 3) with signals belonging to the same spin pattern, as can be observed from the COSY experiment reported in Figure 4.11B. The signal at -4.8 ppm has intensity three; the only

residue with two methyl groups occurring at short distance from one of the H^{α} protons of Gly45 (signal *q*) is Leu86.[14] As signal *l* is much broader than the signal corresponding to the other methyl group, inspection of the X-ray structure[14] suggests the assignment of *l* to δ^2-CH_3 of Leu86 (*i.e.*, the methyl group closer to the metal ion). This conclusion is supported by the network of interresidue connectivities (see caption to Figure 4.11) that involve Leu86 with Lys41 and Leu68. The COSY spectrum (Figure 4.11B) allows us to identify every resonance of Lys41, which, along with Leu86, is one of the residues close to the active site but not coordinated to the metal ion. All the signals of Lys41 experience a slight upfield pseudocontact shift (0-6 ppm). The signal of δ^1-CH_3 of Leu86 is also dipole-dipole coupled to another signal of a methyl group that can be assigned on the basis of the X-ray structure[14] to Leu68. In summary, the NOESY and COSY maps (Figure 4.11) have allowed us to assign almost all the upfield-shifted signals (because of pseudocontact shifts) in the region -14 to -0.3 ppm. The NOEs observed upon saturation of upfield signal *q* are all consistent with these assignments and are reported in the caption to Figure 4.10. In agreement with this reassignment of WT, the homologous methyl signal *m* in the mutant is dipolarly connected to signal *b* (H^{α} of Gly45), as observed clearly from 1D NOE data (Figure 4.8). Such an NOE is definitely inconsistent with the assignment of signal *m* to the ε-CH_3 protons of Met121, but it is consistent with the assignment of *m* to one of the δ-CH_3 protons of Leu86. We conclude that the ε-CH_3 signal of Met121 is unobserved in both derivatives (it should fall in the diamagnetic region of the spectrum). Mutant signal *n* gives an NOE to signal *m*. From an inspection of the X-ray crystal structure,[14] a plausible candidate for signal *n* is one of the β-CH_2 protons of Phe114.

There are no hyperfine-shifted signals in the mutant that can be related to WT signals *j* and *p*. A possible explanation is that the mutant γ-CH_2 protons of Met121 also fall in the diamagnetic region. Such a decrease in the hyperfine shifts of the γ-CH_2 protons of Met121 could arise from the fact that the methionine sulfur atom is not coordinated to the

Co^{II} ion in the Cys112Asp mutant. The absence of the two upfield-shifted signals (~10 ppm) in the mutant (signals *n* and *o* in WT) is consistent with this explanation. All of the above observations point to modest hyperfine shifts experienced by all protons of Met121 in the WT protein and even smaller shifts by those of the mutant protein. In light of the present finding of very large hyperfine shifts for the β-CH_2 protons adjacent to a regularly coordinated sulfur atom of Cys112, the most likely interpretation of the data is that Met121 is *at most* semi-coordinated in the WT structure and essentially not coordinated in the mutant. The larger downfield shifts of the Gly45 α-CH and NH and His46 NH protons are consistent with this view of the Co^{II} coordination environment in the Asp112 protein.

Assignments of the hyperfine-shifted NMR signals of both Co^{II} WT and Cys112Asp azurins are compiled in Table 4.1. A map of the protons that exhibit the hyperfine-shifted resonances (Figure 4.12) shows pictorially the differences observed between Co^{II} WT and Cys112Asp azurins. Our assignments are wholly consistent with those from a more recent and more extensive paramagnetic NMR study of Co^{II} WT *P. aeruginosa* azurin,[9] in which WT signal *k* (unassigned in our study) has been assigned to one of the γ-CH_2 protons of Met13, and a moderately hyperfine-shifted signal corresponding to the ε-CH_3 protons of Met121 was observed near the signal for the δ^2-CH_3 protons of Leu86 (WT signal *l*).

Based on both electronic absorption and NMR data, it is likely that the Co^{II} coordination geometry of Co^{II} WT azurin is similar to that of the pseudotetrahedral Zn^{II} ion observed in the crystal structure of Zn^{II} WT azurin,[23] in which the metal is coordinated by the main chain carbonyl group of Gly45 and the side chains of His46, Cys112, and His117. Furthermore, the closely similar absorption spectra of the Co^{II} derivatives of Met121Leu azurin and the WT protein suggest that Met121 is not a ligand.[24] Although the NMR data accord with this conclusion, we still cannot rule out completely the possibility of some type

of weak Met121-Co^{II} bonding interaction (especially in view of the finding of a hyperfine-shifted resonance for the ε-CH_3 protons of Met121 (ref 9)). As in Co^{II} WT azurin, the Co^{II} ion of Co^{II} Cys112Asp azurin is likely coordinated by the Gly45 carbonyl group and the side chains of His46 and His117. Coordination by the Asp112 side chain is also clearly indicated; coordination by Met121, however, is unlikely. In order to assess the possible bonding modes of the Asp112 carboxylate group, which can, in principle, coordinate metal ions in either a monodentate or bidentate fashion,[25] a computer model of the active site was generated.

Computer Modeling. It has been shown that the structures of the apo and Cu^{II} forms of WT *P. aeruginosa* azurin are nearly superposable.[26] Furthermore, qualitative modeling studies (described in Chapter 3) showed that the Cys112 residue can be replaced with an Asp without introducing steric clashes within the azurin active site. Therefore, we propose that the calculated positions of the active-site side chains of apo Cys112Asp azurin will constitute a valid approximation of the structure of the mutant metal binding site. The minimized apo WT azurin structure exhibited a positional rms deviation of all non-hydrogen main-chain and side-chain atoms of 1.5 Å with the crystal structure of the holo protein,[14] and the displacements of the copper-site ligands were similar to those reported for the crystal structure of apo WT azurin.[26] The positions of the native copper ligands of all the calculated structures were nearly superposable.

The Asp112 carboxylate group can apparently adopt several reasonable conformations with respect to rotations about its C^{β}-C^{γ} bond; monodentate or bidentate coordination can be accommodated depending on its orientation within the active site. A minimized structure of the metal binding site with the carboxylate group in a potentially bidentate binding mode is shown in Figure 4.13. Standard metal-ligand bond distances (~2 Å) can be achieved with the Gly45 carbonyl group, His46, and His117. Interestingly, the Asp112 carboxylate group can be positioned in such a way that both oxygens are

located within reasonable bonding distances but in which one is significantly closer than the other (2.1 *vs.* 2.5 Å). Such a model can be considered intermediate between four and five coordination and would be consistent with the observed intensities of the d-d bands of Co^{II} Cys112Asp azurin. The model also suggests the existence of a *bent* bond[25] between Co^{II} and the Asp112 carboxylate group, owing to constraints placed on the 112 side chain by the global fold of the protein. The apparent movement of the Co^{II} ion away from Met121 toward the Gly45 carbonyl is not surprising because the Asp oxygen donor atoms should harden the Co^{II} center.[27] Thus, the Co^{II} ion in the mutant should have a greater affinity for the Gly45 carbonyl oxygen than for the softer sulfur atom of Met121.

References

(1) For a review on the use of Co^{II} to study metalloprotein active sites, see: Bertini, I.; Luchinat, C. In *Advances in Inorganic Biochemistry*; Eichhorn, G. L.; Marzilli, L. G., Eds.; Elsevier: New York, 1984; Vol. 6, pp 71-111.

(2) For a discussion of metal-binding sites in proteins, see: Tainer, J. A.; Roberts, V. A.; Getzoff, E. D. *Curr. Opin. Biotech.* **1991**, *2*, 582-591.

(3) For a review of paramagnetic NMR spectroscopy of metalloproteins, see: Bertini, I.; Turano, P.; Vila, A. J. *Chem. Rev.* **1993**, *93*, 2833-2932.

(4) Gray, H. B.; Solomon, E. I. In *Copper Proteins*, Spiro, T. G., Ed.; Wiley: New York, 1981; Chapter 1, pp 1-39.

(5) McMillan, D. R.; Holwerda, R. A.; Gray, H. B. *Proc. Natl. Acad. Sci. USA* **1974**, *71*, 1339-1341.

(6) McMillan, D. R.; Rosenberg, R. C.; Gray, H. B. *Proc. Natl. Acad. Sci. USA* **1974**, *71*, 4760-4762.

(7) van de Kamp, M.; Canters, G.W.; Wijmenga, S. S.; Lommen, A.; Hilbers, C. W.; Nar, H.; Messerschmidt, A.; Huber, R. *Biochemistry* **1992**, *31*, 10194-10207 and references therein.

(8) Hill, H. A. O.; Smith, B. E.; Storm, C. B. *Biochem. Biophys. Res. Commun.* **1976**, *70*, 783-790.

(9) Salgado, J.; Jiménez, H. R.; Donaire, A.; Moratal, J. M. *Eur. J. Biochem.* **1995**, *231*, 358-369.

(10) Parts of the work described in this chapter have been published: Piccioli, M.; Luchinat, C.; Mizoguchi, T. J.; Ramirez, B. E.; Gray, H. B.; Richards, J. H. *Inorg. Chem.* **1995**, *34*, 737-742.

(11) Inubushi, T.; Becker, E. D. *J. Magn. Reson.* **1983**, *51*, 128-133.

(12) Banci, L.; Bertini, I.; Luchinat, C.; Piccioli, M.; Scozzafava, A.; Turano, P. *Inorg. Chem.* **1989**, *28*, 4650-4656.

(13) Marion, D.; Wüthrich, K. *Biochem. Biophys. Res. Commun.* **1983**, *113*, 967-974.

(14) Nar, H.; Messerschmidt, A.; Huber, R.; van de Kamp, M.; Canters, G. W. *J. Mol. Biol.* **1991**, *221*, 765-772.

(15) Lee, F. S.; Chu, Z. T.; Warshel, A. *J. Comput. Chem.* **1993**, *14*,161-185.

(16) Mayo, S. L.; Olafson, B. D.; Goddard, W. A., III *J. Phys. Chem.* **1990**, *94*, 8897-8909.

(17) Mizoguchi, T. J.; Di Bilio, A. J.; Gray, H. B.; Richards, J. H. *J. Am. Chem. Soc.* **1992**, *114*, 10076-10078.

(18) Rosenberg, R. C.; Root, C. A.; Wang, R.-H.; Cerdonio, M.; Gray, H. B. *Proc. Natl. Acad. Sci. USA* **1973**, *70*, 161-163.

(19) Moratal, J.-M.; Salgado, J.; Donaire, A.; Jiménez, H. R.; Castells, J. *Inorg. Chem.* **1993**, *32*, 3587-3588.

(20) (a) Bertini, I.; Gerber, M.; Lanini, G.; Luchinat, C.; Maret, W.; Rawer, S.; Zeppezauer, M. *J. Am. Chem. Soc.* **1984**, *106*, 1826-1830. (b) Bertini, I.; Luchinat, C.; Messori, L.; Vasák, M. *J. Am. Chem. Soc.* **1989**, *111*, 7296-7300. (c) Moura, I.; Teixeira, M.; LeGall, J.; Moura, J. J. G. *J. Inorg. Biochem.* **1991**, *44*, 127- 139.

(21) (a) Bertini, I.; Canti, G.; Luchinat, C.; Mani, F. *J. Am. Chem. Soc.* **1981**, *103*, 7784-7788. (b) Bertini, I.; Luchinat, C.; Piccioli, M. *Progr. Nucl. Magn. Reson. Spectrosc.* **1994**, *26*, 91-139.

(22) (a) Holz, R. C.; Que, L., Jr.; Ming, L.-J. *J. Am. Chem. Soc.* **1992**, *114*, 4434-4436. (b) Bertini, I.; Lanini, G.; Luchinat, C.; Messori, L.; Monnanni, R.; Scozzafava, A. *J. Am. Chem. Soc.* **1985**, *107*, 4391-4396.

(23) Nar, H.; Huber, R.; Messerschmidt, A.; Filippou, A. C.; Barth, M.; Jaquinod, M.; van de Kamp, M.; Canters, G. W. *Eur. J. Biochem.* **1992**, *205*, 1123-1129.

(24) Di Bilio, A. J.; Chang, T. K.; Malmström, B. G.; Gray, H. B.; Karlsson, B. G.; Nordling, M.; Pascher, T.; Lundberg, L. G. *Inorg. Chim. Acta* **1992**, *198-200*, 145-148.

(25) For a discussion of metal binding by carboxylate groups in proteins, see: Glusker, J. P. *Adv. Protein Chem.* **1991**, *42*, 1-76.

(26) Nar, H.; Messerschmidt, A.; Huber, R.; van de Kamp, M.; Canters, G. W. *FEBS Lett.* **1992**, *306*, 119-124.

(27) Pearson, R. G. *Inorg. Chem.* **1988**, *27*, 734-740.

Table 4.1 ^{1}H-NMR assignments of the hyperfine-shifted signals of Co^{II} WT and Cys112Asp *P. aeruginosa* azurins that are discussed in the text (n/a = not applicable). WT signal *k* has subsequently been assigned to one of the γ-CH_2 protons of Met13.[9]

Signal	Co^{II} WT Azurin	Co^{II} Cys112Asp Azurin
a	β-CH_2 Cys112	$H^{\varepsilon 1}$ His46/117
b	β-CH_2 Cys112	α-CH_2 Gly45
c	$H^{\varepsilon 1}$ His46/117	$H^{\varepsilon 2}$ His46
d	$H^{\varepsilon 1}$ His46/117	$H^{\delta 2}$ His117
e	$H^{\varepsilon 2}$ His46	$H^{\varepsilon 2}$ His117
f	$H^{\varepsilon 2}$ His117	$H^{\delta 2}$ His46
g	$H^{\delta 2}$ His117	β-CH_2 Asp112
h	$H^{\delta 2}$ His46	β-CH_2 Asp112
i	α-CH_2 Gly45	NH His46
j	γ-CH_2 Met121	$H^{\varepsilon 1}$ His46/117
k	(unassigned)	NH Gly45
l	δ-CH_3 Leu86	α-CH_2 Gly45
m	NH Gly45	δ-CH_3 Leu86
n	β-CH_2 Met121	β-CH_2 Phe114
o	β-CH_2 Met121	n/a
p	γ-CH_2 Met121	n/a
q	α-CH_2 Gly45	n/a

Figure 4.1 Electronic absorption spectrum of Co^{II} WT *P. aeruginosa* azurin in 10 mM DEA·HCl/~40 mM NaCl (pH 8.8) at room temperature.

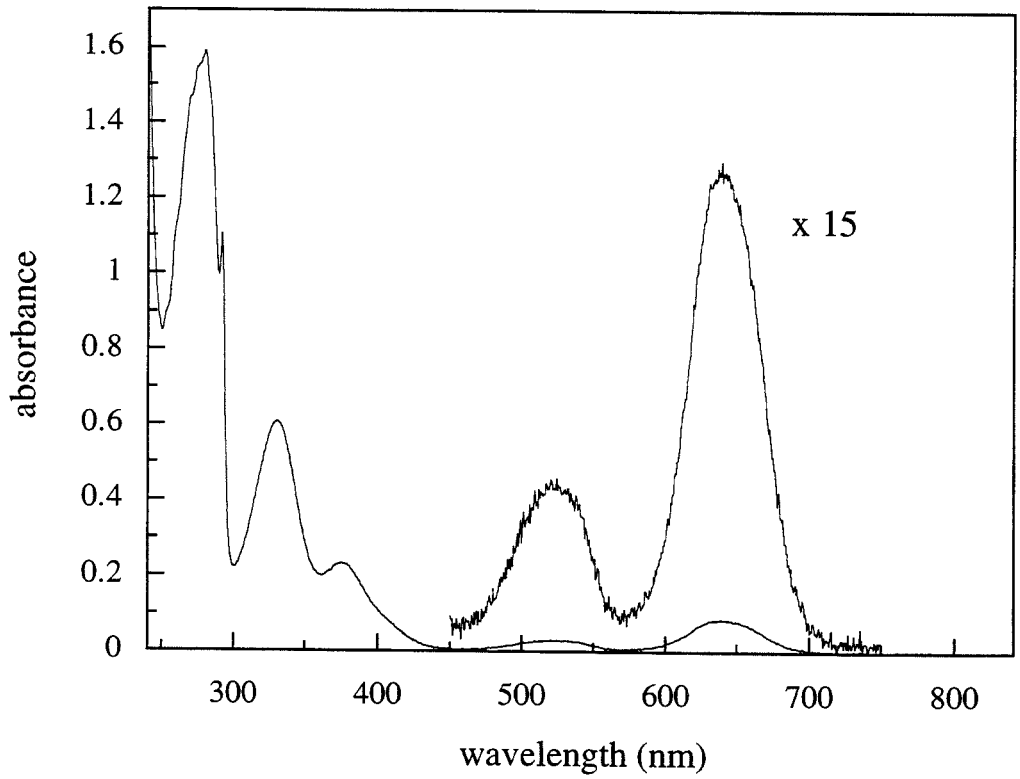
absorbance
1.6
1.4
1.2
1
0.8
0.6
0.4
0.2
0
x 15
300
400
500
600
700
800
wavelength (nm)

Figure 4.2 Absorption changes accompanied by the titration of apo WT (**A**) and Cys112Asp (**B**) *P. aeruginosa* azurins with Co^{II}.

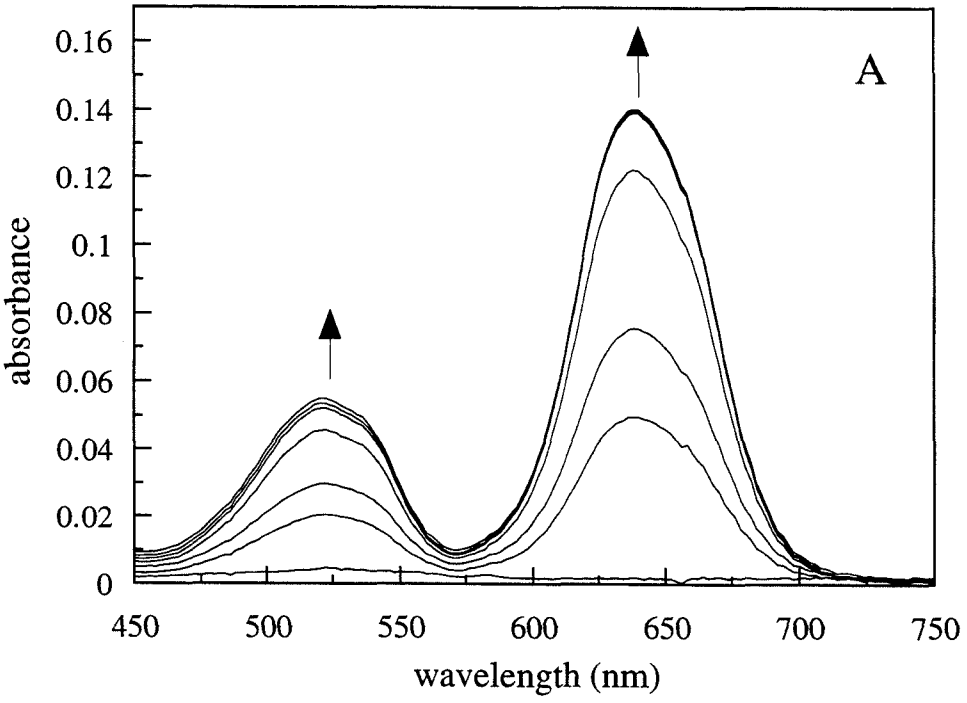
A
absorbance
0.16
0.14
0.12
0.1
0.08
0.06
0.04
0.02
0
450
500
550
600
650
700
750
wavelength (nm)

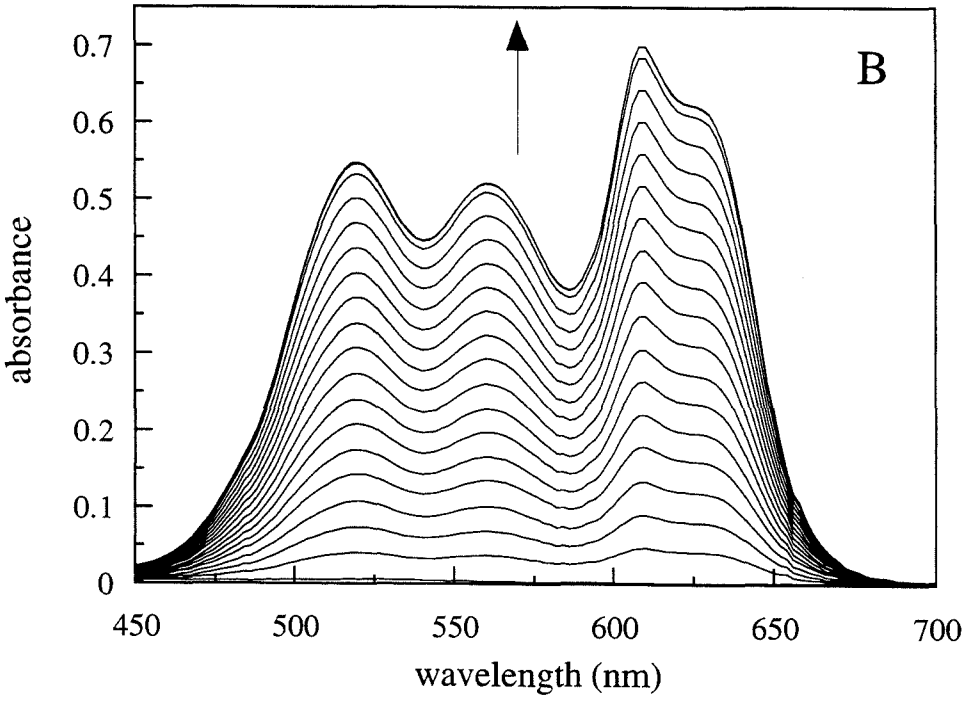
B
absorbance
0.7
0.6
0.5
0.4
0.3
0.2
0.1
0
450
500
550
600
650
700
wavelength (nm)

Figure 4.3 Titration plots derived from the data from Figure 4.2 with accompanying fits to two lines for WT (λ_{obs} = 638 nm) (**A**) and Cys112Asp (λ_{obs} = 610 nm) (**B**) azurins.

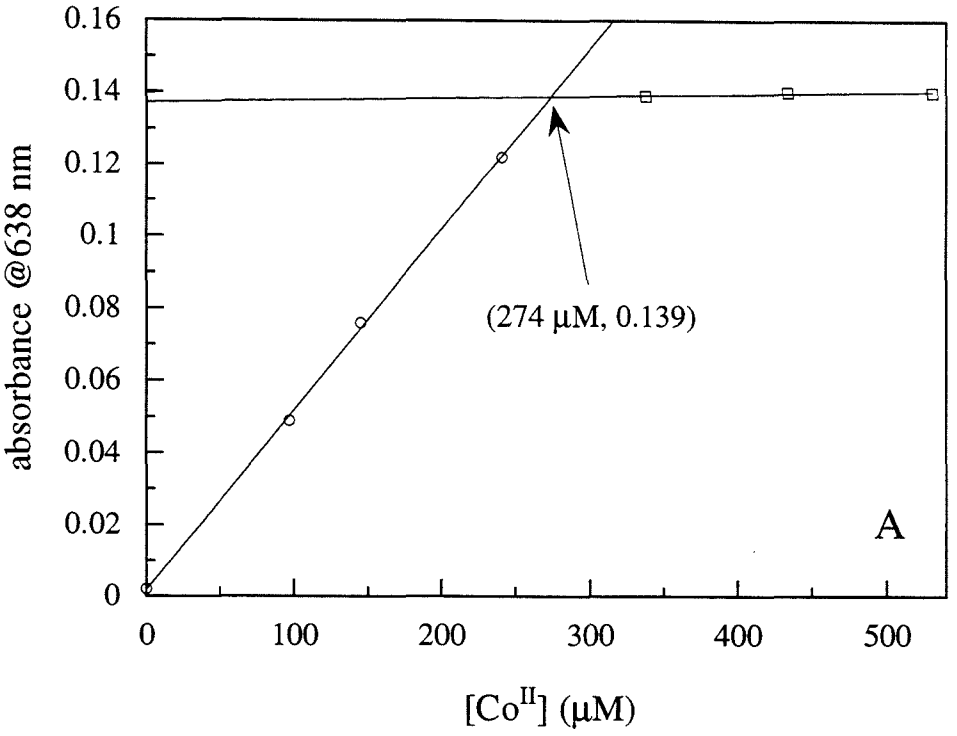
absorbance @638 nm
0.16
0.14
0.12
0.1
0.08
0.06
0.04
0.02
0
0
100
200
300
400
500
(274 µM, 0.139)
A
[Co^II] (µM)

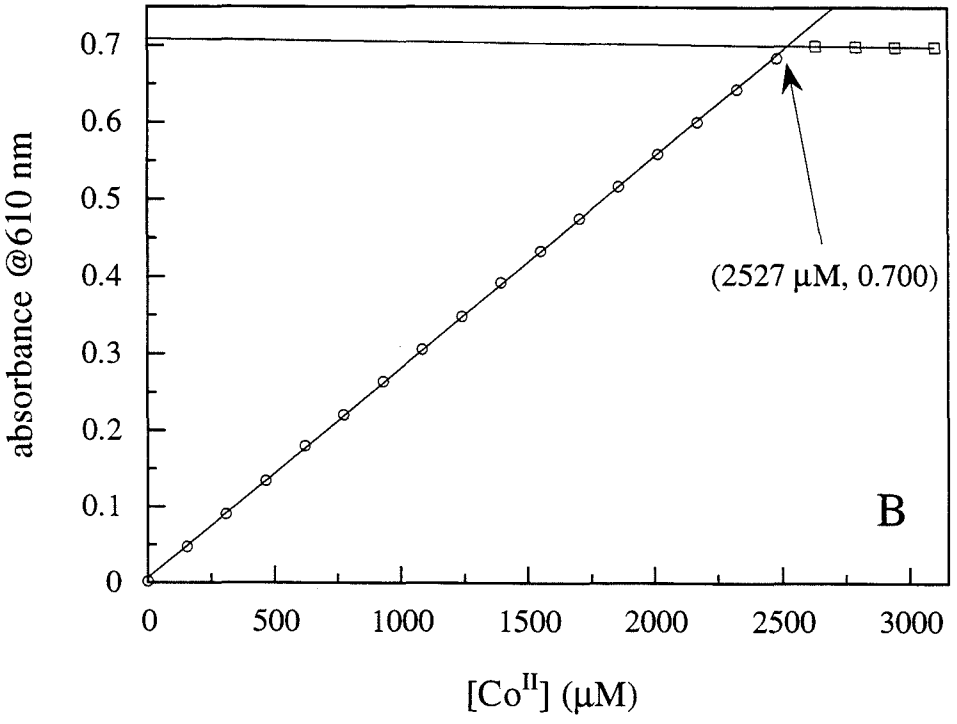
absorbance @610 nm
0.7
0.6
0.5
0.4
0.3
0.2
0.1
0
0
500
1000
1500
2000
2500
3000
(2527 µM, 0.700)
B
[Co^II] (µM)

Figure 4.4 Electronic absorption spectrum of Co^{II} Cys112Asp *P. aeruginosa* azurin in 10 mM DEA·HCl/~40 mM NaCl (pH 8.8) at room temperature.

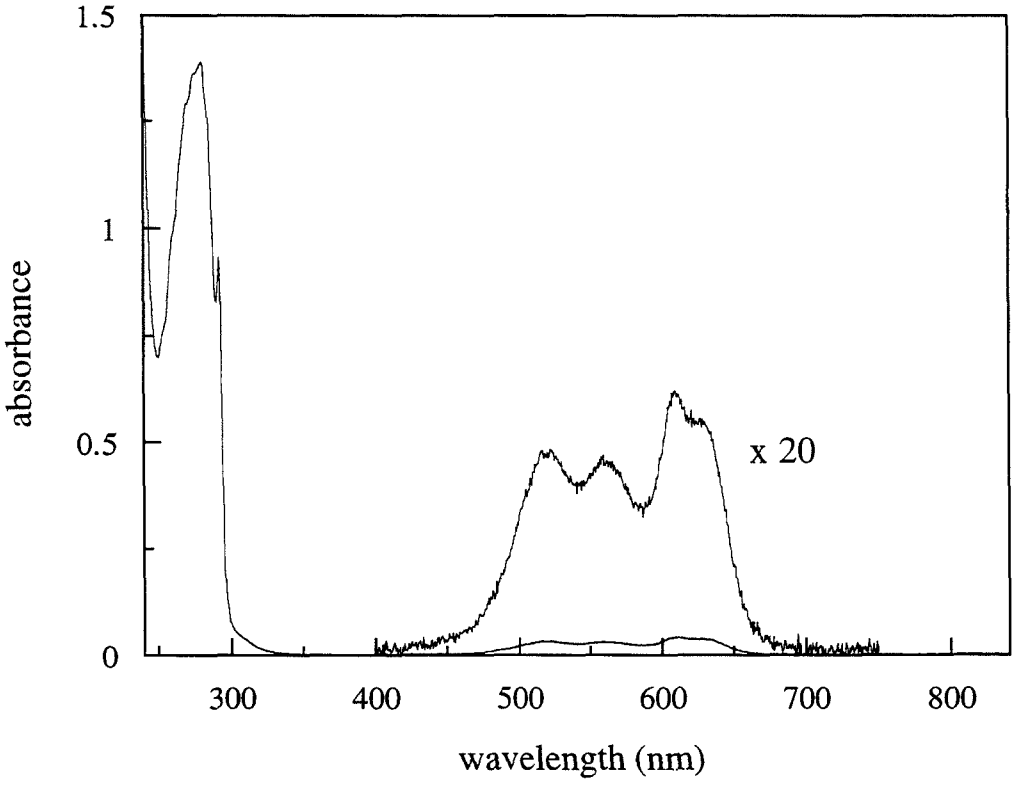
1.5
1
0.5
0
absorbance
x 20
300
400
500
600
700
800
wavelength (nm)

Figure 4.5 Overlay of the visible absorption spectra of Co^{II} WT (λ_{max} = 521, 638 nm) and Cys112Asp (λ_{max} = 521, 560, 609 nm) *P. aeruginosa* azurins in 10 mM DEA·HCl/ ~40 mM NaCl (pH 8.8) at room temperature.

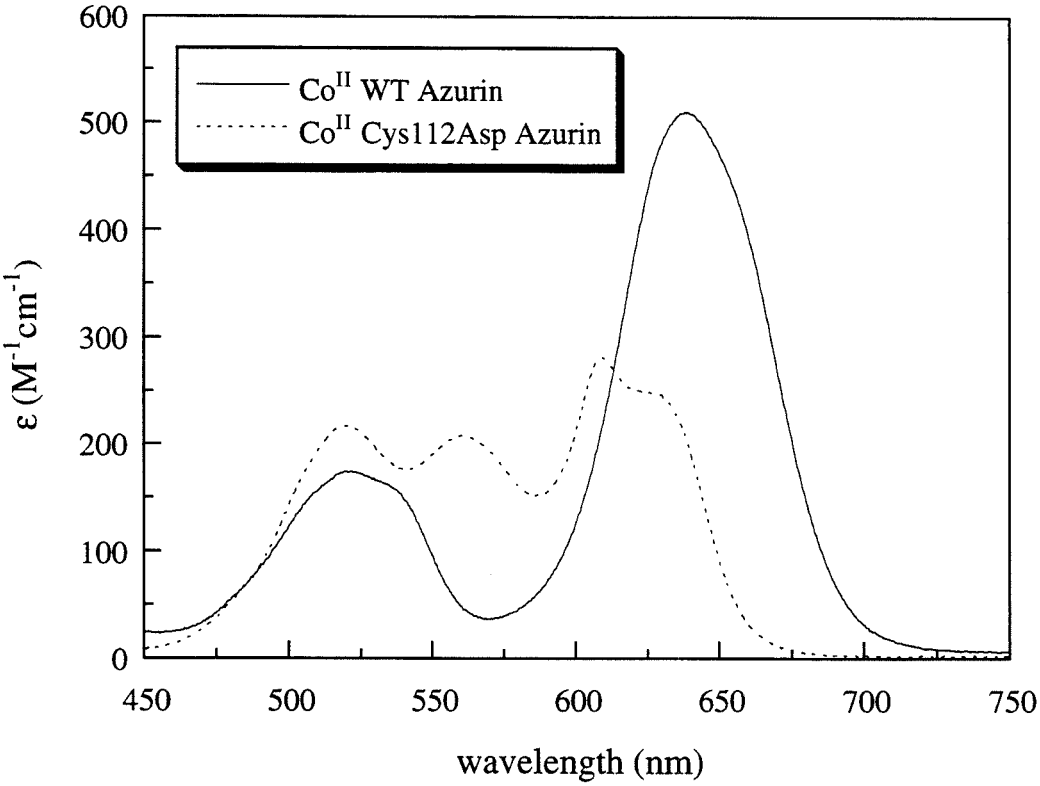
Co^II WT Azurin
Co^II Cys112Asp Azurin
ε (M^-1cm^-1)
wavelength (nm)
600
500
400
300
200
100
0
450
500
550
600
650
700
750

Figure 4.6 200-MHz ^{1}H-NMR spectra (298 K) of Co^{II} WT (pH 8.0) in D_2O (**A**) and H_2O (**B**) and Co^{II} Cys112Asp *P. aeruginosa* azurins (pH 7.0) in D_2O (**C**) and H_2O (**D**).

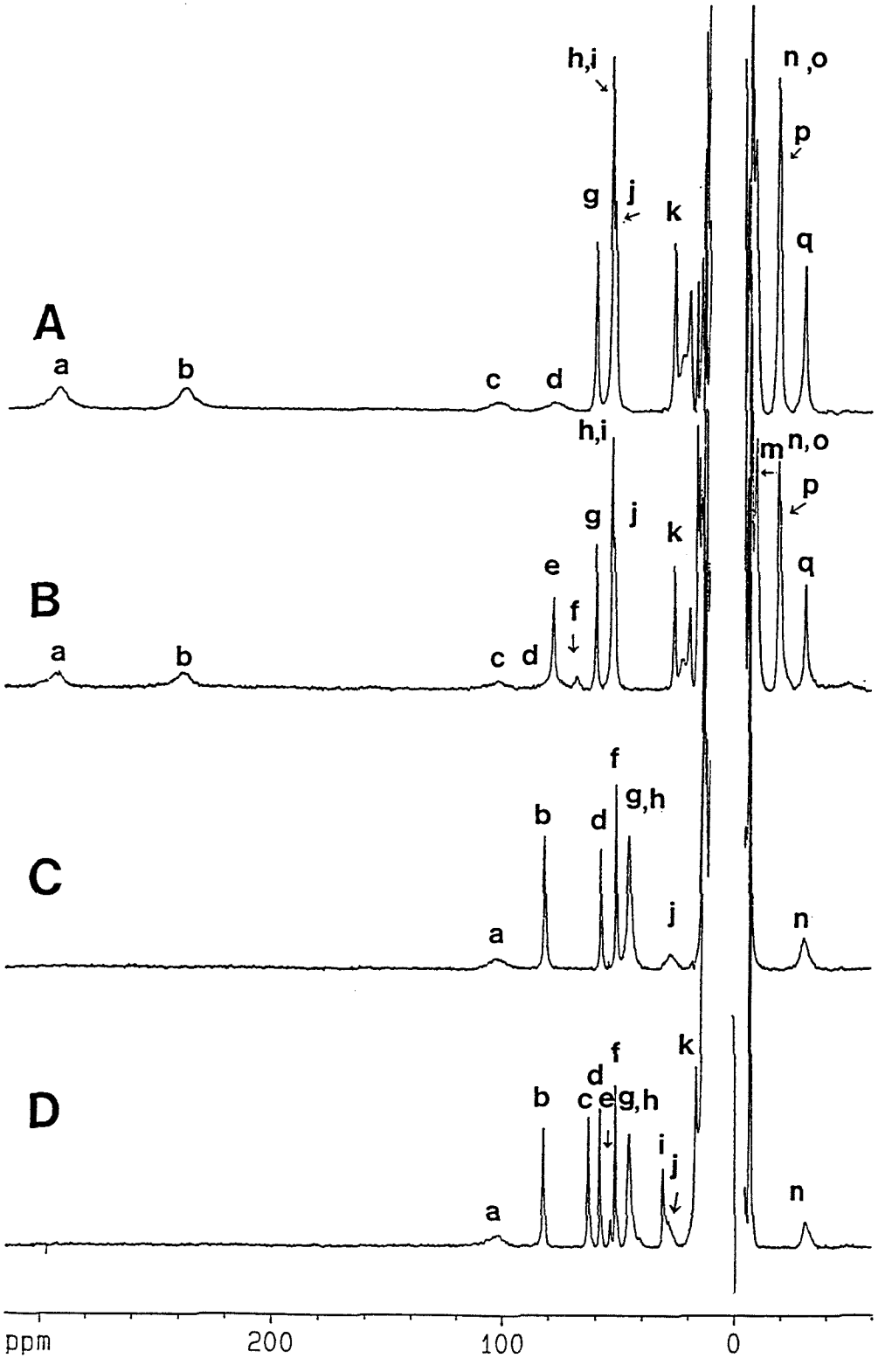
A
a
b
c
d
h,i
g
j
k
n,o
p
q
B
a
b
c
d
e
f
h,i
g
j
k
m
n,o
p
q
C
a
b
d
f
g,h
j
n
D
a
b
c
d
e
f
g,h
i
j
k
n
ppm
200
100
0

Figure 4.7 600-MHz NOESY spectrum (298 K) of Co^{II} Cys112Asp *P. aeruginosa* azurin (pH 7.2). The 35 to 70 ppm region is reported. The *d-e* cross peak is weaker than the *c-f* cross peak because signal *e* is of fractional intensity at this pH.

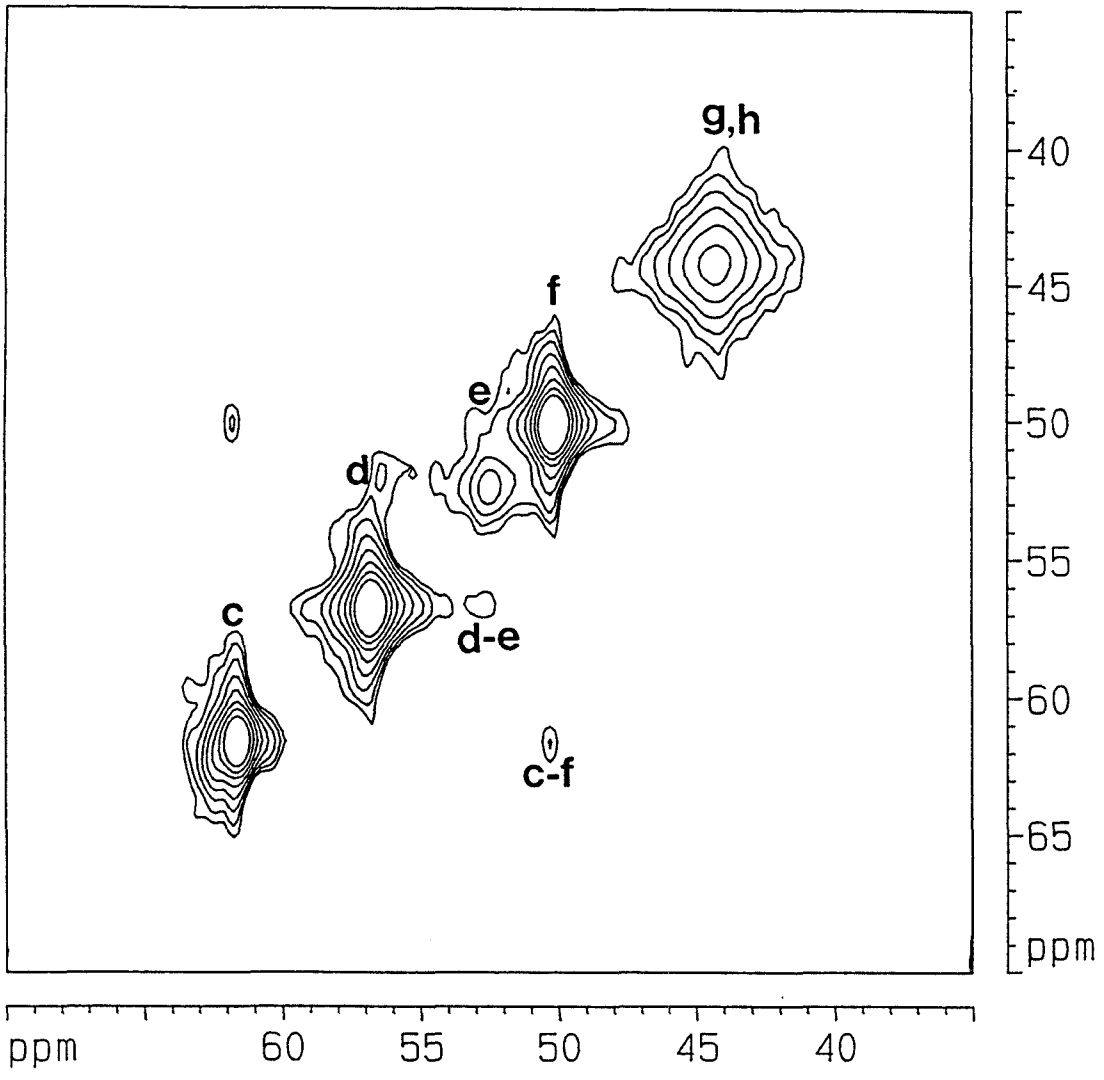
g,h
f
e
d
c
d-e
c-f
40
45
50
55
60
65
ppm
ppm
60
55
50
45
40

Figure 4.8 (**A**) 600-MHz 1D NOE difference spectra (298 K) obtained upon selective saturation of signal *b* of Co^{II} Cys112Asp *P. aeruginosa* azurin (pH 5.5). Trace (a) is the 1D difference spectrum in H_2O, and trace (b) is the 1D difference spectrum in D_2O. Connectivities between signals *b* and two exchangeable signals *i* and *k* are observed. The reference spectrum is also given. (**B**) An expanded plot of the -15 to 20 ppm region of the difference spectrum of trace (b), together with the reference spectrum in D_2O. Besides several other NOEs that are not discussed, a strong NOE is observed with broad signal *l* as well as a weak NOE with signal *m*, which corresponds to a methyl resonance.

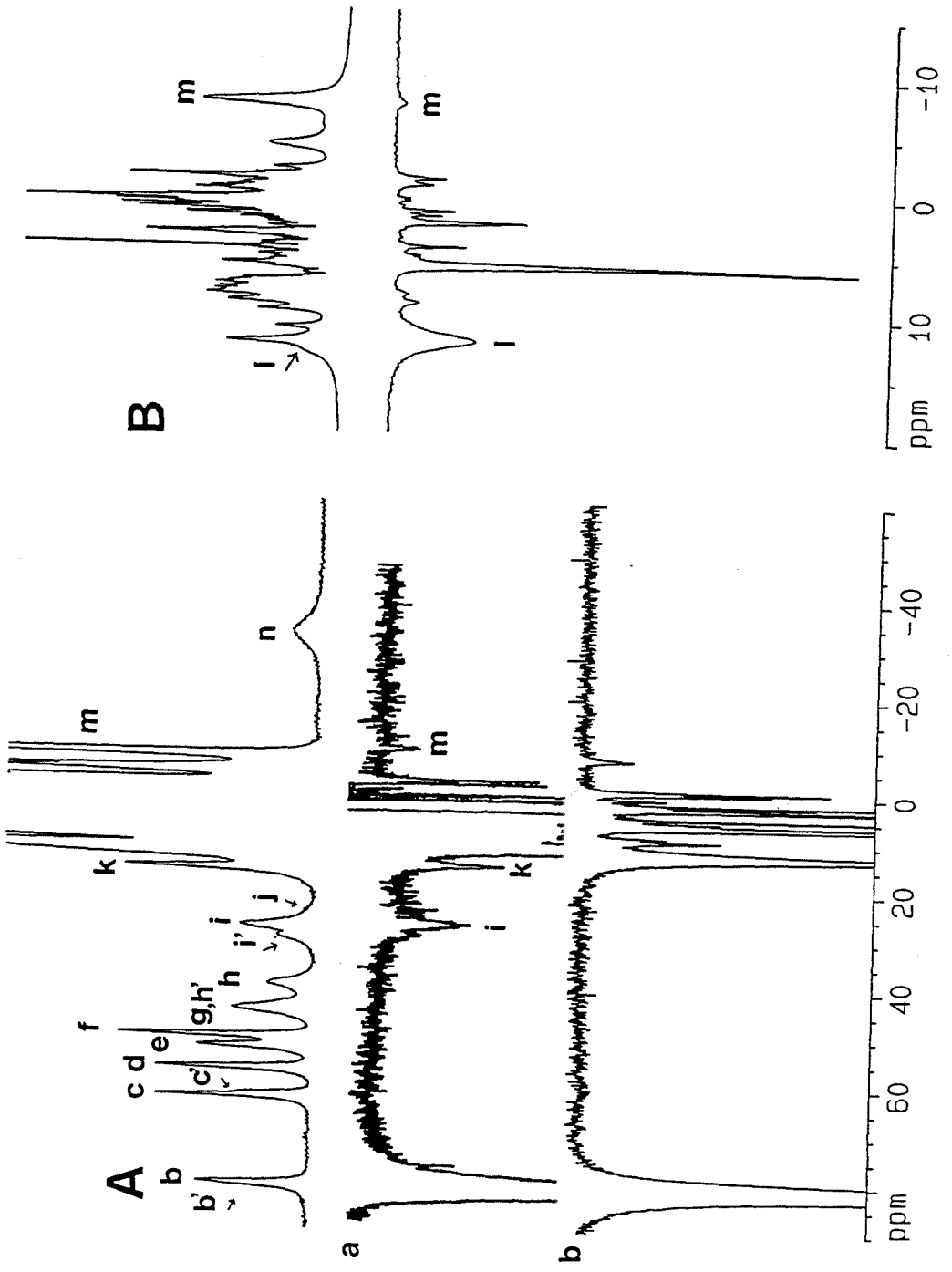
A
B
a
b
ppm
ppm

Figure 4.9 200-MHz 1D NOE difference spectra (298 K) obtained upon selective saturation in D_2O (pH 8.0) of signals *a* (**A**) and *b* (**B**) of Co^{II} WT *P. aeruginosa* azurin. An NOE with one of the two overlapped signals *n* and *o* is observed when saturating signal *b*. The reference spectrum is also given.

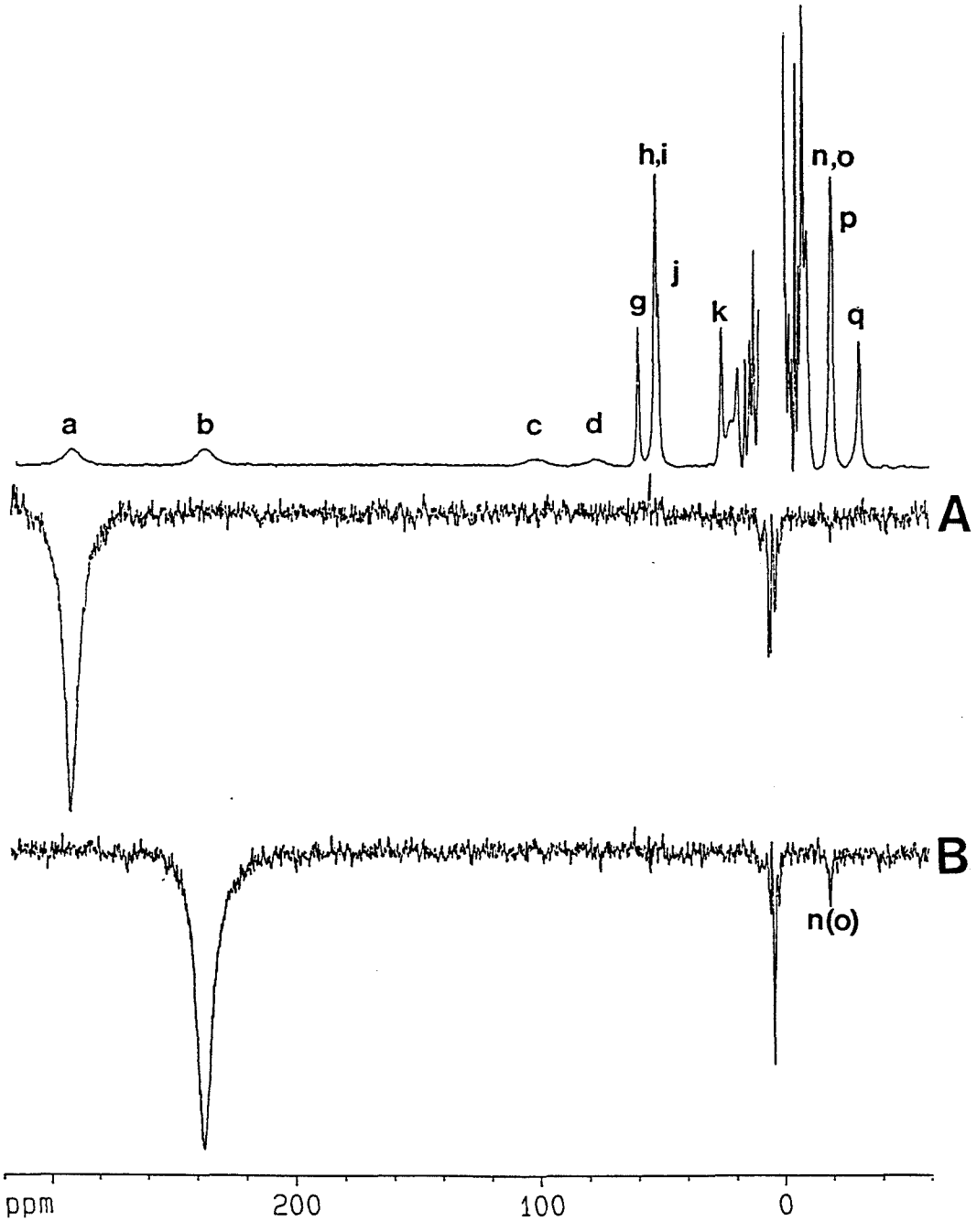
h,i
n,o
p
j
g
k
q
a
b
c
d
A
B
n(o)
ppm
200
100
0

Figure 4.10 600-MHz 1D NOE difference spectrum (298 K) obtained upon saturation of signal *q* in Co^{II} WT *P. aeruginosa* azurin in H_2O (pH 7.2). The NOE peaks indicated with numbers are assigned (mainly on the basis of NOESY and COSY data in Figure 4.11) as follows: (1) NH-Gly45, (2) δ^2-CH_3(Leu86), (3) H^{γ}(Leu86), (4) δ^1-CH_3(Leu86), (5) $H^{\gamma 1}$(Lys41) and H^{β}(Lys41), (6) H^{α}(Lys41), (7) δ-CH_3(Leu68), (8) $H^{\gamma 2}$(Lys41), (9) H^{β}(Lys41), (10) H^{δ}(Lys41). Small cross peaks 7, 8, and 10 are likely due to spin diffusion. The reference spectrum in the -13 to 2 ppm region is also reported.

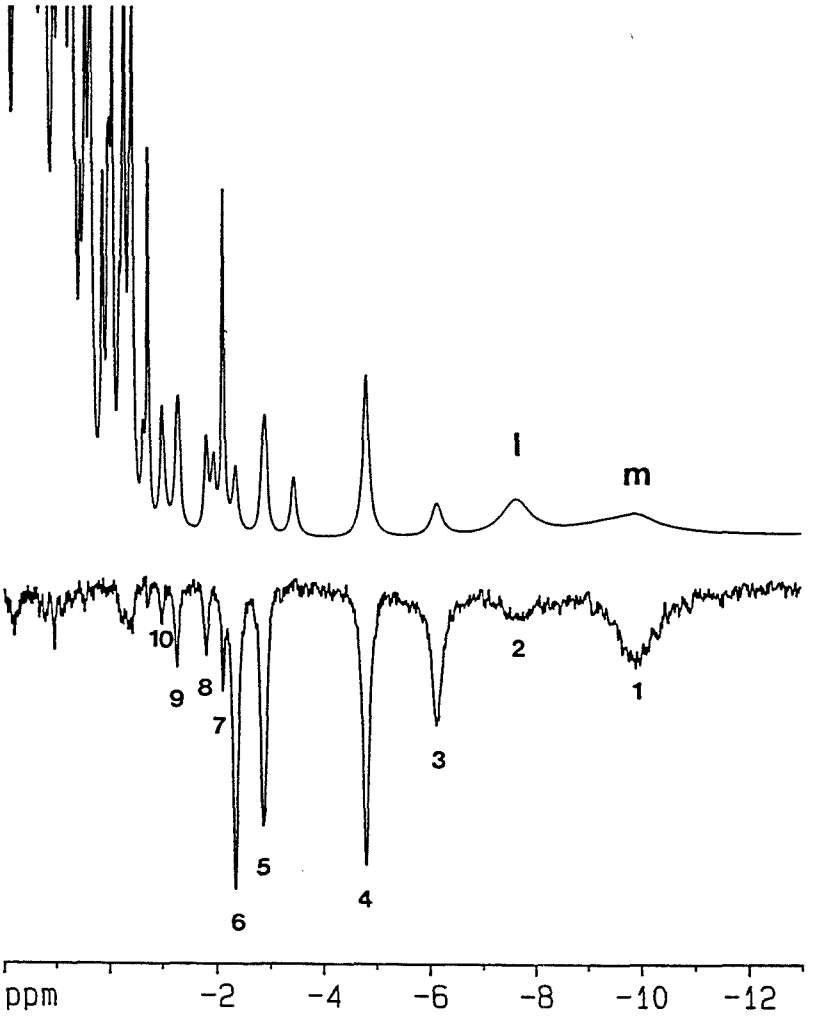
l
m
10
9
8
7
6
5
4
3
2
1
ppm
-2
-4
-6
-8
-10
-12

Figure 4.11 600-MHz NOESY (**A**) and COSY (**B**) spectra (298 K) of Co^{II} WT *P. aeruginosa* azurin in H_2O (pH 7.2) in the -9 to 2 ppm region. In the NOESY spectrum (**A**), cross peaks are labeled as follows: (1) δ^2-CH_3(Leu86)—Hγ(Leu86), (2) δ^2-CH_3(Leu86)—δ^1-CH_3(Leu86), (3) δ^2-CH_3(Leu86)—Hβ(Leu86), (4) Hγ(Leu86)—δ^1-CH_3(Leu86), (5) Hγ(Leu86)—Hγ^1(Lys41), (6) Hγ(Leu86)—Hβ(Leu86), (7) δ^1-CH_3(Leu86)—Hγ^1(Lys41), (8) δ^1-CH_3(Leu86)—δ-CH_3(Leu68), (9) δ^1-CH_3(Leu86)—Hδ(Lys41), (10) δ^1-CH_3(Leu86)—Hβ(Leu86), (11) Hβ(Lys41)—Hα(Lys41), (12) Hγ^1(Lys41)—δ-CH_3(Leu68), (13) Hγ^1(Lys41)—Hγ^2(Lys41), (14) Hβ(Lys41)—Hβ(Lys41), (15) Hγ^1(Lys41)—Hδ(Lys41), (16) Hγ^1(Lys41)—Hδ(Lys41), (17) Hα(Lys41)—Hβ(Lys41), (18) Hδ(Lys41)—Hγ^2(Lys41). Cross peaks 5, 7, 8, 9 identify the connections of the spin system of Leu86 to the spin system of Lys41 and to the spin system of Leu68. In the COSY spectrum (**B**), letters indicate cross peaks belonging to the same spin system. The spin systems are labeled as follows: (a) Leu86, (b) Lys41, (c) Leu68. Cross peaks indicated with (d) belong to a spin system that does not give rise to any dipolar connectivity with Hα of Gly45 or any other resonance of the above assigned residues. NOESY (**A**): A higher field threshold level was used for the contour plot of the left panel; the right panel was obtained upon Fourier transformation of a 512 x 256 data-point matrix. COSY (**B**): The upper and lower right panels were obtained upon Fourier transformation of 600 x 300 and 360 x 180 data-point matrices, respectively.

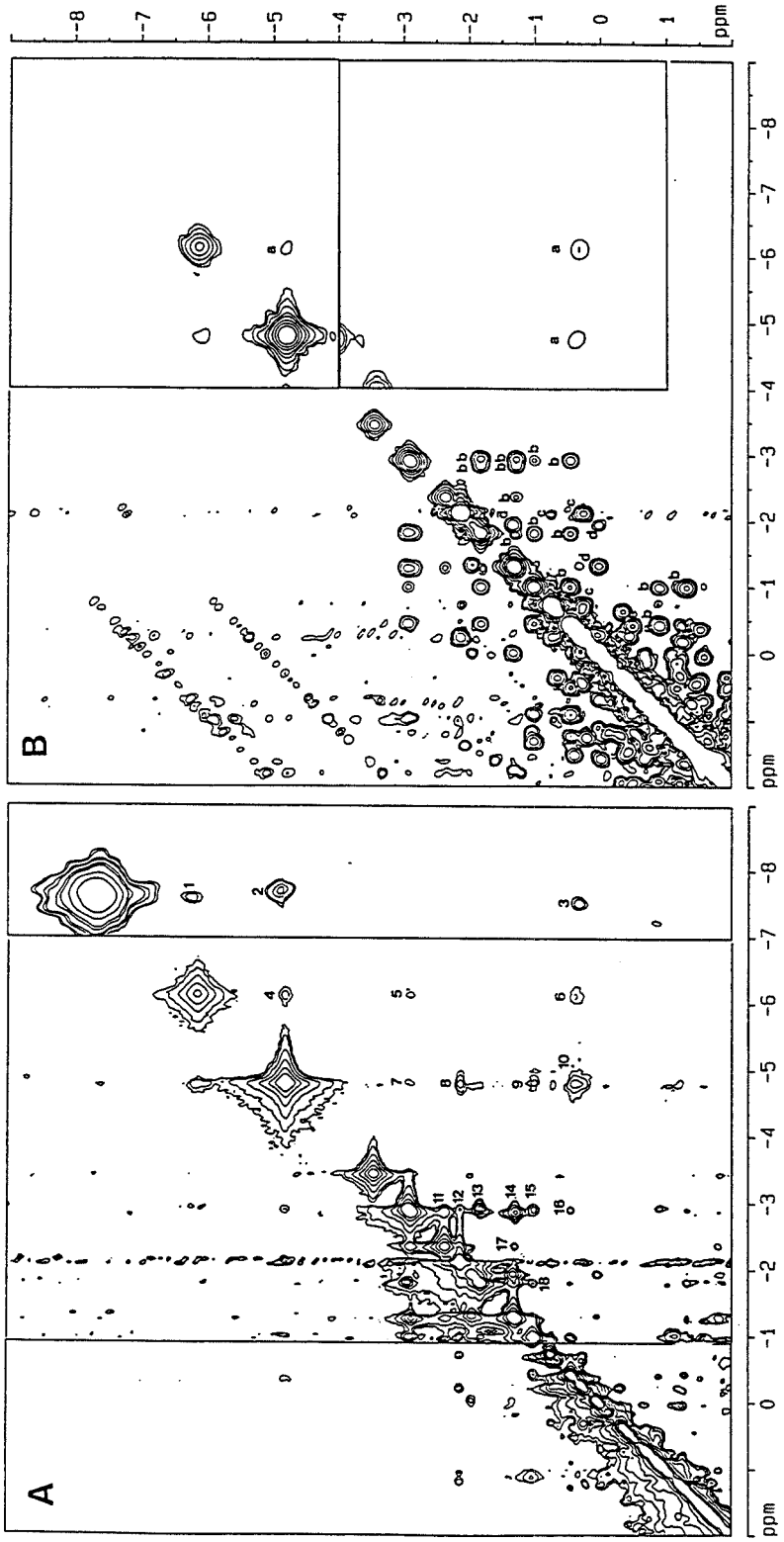
ppm
A
B
ppm

Figure 4.12 Representation of the protons of Co^{II} WT and Cys112Asp *P. aeruginosa* azurins that possess large hyperfine-shifted NMR signals.

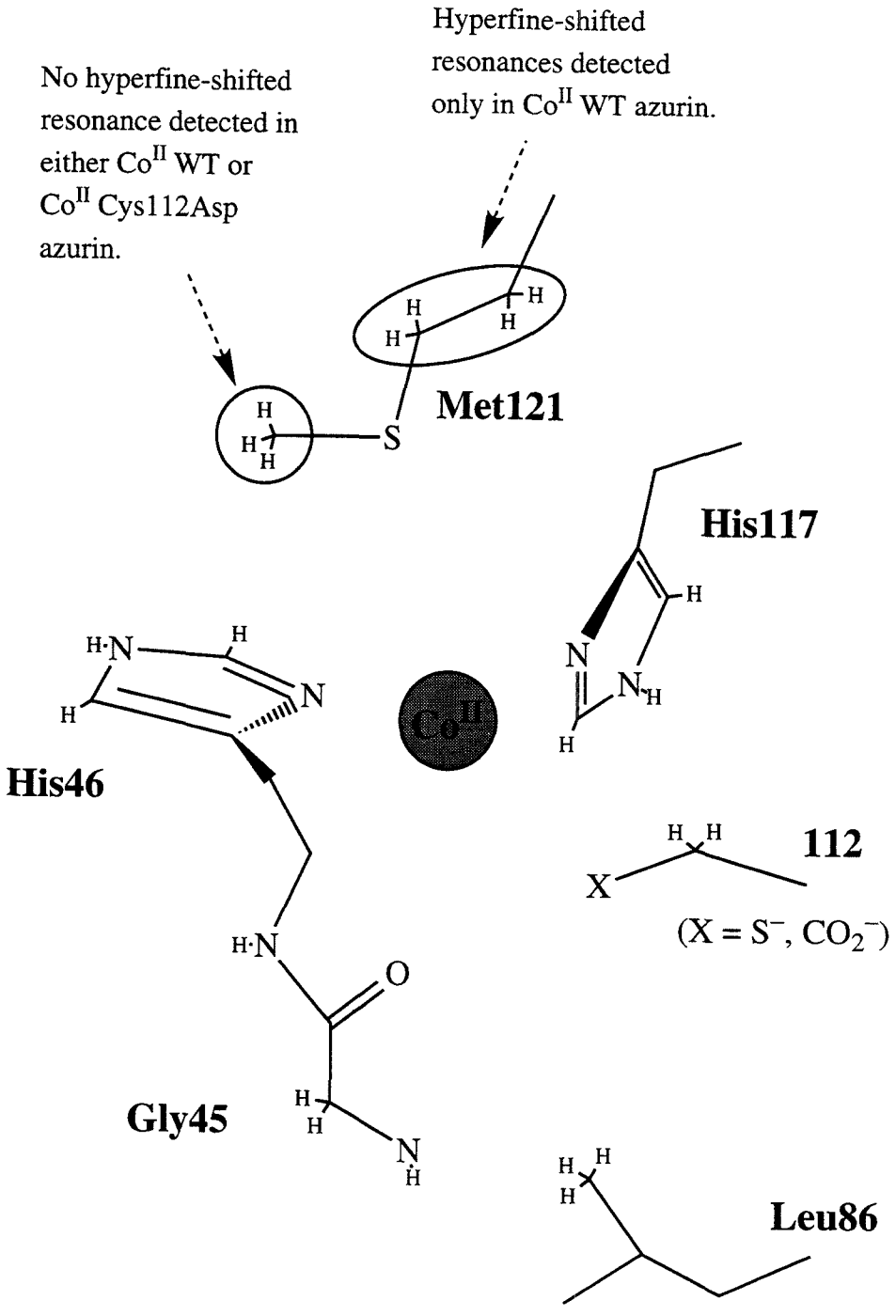
No hyperfine-shifted resonance detected in either Co^II WT or Co^II Cys112Asp azurin.
Hyperfine-shifted resonances detected only in Co^II WT azurin.
Met121
His117
His46
Co^II
112
(X = S⁻, CO2⁻)
Gly45
Leu86

Figure 4.13 Computer-generated model of the active-site structure of Co^{II} Cys112Asp *P. aeruginosa* azurin. The Co^{II} ion was added manually to the minimized apo protein structure. Reasonable bond distances could be achieved between the Co^{II} center and the Gly45 carbonyl (2.3 Å), N^{δ}(His46) (2.1 Å), $O^{\delta 1}$(Asp112) (2.1 Å), $O^{\delta 2}$(Asp112) (2.5 Å), and N^{δ}(His117) (2.1 Å). According to this model, the Co^{II}-S^{δ}(Met121) distance is 3.7 Å, the metal is displaced ~1.4 Å out of the pseudosquare plane towards Gly45, and the C^{β}(Asp112)-C^{γ}(Asp112)-Cu angle is ~145°.

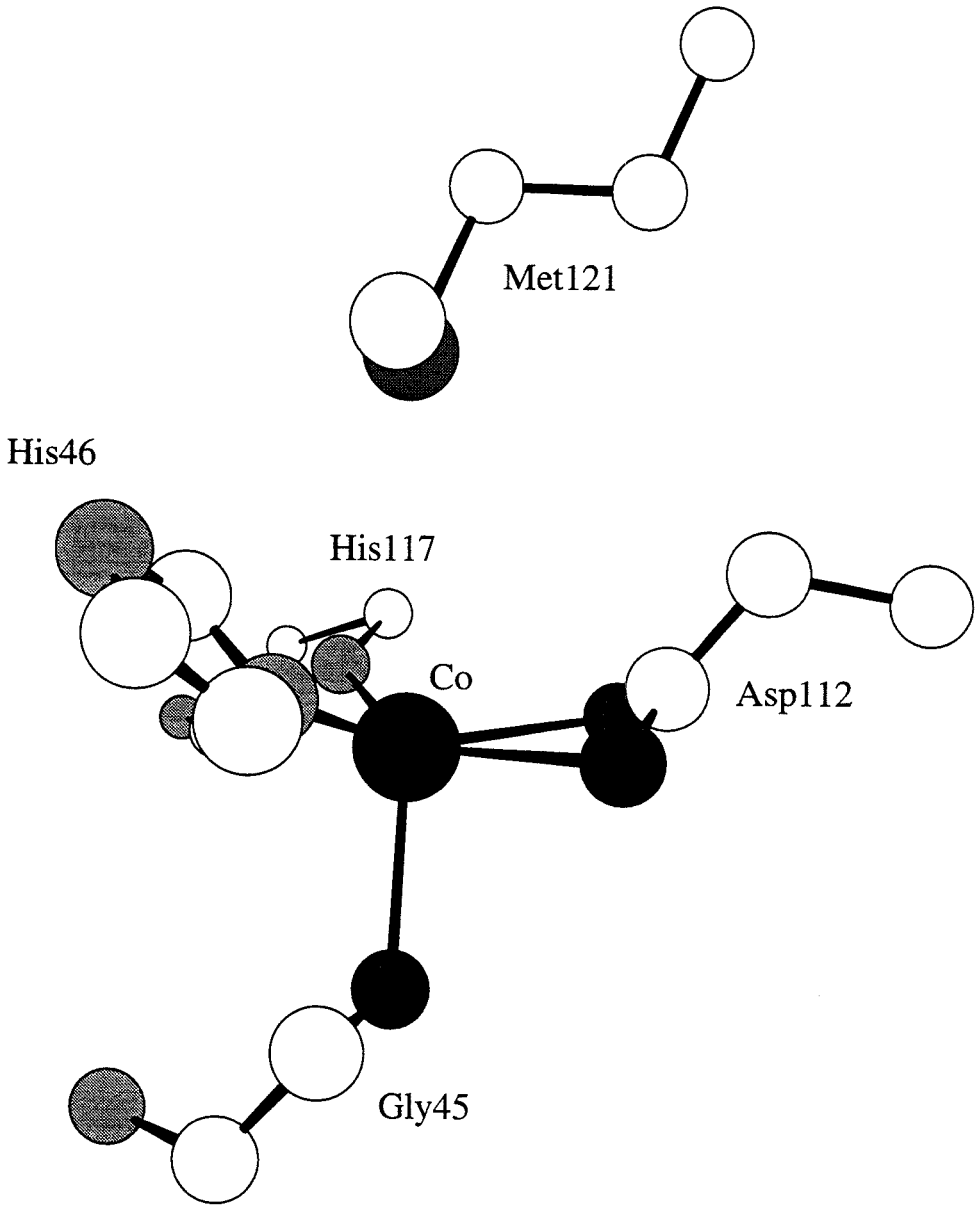
Met121
His46
His117
Co
Asp112
Gly45

Chapter 5

Nickel(II) Cys112Asp Azurin

Introduction

Like Co^{II} substitutions of blue copper sites in proteins (see Chapter 4), substitutions with Ni^{II} result in similar changes: (1) the Cys(thiolate)-to-metal(II) charge-transfer transitions shift to higher energy[1] due to the relative instability of Ni^{I}, and (2) the high-spin character of the d^8 Ni^{II} centers in blue copper active sites allows paramagnetically shifted NMR signals in and around the active sites to be detected owing to favorable electronic spin-relaxation times.[2] In particular, the absorption spectrum of Ni^{II} WT *P. aeruginosa* azurin (Figure 5.1) shows two relatively intense bands centered at 357 and 440 nm, both of which are attributable to Cys(thiolate)-to-Ni^{II} charge-transfer transitions; the energies of these transitions are not as blue-shifted as in Co^{II} WT azurin (Figure 4.1), implying that the Ni^{II} center is more easily reduced than the Co^{II} center. The crystal structure of Ni^{II} WT *P. aeruginosa* azurin has been reported,[3] and shows a pseudotetrahedral Ni^{II} coordination geometry defined by His46, His117, Cys112, and the backbone carbonyl of Gly45. To investigate further the coordination chemistry of the Cys112Asp mutant of *P. aeruginosa* azurin, we examined the spectroscopic properties of its Ni^{II} derivative.

Materials and Methods

Metal Titration. Molar extinction coefficients of the absorption bands of Ni^{II} Cys112Asp azurin were determined from a titration experiment. To an appropriately concentrated solution of a known volume of pure recombinant apo Cys112Asp *P. aeruginosa* azurin in 10 mM DEA·HCl/~40 mM NaCl (pH ~8.5) was added aliquots of a standardized solution of aqueous $NiCl_2$ ($\varepsilon_{394} = 5.0\ M^{-1}cm^{-1}$) in a 1-cm pathlength quartz cuvette. Absorption changes were monitored using a Hewlett-Packard 8452A Diode Array Spectrophotometer and were allowed to stabilize after each addition.

The data at a given wavelength were plotted as (observed absorbance) *vs.* (concentration Ni^{II} added). The data were not corrected for volume changes as the

maximum change was < 5%. The resultant titration plot was fit using KaleidaGraph 3.0 (Abelbeck Software) to the following function:

$$A = \frac{1}{2}\left[\varepsilon_{Ni}\left([M]_{tot} + [P]_{tot} + K_d\right) - \sqrt{\varepsilon_{Ni}{}^2\left([M]_{tot} + [P]_{tot} + K_d\right)^2 - 4\varepsilon_{Ni}{}^2[P]_{tot}[M]_{tot}}\right] \quad (5.1)$$

where:

$A \equiv$ observed absorbance

$\varepsilon_{Ni} \equiv$ molar extinction coefficient of Ni^{II} Cys112Asp azurin

$[M]_{tot} \equiv$ total $[Ni^{II}]$

$[P]_{tot} \equiv$ total [protein]

$K_d \equiv$ dissociation constant

The derivation of eq 5.1 assumes a simple equilibrium process:

$$Ni^{II} + \text{apo Cys112Asp azurin} \rightleftharpoons Ni^{II}\ \text{Cys112Asp azurin}$$

where:

$$K_d = \frac{[Ni^{II}][\text{apo Cys112Asp azurin}]}{[Ni^{II}\ \text{Cys112Asp azurin}]} \quad (5.2)$$

in which the observed absorbance is due solely to Ni^{II} Cys112Asp azurin. $[P]_{tot}$ was determined using $\varepsilon_{280} = 9.0 \times 10^3\ M^{-1}cm^{-1}$ for apo Cys112Asp azurin. ε_{Ni} and K_d were determined from the fit.

Protein Preparation. For general purposes, Ni^{II} WT azurin was made by the addition of a moderate excess of aqueous $NiCl_2$ to a buffered solution (pH ~9) of apo protein. The resultant yellow solution was allowed to stand for at least 1 hour to assure complete reconstitution. Excess Ni^{II} was chelated with the addition of EDTA, and Ni^{II} WT azurin was then purified by FPLC on a Mono Q (strong anion-exchange) column (Pharmacia) using a NaCl gradient in 10 mM DEA·HCl (pH 8.8). The low salt buffer

(Buffer A) contained no additional NaCl; the high salt buffer (Buffer B) was supplemented with 200 mM NaCl. Protein was detected by UV absorption at 280 nm.

Samples of Ni^{II} Cys112Asp azurin were prepared by the addition of a known excess of Ni^{II} to a solution containing a known amount of pure apo Cys112Asp azurin.

Concentrated protein samples were obtained using Centricon-10 concentrator units (Amicon).

Spectroscopic Measurements. High-resolution absorption spectra were recorded on a modified Cary 14 spectrophotometer.

Results and Discussion

Metal Titration and Instability to Metal Loss. Titration of apo Cys112Asp azurin with Ni^{II} is accompanied by absorption changes that make the solution turn yellow-orange (indicating formation of Ni^{II} Cys112Asp azurin) (Figure 5.2A). However, unlike titrations with Cu^{II} (see Chapter 3) or Co^{II} (see Chapter 4), the absorption changes took much longer to stabilize, were not linear with respect to added Ni^{II}, and did not plateau until well over 1 equivalent of Ni^{II} had been added (Figure 5.2B). These results suggested that an equilibrium process was occurring with relatively weak metal binding. A control experiment using Zn^{II} Cys112Asp azurin showed that exogenous Ni^{II} does not contribute significantly to the overall absorbance of the solution under the conditions of the titration experiment, thereby demonstrating not only that the observed absorbance changes reflect formation of Ni^{II} Cys112Asp azurin but also that the Ni^{II} ion is being bound at the active site of azurin. A fit of the titration plot to eq 5.1 resulted in ε_{330} (ε_{Ni} in eq 5.1) = 3.4×10^2 $M^{-1}cm^{-1}$ and $K_d = 1.1 \times 10^{-4}$ M (Figure 5.2B). The error in these values is estimated to be $< \pm 15\%$. The relatively large dissociation constant of Ni^{II} Cys112Asp azurin is reflected in the ease with which the protein is demetallated by EDTA. Furthermore, Ni^{II} Cys112Asp azurin can not survive the FPLC purification protocol without metal loss.

Electronic Spectroscopy. The absorption spectrum of Ni^{II} Cys112Asp azurin (Figure 5.3) shows no intense charge-transfer bands, as observed in the Ni^{II} WT protein (Figure 5.1). Instead, low-intensity absorptions are observed throughout the near-UV, visible, and near-IR. The presence of low-energy absorption bands are suggestive of high-spin Ni^{II}. This conclusion has been confirmed with the detection of hyperfine-shifted NMR signals (data not shown), since low-spin Ni^{II} is diamagnetic. Therefore, the possibility of a square planar Ni^{II} geometry can effectively be ruled out.

The nature of the most intense absorption band centered at 330 nm remains somewhat of a mystery. The relatively high energy of the transition argues strongly against it being a d-d band. If so, we are forced to assign the band to a charge-transfer transition, and the most reasonable active-site ligand that might produce such a low-energy charge-transfer transition with Ni^{II} is the thioether of Met121. In fact, octahedral Ni^{II} thioether complexes that employ thia crown ethers exhibit intense bands ~300-320 nm which have been assigned to thioether-to-Ni^{II} charge-transfer transitions.[4] Although, these bands are significantly more intense than the one observed for Ni^{II} Cys112Asp azurin, this discrepancy may result from poor orbital overlap between the thioether of Met121 and the Ni^{II} center caused by structural constraints imposed by the protein fold. If we assume that the other well resolved band at 444 nm represents the highest energy d-d transition of Ni^{II} Cys112Asp azurin, its intensity is too low and its energy still too high to consider tetrahedral Ni^{II} coordination.[5] Distorted square pyramidal, trigonal bipyramidal and octahedral geometries remain viable possibilities.

Based on results from the Cu^{II} (see Chapter 3) and Co^{II} (see Chapter 4) derivatives of Cys112Asp azurin, it is reasonable to assume that both native histidine residues (His46 and His117) and the carboxylate group of Asp112 are involved in Ni^{II} binding. In contrast, however, the Ni^{II} derivative may possess a Met121(thioether)-metal bonding interaction that is strong enough to give rise to an observable electronic transition. Paramagnetic NMR

studies are currently in progress to help further elucidate the coordination structure of Ni^{II} Cys112Asp azurin.

References

(1) (a) Tennet, D. L.; McMillan, D. R. *J. Am. Chem. Soc.* **1979**, *101*, 2307-2311. (b) Lum, V.; Gray, H. B. *Isr. J. Chem.* **1981**, *21*, 23-25. (c) Di Bilio, A. J.; Chang, T. K.; Malmström, B. G.; Gray, H. B.; Karlsson, B. G.; Nordling, M.; Pascher, T.; Lundberg, L. G. *Inorg. Chim. Acta* **1992**, *198-200*, 145-148.

(2) (a) Blaszak, J. A.; Ulrich, E. L.; Markley, J. L.; McMillan, D. R. *Biochemistry* **1982**, *21*, 6253-6258. (b) Moratal, J.-M.; Salgado, J.; Donaire, A.; Jiménez, H. R.; Castells, J. *J. Chem. Soc. Chem. Commun.* **1993**, 110-112. (c) Moratal, J.-M.; Salgado, J.; Donaire, A.; Jiménez, H. R.; Castells, J.; Martínez-Ferrer, M.-J. *Mag. Res. Chem.* **1993**, *31*, S41-S46.

(3) Moratal, J. M.; Romero, A.; Salgado, J.; Perales-Alarcón, A.; Jiménez, H. R. *Eur. J. Biochem.* **1995**, *228*, 653-657.

(4) (a) Blake, A. J.; Gould, R. O.; Halcrow, M. A.; Holder, A. J.; Hyde, T. I.; Schröder, M. *J. Chem. Soc. Dalton Trans.* **1992**, 3427-3431. (b) Blake, A. J.; Reid, G.; Schröder, M. *J. Chem. Soc. Dalton Trans.* **1994**, 3291-3297.

(5) Sacconi, L.; Mani, F. In *Comprehensive Coordination Chemistry*; Wilkinson, G.; Gillard, R. D.; McCleverty, J. A., Eds.; Pergamon: Oxford, 1987; Vol. 5, pp 1-347.

Figure 5.1 Electronic absorption spectrum of Ni^{II} WT *P. aeruginosa* azurin in 10 mM DEA·HCl/~40 mM NaCl (pH 8.8) at room temperature.

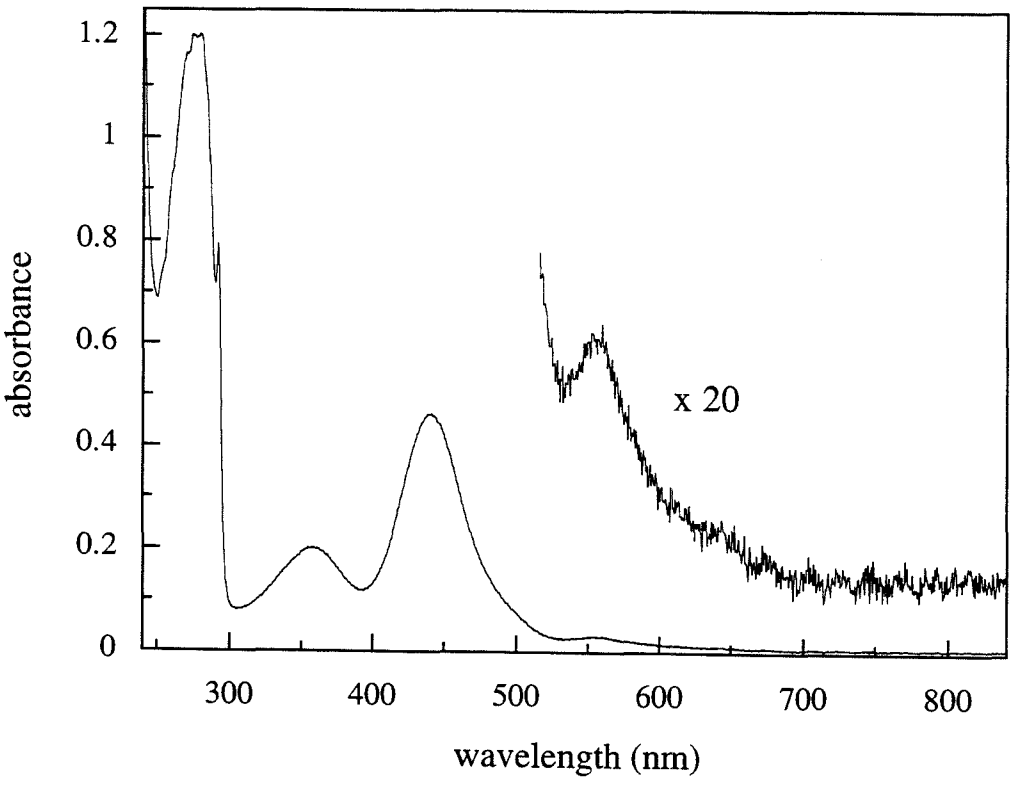
absorbance
1.2
1
0.8
0.6
0.4
0.2
0
x 20
300
400
500
600
700
800
wavelength (nm)

Figure 5.2 Absorption changes accompanied by the titration of apo Cys112Asp *P. aeruginosa* azurin with Ni^{II} (**A**) and the corresponding titration plot (λ_{obs} = 330 nm) with accompanying fit to eq 5.1 ($[P]_{tot} \equiv 0.55$ mM) (**B**).

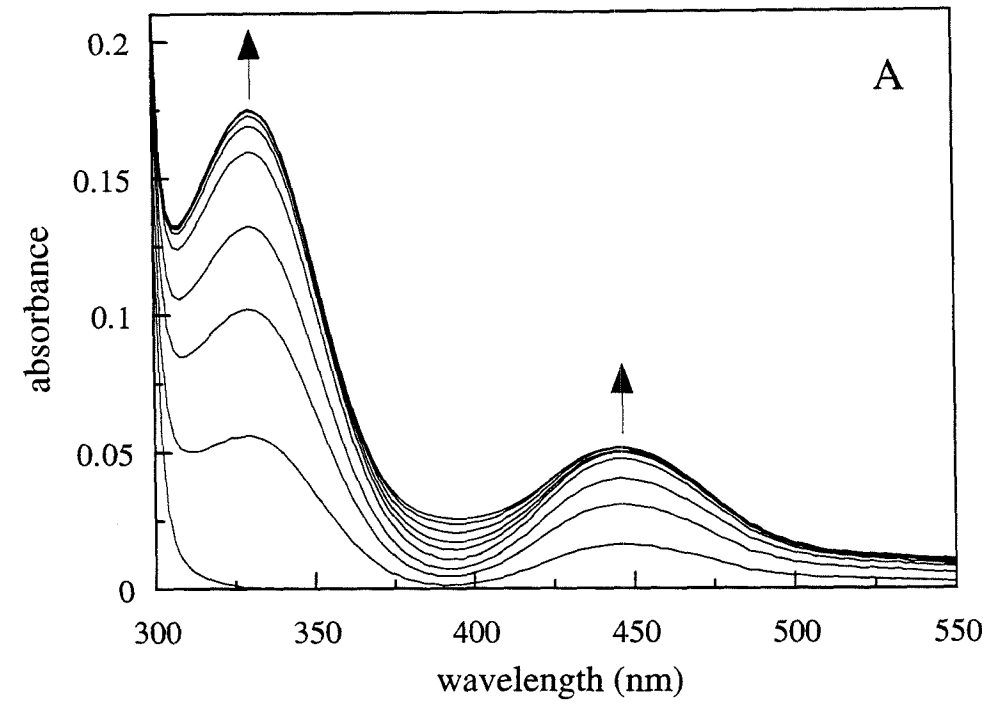
A
absorbance
0.2
0.15
0.1
0.05
0
300
350
400
450
500
550
wavelength (nm)

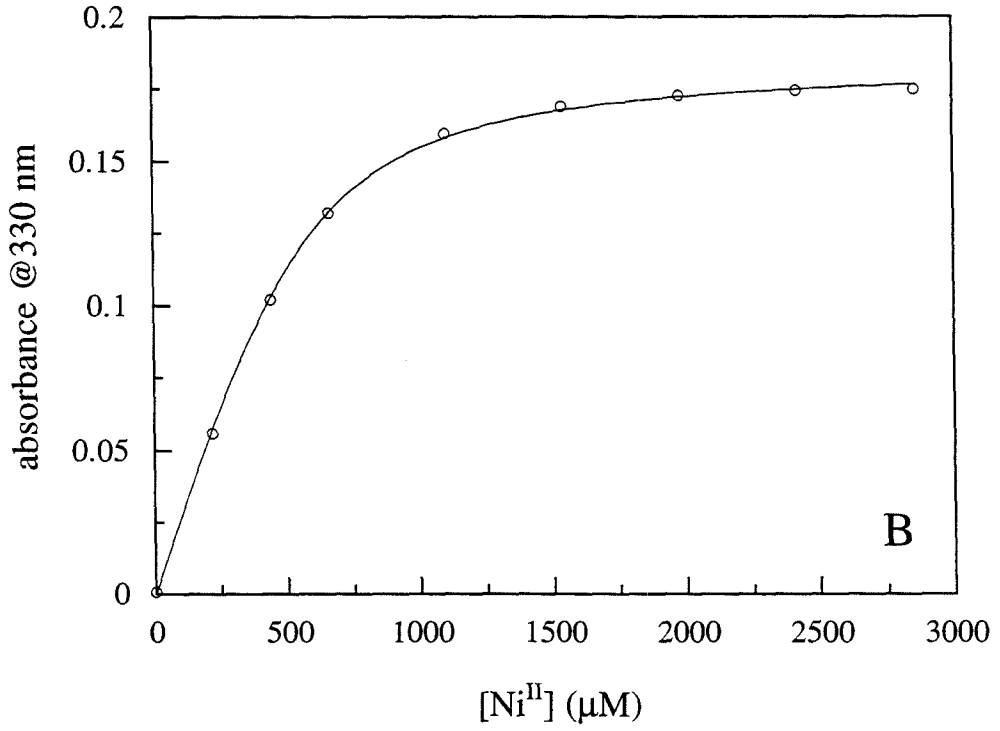
B
absorbance @330 nm
0.2
0.15
0.1
0.05
0
0
500
1000
1500
2000
2500
3000
[Ni^II] (μM)

Figure 5.3 Electronic absorption spectrum of Ni^{II} Cys112Asp *P. aeruginosa* azurin (λ_{max} = 330, 444 nm) in 10 mM DEA·HCl/~40 mM NaCl (pH ~8) at room temperature (contains ~0.4 mM free Ni^{II} which contributes a background absorption of < 0.002 absorbance units).

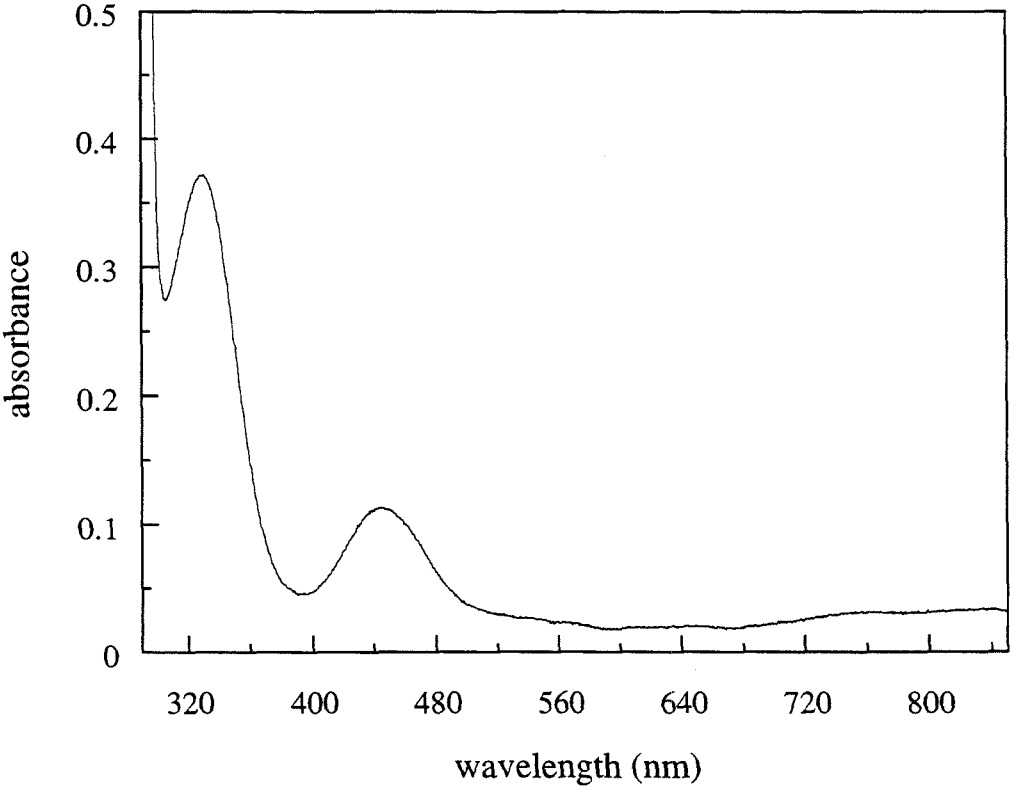
0.5
0.4
0.3
0.2
0.1
0
absorbance
320
400
480
560
640
720
800
wavelength (nm)

Chapter 6

Summary

We have found that replacement of the active-site Cys (at position 112) of *P. aeruginosa* azurin with an Asp does not compromise the inherent stability of the protein nor abolish its ability to bind metal ions (*viz.*, Cu^{II}, Cu^{I}, Co^{II}, Ni^{II}, Zn^{II}). Nevertheless, the spectroscopic properties of holo Cys112Asp azurins are significantly different from those of the analogous metal-bound forms of the WT protein (except for the Zn^{II} derivatives), thereby reinforcing the importance of the thiolate sulfur ligand to the electronic structure of the WT active site. The electronic spectroscopy of the various open-shell metal derivatives of Cys112Asp azurin all show d-d bands that are consistent with five-coordinate geometries.

Data from a combination techniques (paramagnetic NMR spectroscopy, electronic absorption spectroscopy, X-ray crystallography (of Cu^{II} WT azurin)) provided the basis for the generation of a computer model of the Cys112Asp active site. Subsequent X-ray crystallographic studies of Cu^{II} Cys112Asp azurin revealed a remarkably similar active-site structure: a distorted square pyramidal coordination structure with an out-of-plane metal-binding interaction with a bidentate, asymmetrically bound carboxylate group. The metal ion, however, is not as removed from the plane of the carboxylate group as in the computer model structure. This difference probably reflects the desire of Cu^{II} to adopt a more standard planar metal-carboxylate interaction, an energetic term that was not included in the computer calculations. Regardless, the perturbation caused by the local Cys-to-Asp change is transmitted to surrounding residues leading to small but significant positional changes of atoms within the entire active-site region and beyond.

Our inability to observe intramolecular electron transfer in systems that exhibit fast kinetics in analogous WT protein systems demonstrates the criticality of the Cys residue to the reaction. The reason for the intramolecular electron-transfer-impaired nature of the mutant has been determined to result at least in part by a significant reduction in the electronic coupling between the donor and acceptor groups. Nevertheless, the bimolecular

electron transfer between Cys112Asp azurin and either WT azurin or cytochrome c_{551} is still observed and the reactions quantifiable. The difference between the intramolecular and intermolecular electron-transfer systems most likely reflects the fact that the intermolecular reactions involve the hydrophobic patch of azurin and the transfer of electrons through the partially solvent-exposed ligand His (at position 117), thereby bypassing the Cys112 ligand altogether. Therefore, the Cys ligand appears to be important for promoting long-range electron transfer, a property that may be necessary for the proper *in vivo* function of blue copper proteins, in general.

We hope that further studies of Asp112-containing azurins will be pursued to understand better the role of the Cys112 ligand to electron transfer in azurin. For example:

(1) A pulsed laser experiment (λ = ~290 nm) may allow intramolecular electron transfer to occur between the highly oxidizing and the very long-lived triplet excited-state of Trp48 and the Cu^{II} center. If excited-state quenching occurs by electron transfer at an appreciable rate, the ground-state electron-transfer reaction between the Cu^{I} center and the Trp48 cation radical may be observable by transient absorption spectroscopy.

(2) It may be possible to obtain crystals of Cu^{I} Cys112Asp azurin by chemical reduction of crystals of the oxidized protein. A determination of the active-site structure of Cu^{I} Cys112Asp azurin is important to know what kind of structural changes, including the possibility of ligand loss, accompany change in redox state.